Development of Enzyme Replacement Therapy in Mammalian Models of Barth Syndrome

Ana A. Dinca

A dissertation submitted in partial fulfillment of

the requirements for the degree of

Doctor of Philosophy

University of Washington

2017

Reading Committee:

Michael Chin, Chair

David Marcinek

Peter Rabinovitch

Program Authorized to Offer Degree:

Pathology

University of Washington

Abstract

Development of Enzyme Replacement Therapy

in Mammalian Models of Barth Syndrome

Ana A. Dinca

Chair of the Supervisory Committee:

Micahel Chin, Associate Professor of Medicine

Department of Pathology

Barth Syndrome (BTHS) is a devastating disorder caused by a single gene mutation in the mitochondrial transacylase, tafazzin (TAZ), which results in impaired lipid metabolism leading to dysfunction in highly energetic tissues, such as the heart and skeletal muscle. TAZ remodels, cardiolipin (CL), a multifaceted phospholipid with roles in mitochondrial bioenergetics, protein import and apoptosis. BTHS, the first known disorder of CL metabolism, manifests through a wide range of symptom, from severe impairment in cardiac function to hypotonia and recurring infections. Current treatment strategies are merely ameliorative in nature and up to 30% of patients still succumb to the disease early in life. A curative treatment is still an unmet need. TAZ enzyme replacement therapy (ERT) could significantly benefit patients suffering from this disorder.

The studies presented here focus on the design and development of a recombinant TAZ protein containing a cell penetrating peptide for the treatment of BTHS, along with characterization of tafazzin deficient mammalian models critical for efficacy tests. To better understand the structure of

TAZ, the mitochondrial localization signal of TAZ was determined. If successful, these studies could lead to significant improvements in quantity and quality of life for BTHS patients.

TABLE OF CONTENTS

LIST OF FIGURES

LIST OF TABLES

1 Introduction

Barth Syndrome (BTHS) is a rare, but debilitating disorder of infancy, characterized by cardiomyopathy and severe infections. The effects can be lethal for patients and devastating for family members. The only available therapies are ameliorative in nature and patients could benefit enormously from a curative treatment. My thesis aims to address this unmet need, by studying the biology of tafazzin (TAZ), the gene responsible for BTHS, and developing an enzyme replacement therapy (ERT).

1.1 BTHS, a devastating disorder

BTHS (OMIM #302060) is a recessive X-linked mitochondrial disorder first described in 1983 in a large Dutch pedigree by Dr. Peter Barth [1]. The multi-system syndrome manifests with cardiomyopathy, neutropenia, skeletal muscle weakness, growth deficiencies and methylglutaconic aciduria [2,3]. It was later found to result from mutations in a single gene, the mitochondrial transacylase, TAZ [4]. The result is an impairment of lipid metabolism leading to mitochondrial dysfunction in highly energetic tissues [5–7].

Cardiolipin (CL), an exclusive mitochondrial phospholipid, is not properly remodeled in the absence of TAZ. The mitochondrial defects that lie at the basis of this syndrome are based on the many functions of CL, but ultimately result in reduced performance of the electron transport chain and a loss of energy coupling efficiency [1,8,9].

The exact prevalence and incidence of the disease are unknown and reported estimates (from different countries) show significant variability. The BTHS Foundation in the United States (US), which maintains a Registry and Repository with patient data and samples from around the globe, reports fewer than 500 cases worldwide. They also estimate around 10 new cases, or 1 in 300,000-400,000 live births, occur each year in the US [10]. This is in agreement with estimates from a study

of the French BTHS patient population, reporting an incidence of 1.5/1,000,000 [11]. In contrast, a British study estimates the disease is under-diagnosed and incidence may be as high as 1 in 140,000 births [12,13]. BTHS could also be an unrecognized cause of prenatal deaths [14].

1.1.1 Clinical Features

BTHS is considered a multi-system disorder, manifesting with cardiomyopathic features, skeletal myopathy, neutropenia and other blood abnormalities, growth delays, and 3-methylglutaconic aciduria. There is significant variability in the manifestation of symptoms, both between patients and in a single patient over time [15,16]. This is likely a contributing factor to the presumed underdiagnosis of BTHS.

1.1.1.1 Cardiomyopathy and Skeletal Myopathy

Cardiomyopathy has a high prevalence in BTHS and is one of the leading causes of morbidity among these patients. The BTHS Registry reports 94% of subjects have some form of cardiomyopathy, with the majority of diagnoses (70%) occurring during the first 6 months of life [16]. This is in agreement with studies from the United Kingdom (UK) and France that examined their respective populations only [11,17]. All subjects in the Registry had the first manifestation of cardiac symptoms prior to 5 years of age and 80% of cardiac transplants occurred prior to this age, suggesting a critical role for TAZ during development [13]. After age 5, cardiac function maintains relatively stable, with only mild abnormalities [13,17,18].

Patients most commonly exhibit dilated cardiomyopathy (DCM), which results in increased left ventricular (LV) mass, enlargement of the LV chamber and a decrease in systolic function [19]. Endocardial fibroelastosis (EFE), or thickening of the endocardium layer, can accompany DCM [13,20]. Tissue architecture often undergoes remodeling during this process. This includes cardiomyocyte elongation and death, followed by cardiac fibroblast proliferation and formation of fibrotic scars. Myocardial fibrosis has been documented in BTHS patients [21].

About 50% of patients present with LV non-compaction (LVNC) or hypertrabeculation, a condition commonly associated with monogenic disorders [22]. This condition may overlap with DCM, although it doesn't appear to impact the functional severity of the already existing cardiomyopathy [17]. LVNC is a structural abnormality of the myocardial wall, characterized by a spongy appearance, and believed to result from a failure of the heart muscle to compact during development. It manifests clinically with cardiac arrhythmias and ventricular dysfunction, both systolic and diastolic [23]. In rare cases, blood clots formed in the trabeculae can cause stroke. An intriguing feature of hypertrabeculation in children is the 'undulating phenotype', in which cardiac morphology undergoes changes. This can result in a transition, for instance, from a dilated to a hypertrophic and hypercontractile LVNC [24,25]. Periods of significant improvement in ventricular function are sometimes seen in LVNC pediatric patients, followed by regression, adding to the inconsistency in phenotype already seen with BTHS.

Less often, hypertrophic cardiomyopathy (HCM) is also encountered in BTHS. Hypertrophy, a primarily compensatory reaction in response to higher workload imposed on the heart, leads to thickening of the septal wall and left ventricle. As mature cardiomyocytes are unable to significantly proliferate, the primary mechanism is an increase in cardiomyocyte diameter and/or length; interstitial fibrosis also often accompanies HCM [26,27]. On rare occasions, a transition from one form of cardiomyopathy to another can occur. Kang *et al* report a case where a BTHS patient initially presenting with HCM later evolved to the more commonly encountered, DCM [17].

Although rare, some BTHS patients never report cardiomyopathy. In these cases, they are diagnosed due to a positive family history [15,16].

Two important indicators of ventricular function that can be gleaned from echocardiograms are ejection fraction (EF) and fractional shortening (FS), which measure the percentage of blood volume pumped out and the change in diameter of the LV with each beat, respectively [28].

Although there are appreciable differences in cardiac function in the BTHS population, particularly during the first few years of life, EF and FS data showed similar patterns over time, namely a decrease in variation and an increase in function with increase in age. The majority of patients for whom EF and FS data was available show only mild decreases in function after age 5 [11,16].

Ventricular arrhythmias leading to cardiac arrest, and sometimes resulting in sudden death, have also been documented in BTHS patients [15,29]. These episodes are more predominant in adolescents, rather than early childhood and do not appear to correlate with the degree of ventricular dysfunction, suggesting an independent mechanism, directly rooted in mitochondrial abnormalities. One theory suggests that altered fatty acid distribution of mitochondrial phospholipids could disturb lipid–protein interactions and change mitochondrial ion channels and polarization status. Mitochondrial depolarization via adenosine triphosphate (ATP)–sensitive potassium (K_{ATP}) channels in the IMM of cardiomyocytes has cardioprotective effects during ischemia and ischemia-related arrhythmia and any aberrant alteration in polarization status could predispose to arrhythmia [29,30].

In addition to CM, boys with BTHS often experience skeletal myopathy. Typical manifestations include developmental motor delays, non-progressive weakness of the lower limbs and low weight due to reduction of muscle mass [13,15]. Biopsies of affected muscles demonstrate atrophy of type I muscle fibers and increased subsarcolemmal spaces. No involvement of the diaphragm has been demonstrated. Defects in the Krebs cycle that affect anaplerosis and amino acid metabolism are thought to result in insufficient muscle protein synthesis [13].

1.1.1.2 Exercise Intolerance

Boys with BTHS are easily fatigued and exercise intolerance is a frequent complaint. Some require the use of mobility aids to conserve energy. The increased fatigability is mediated by a combination of both skeletal and cardiac impairments. O_2 extraction and utilization (determined by

measurements of hemoglobin with near-infrared spectroscopy during graded exercise tests) is reduced in the skeletal muscle of BTHS patients, which leads to increased reliance on glycolytic metabolism earlier during exercise and, consequently, premature exhaustion. Impaired cardiac contractile reserve and lower cardiac output were also evident, which is incompatible with sustained exercise [13,31]. This feature severely limits the ability of boys with BTHS to perform many of the physical activities healthy children engage in regularly.

1.1.1.3 Haematological Features

Disturbances in white blood cell counts have been detected as a recurring feature in BTHS patients, most commonly manifesting as neutropenia. An estimated 70% to 90% of patients have reported a low neutrophil count ($<1.5 \times 10^9$/L) over the course of their follow-up [11,13,16]. While a previous report had estimated neutropenia is present in only 25% of cases [15], it is important to note the intermittent nature of this symptom and that up to 30% of patients are not neutropenic at initial presentation, which could lead to failure to recognize this feature in some cases [13]. In contrast, for about 20% of cases, neutropenia, accompanied by the resulting infections, is the presenting feature [11].

Neutropenia in BTHS can be persistent, cyclical or intermittent and unpredictable. A recent study reports 31% of patients have chronic neutropenic measurements ($<1.5 \times 10^9$/L), while 9%-14% have persistent severe neutropenia ($<0.5 \times 10^9$/L) [32]. The majority of cases, however, are intermittent with no discernable pattern. Measurements can further be confounded by a developing infection, as this can cause neutrophil numbers to normalize. As is commonly seen with congenital neutropenias, BTHS patients also demonstrate compensatory monocytosis and an increase in lymphocyte numbers [11,13,32,33].

The effects of neutropenia range from mouth ulcers, inflamed gums and upper respiratory tract infections to myocarditis and sepsis on the severe end of the spectrum. A majority of patients

(60%) report experiencing mouth ulcers, sometimes recurring, while 28% report pneumonia. Septicemia is rare, occurring in only 10 – 13% of patients, however it is responsible for approximately 20% of deaths [11,16].

The exact mechanism leading to the development of neutropenia in BTHS is not completely clear, although evidence is mounting that myelocyte maturation arrest may be to blame. In their initial studies, Barth *et al* examined neutrophil function, but had no abnormal findings. Other early studies focused on the apoptotic activity of neutrophils and the possibility of increased clearance by macrophages. While neutrophils from BTHS patients do show increased annexin V binding compared to normal cells, generally considered an early sign of apoptosis, this does not translate to increased programmed cell death in these cells [34,35]. Annexin V avidly binds to phosphatidyl serine (PS), a phospholipid normally found on the cellular side of the plasma membrane, following scrambling of the cell membrane lipids during the apoptotic process. More detailed analysis, however, revealed that BTHS neutrophils do not display lipid scrambling, raising the possibility that PS in BTHS neutrophils could have a different stereometry or that annexin V is binding an as of yet unknown molecule. Kuijpers *et al* also examined other processes indicative of apoptosis, such as cellular and nuclear morphology, mitochondrial clustering, and activated caspase activity, and found no evidence that neutrophils were undergoing early or increased apoptosis. Another proposed possibility is that macrophages, which express PS-recognizing receptors on their surface, are phagocytosing neutrophils at an increased rate. Initial experiments with macrophages derived from healthy isolated monocytes indicate this is not the case [34], however, *in vitro*-derived macrophages may not be able to replicate the function and receptor expression pattern of resident tissue macrophages that are likely responsible for neutrophil clearance [35]. Van Raam *et al* suggest that the mitochondrial defects in neutrophils, which led to a decreased mitochondrial membrane potential and increased reactive oxygen species (ROS) production, ultimately result in upregulation of lipid

scramblases in the plasma membrane and, consequently, increased PS presence in the outer leaflet [35].

A competing theory is that the decrease in neutrophil numbers in BTHS is a result of defects at the level of precursor cells in the bone marrow. Neutrophils develop from the differentiation of myeloid cells, a progenitor that also gives rise to basophils, eosinophils and monocytes. Examination of bone marrow samples from neutropenic BTHS patients shows maturation arrest during the early stages of myeloid differentiation in a subset of the cases [11,32,36]. Interestingly, although monocytes come from the same cell lineage, there is often a compensatory increase in their numbers, rather than monocytopenia, indicating that the maturation arrest happens after the myeloblasts have committed to either the monocyte or granulocyte pathway. Eosinophilia has also been reported [36]. Further supporting this hypothesis, Makaryan *et al* showed that TAZ knockdown in a human myeloid progenitor cell lines (HL60), but not in lymphoid lines, leads to increased apoptosis [37]. Without a better mechanistic insight in the causes underlying this deadly symptom of BTHS, the need for a curative ERT becomes vital to reduce the mortality rates associated with it.

1.1.1.4 Metabolism

A common feature of metabolic disorders is the presence of increased levels of 3-methylglutaconic acid (3-MGCA) in urine, often along with methylglutaric acid, both of which are found only in trace amounts in the healthy population. About half of BTHS patients show this phenotype, which led to the classification of BTHS as type II 3-methylglutaconic aciduria. Similar to other clinical features of BTHS, 3-MGCA levels are not consistent, even when re-testing a patient [11,13]. The mechanism underlying the aciduria is not well known, though some have proposed that it may be a direct effect of the electron transport chain dysfunction demonstrated in BTHS, which mediates a decrease in the NADH/NAD+ ratio that, through feedback mechanisms, results in

inhibition of specific Krebs cycle enzymes and redirection of acetyl-CoA toward 3-MGCA production [38,39].

A range of other metabolic abnormalities have been documented in boys with BTHS, with various incidence rates. Most notable are low plasma arginine and carnitine levels, hypocholesterolemia, lactic acidosis, hypoglycemia and mild hyperammonemia [1,11,13,31]. The extent to which these metabolic abnormalities affect patients' lives is unknown, as most of the time these defects are rather minor, however there have been documented cases of life threatening metabolic decompensation in infants with BTHS [13,40].

1.1.1.5 Female Carriers

Women who are carriers of a TAZ mutation do not show any observable signs of the disease. This is believed to be due to skewed X-inactivation of the affected chromosome, in the range of 80:20 to >95:5, which was shown to happen almost 70% of the time, in a study of 16 carriers [41]. Members of the same family can display different levels of inactivation, suggesting additional factors may also play a role.

1.1.2 Mitochondrial Defects Associated with BTHS

Several molecular level defects are evident in BTHS derived cells and tissues. Electron microscope examination of biopsies obtained from heart and skeletal muscles of patients show mitochondria have significant structural abnormalities, appearing more fragmented, with reduced cristae alignment, and containing densely packed cristae [1,42]. Similarly, patient lymphoblasts demonstrate disorganized cristae, reduced alignment and the presence of multiple aberrant structures, likely to be abnormally packed cristae [43,44].

Lymphoblasts from patients also demonstrate reduced levels of electron transport chain (ETC) respiratory complexes and impaired ability to organize into supercomplexes, ultimately

resulting in a decrease in mitochondrial oxygen consumption rates [9,45]. These abnormalities have also been documented in patient-derived fibroblasts [8,46].

Mass spectrometric analysis revealed significant changes in the mitochondrial lipidome of both tissues and cells, with a reduction of specific forms of mature CL, most notably tetralinoleoyl CL (L4CL), an increase in MLCL and increases in phosphatydyl choline along with decreases in the levels of phosphatydyl ethanolamine. The degree of lipid profile alteration was not correlated to the severity of the disease in the patients examined [44,47]. This disconnect potentially reflects the presence of additional disease modifying factors.

1.1.1 Management and Prognosis of BTHS

There is no curative treatment for BTHS. Current treatment strategies aim to address each symptom individually with standard clinical practices. Management of LV dysfunction and heart failure is tailored to the particular cardiac phenotype exhibited by the patient. For the most commonly occurring DCM, angiotensin converting enzyme inhibitors (ACEi) in combination with diuretics and ß-blockers are a typical strategy. Digoxin and ionotoropic drugs are also considered [19]. BTHS patients respond well to these treatments, with the majority showing relatively good LV function (EF and FS values) into adulthood. For the rare cases of refractory heart failure, where the above strategies do not improve function, heart transplant is considered. Around 14% of BTHS patients underwent transplant surgery and most show good survival. Curiously, some patients spontaneously recover from severe heart failure and can be withdrawn from the transplant list [3,11,16].

Ventricular arrhythmia is addressed by placement of an implantable cardioverter defibrillator (ICD). In some cases ICDs are placed preventively, without evidence of arrhythmia, due to the documented risk of BTHS boys experiencing life-threatening cardiac arrests [3,29].

Granulocyte colony stimulating factor (G-CSF) is used in neutropenic patients to prevent infection. The treatment is used short- or long-term, depending on the nature of the neutropenia (i.e. persistent, cyclic) in each case. In addition, antibiotics are used both prophylactically and during acute infectious episodes. With few exceptions, patients respond well to these treatments [13,16].

Highest mortality is associated with the first 3 years of life, however, due to improvement in heart failure management strategies and neutropenia-associated risks, a large increase in survival rate has been seen in boys diagnosed with BTHS. Rigaud *et al* report a drastic change in survival rate, with patients born after the year 2000 having a 70% survival rate, compared to 20% survival for those born before [3,11]. Most patients succumb to heart failure (70%), while some experience sepsis or other complications [16].

Despite improvements in survival, this disorder remains deadly for a significant number of patients and cuts short the life expectancy of most. Novel therapeutic interventions are needed to improve patient quality and quantity of life.

1.2 Pathophysiology of BTHS – TAZ mutations and CL remodeling

Mutations in the gene encoding TAZ have been identified as the cause of BTHS. TAZ is a highly conserved, nuclear-encoded, mitochondrial transacylase, responsible for remodeling the phospholipid CL [48].

Over 160 mutations in the TAZ gene have been identified from Barth Syndrome patients. The mutations range from single amino acid substitutions to large deletions, insertions and truncations and they affect every exon and intron of the gene [5,49]. Intriguingly, the prognosis and severity of disease can vary from patient to patient [3,15], including patients who carry identical mutations, suggesting that other factors, aside from TAZ, may have an impact on the phenotype [14].

1.1.1 TAZ Structure and Mutations

Four TAZ isoforms have been confirmed in humans, which include a full-length transcript

containing 11 exons (FL), a transcript lacking exon 5 (Δ5), a transcript lacking exon 7 (Δ7) and a transcript lacking both (Δ5Δ7) [49]. Alternative splicing of exon 5 has only been reported in primates. Of the four transcripts, only TAZ FL and TAZ Δ5 transcripts have demonstrated enzymatic activity, with TAZ Δ5 being the predominantly expressed isoform. The exact function of the other two isoforms is not yet known, although experimental evidence suggests they are also located in mitochondria.

Although TAZ FL is only expressed in primates, complementation assays in Drosophila show that it is able to not only function and restore the phenotype in a TAZ null strain, it is the only human isoform able to rescue all aspects of the phenotype, whereas TAZ Δ5 does not restore motor function defects [49]. In contrast, TAZ FL is not able to rescue a TAZ null yeast strain, suggesting it may only be able to function in higher organisms [6,50]. The crystal structure of TAZ has not yet been resolved, however, a recent in-silico prediction model of TAZ protein structure determined the exon 5 of human TAZ FL to be an area of unstructured protrusion which does not interfere with the conformation of the rest of the protein [51]. Data from both yeast and mammalian cells show that TAZ assembles in several distinct protein complexes, ranging in size from 100-400 kD, though the identity of their members remains unknown, and at least one of these complexes fails to form in TAZ mutants [49,52]. As unstructured regions of proteins are likely to be involved in interactions with other proteins [53], it is possible that exon 5 plays a role in modulating TAZ's interactions with other protein complexes, modifying its function. This is supported by the fact that both TAZ FL and TAZ Δ5 assemble in similar complexes, however, TAZ FL seems to be more readily released by protease treatment, suggesting that it is less integrated into the mitochondrial membrane.

Biochemical studies in yeast and mammalian cells show TAZ is an integral monotopic protein, embedded into, but not protruding through, the lipid bilayer. It can embed in both the inner and outer mitochondrial membrane (I/OMM), in both cases facing the inter-membrane space (IMS),

and is also present at contact sites between the inner and outer membrane [54,55].

An *in silico* prediction model predicts that a series of positively charged, conserved, residues in human TAZ – Lysine 106, Arginine 123, Lysine 152 and Arginine 233 – constitute the substrate-binding cleft. Located behind these positive residues in the predicted structure, Histidine 69 and Asparagine 74, are suggested as the catalytic residues of the enzyme. The model also suggests a 30 amino acid-long hydrophobic region in the N-terminus of the human protein as the likely membrane-insertion domain [51]. In contrast, studies in yeast had identified a membrane-anchoring region at residues 215-232 of its 381-amino acid orthologue, Taz1p. Several sources of domain prediction had previously suggested two regions of Taz1p as potential membrane spanning regions – amino acids 26-46 and 215-232, but empirical evidence favored the C-terminus site [56]. Several BTHS-patient documented mutations reside within the orthologous region of human TAZ. Subcellular localization experiments modeling these mutations in yeast showed that the defective proteins localized to the mitochondrial matrix, rather than embed in the IMM [55,57].

Of the numerous types of mutations, yeast modeling of frameshift and splice-site mutations resulted in the expression of almost no functional TAZ. Single point mutations, by and large, result in a normally expressed and localized protein that is catalytically inactive, while some retain normal activity, but are degraded by quality control proteases [57]. The spectrum of consequences resultant from TAZ mutations would be expected to result in distinct predictable effects on biochemical and functional markers. Data from patients, however, contradicts this prediction, pointing to the possibility that TAZ-independent modulating factors affect the ultimate outcome.

1.1.2 TAZ Function and Substrates

The half-life of TAZ in mammalian cells was shown to be approximately 3 hours, which is orders of magnitude shorter that of other mitochondrial resident proteins, such as members of the electron transport chain, which have a half-life of approximately 15 days [58]. The short-lived nature

of the protein would suggest the protein is not continuously needed during normal mitochondrial function and only upregulated transiently as necessary, such as during biogenesis of mitochondrial membranes.

Previous findings show that purified fusion maltose binding protein (MBP)-TAZ can react with a wide range of different substrates and it can use a number of phospholipids and lysophospholipids as acyl donors and acceptors, respectively, to remodel monolysocardiolipin (MLCL) [48,59]. *In vitro* work shows that phosphatidyl glycerol (PG), phosphatidyl choline (PC), phosphatidyl ethanolamine (PE), phosphatidyl choline (PC) and phosphatidic acid (PA) can all be remodeled by TAZ.

The enzyme can also use multiple fatty acids for the transacylation reaction, however, the transfer rate for linoleic acid, as compared to other acyl chains, is much higher; as a result, in mammalian muscle, the most common form of mature CL is L4CL [48,60]. Furthermore, previous studies which introduced non-species specific TAZ into TAZ-deficient cells have shown that the foreign TAZ is able to remodel CL to the host-specific profile [6].

Taken together, these data suggest that TAZ is a relatively nonspecific transacylase, however, it does require a lipid membrane domain with specific physical properties in order to produce physiologically relevant CL. In vitro experiments with isolated TAZ show that the enzyme is not able to optimally operate in lipid bilayers, and instead prefers phases characterized by lower lipid packing, which is likely to promote better mixing of phospholipids and lysophospholipids. TAZ was shown to best operate at non-bilayer negative-curvature phases of the mitochondrial membrane, likely to be found at cristae junctions and at contact sites [61,62]. According to this model, the microenvironment of TAZ plays a large role in determining the molecular species pattern of CL, which implies that mislocalization of TAZ could alter the remodeling specificity.

1.2.1 Cardiolipin Remodeling and Mitochondrial Function

CL is a unique phospholipid found exclusively in mitochondrial membranes. In contrast to most phospholipid biosynthetic pathways, which are localized in the endoplasmic reticulum (ER), CL synthesis uniquely occurs in the mitochondrial matrix. Initially, PA is converted to cytidinediphosphate-diacylglycerol (CDP-DAG) by the enzyme CDP-DAG synthase. CDP-DAG can also serve as a precursor for other phospholipids. In the first step of the dedicated CL biosynthetic pathway, CDP-DAG is converted to phosphatidylglycerol phosphate (PGP) by the PGP synthase. PGP is then dephosphorylated, leading to the formation of PG. Finally, cardiolipin synthase (CLS) catalyzes the formation of CL through the condensation of PG and CDP-DAG [63,64]. In its mature conformation, CL contains four acyl chains. The acyl chain composition is the result of post-synthetic remodeling and it varies by tissue [65]. In most cases, however, cardiolipin contains only one or two dominant acyl residues, which promotes structural uniformity [66,67]. The acyl chains are typically polyunsaturated fatty acids. Three transacylases are proposed to have the ability to remodel CLs: monolyso-cardiolipin acyltransferase (MLCLAT), acyl-CoA: lysocardiolipin acyltransferase (ALCAT) and TAZ. While TAZ is accepted as the predominant remodeling transacylase [68,69], ALCAT has been postulated to catalyze the deleterious remodeling of CL that leads to the aberrant CL species found in heart disease, diabetes, and obesity [70,71].

CL is present in both eukaryotes and prokaryotes in energy producing membranes; its role, however, extends beyond bioenergetics [63]. In addition to defective mitochondrial respiration, abnormal cardiolipin species have been linked to defective mitochondrial protein import and decreased mitochondrial fusion [65,72,73]. Through its interaction with cytochrome c, CL also plays a role in apoptosis [73,74].

CL binds the electron transport chain complexes I, II and IV, as well as the ATP synthase, providing structural support [75,76]. At physiological pH, cardiolipin carries one negative charge,

and is postulated to serve as a proton trap [77]. The electron transport chain complexes are typically organized into supramolecular structures known as supercomplexes or respirasomes; in mammalian cells, they are formed by the association of complex I with two units of complex III and multiple units of complex IV [78]. Respirasomes are surmised to increase the efficiency of substrate channeling between the individual complexes. Destabilization of respirasomes is expected to result in increased electron leakage and reactive oxygen species (ROS) formation [79]. Not surprisingly, in BTHS patient-derived cells, formation of respirasomes is significantly reduced and TAZ deficient cardiomyocytes and induced pluripotent stem cells show an increase in the production of ROS which, in turn, can lead to an increase in oxidative damage to the CL acyl chains, ultimately resulting in apoptosis [80,81].

Cytochrome *c* (cyt *c*) is an electron transfer chain protein localized to the outer leaflet of the IMM; under normal conditions, only a small fraction of it interacts with cardiolipin, which is mainly located in the inner leaflet of the IMM [82]. Cyt *c* released from the mitochondria triggers apoptosis, by nucleating the formation of the so-called 'apoptosome' [83]. During apoptosis, CL relocates from the inner leaflet of the IMM to the outer leaflet, thus increasing its chances for interaction with cyt *c* [82]. The formation of a CL/cyt *c* complex causes conformational changes in cyt *c* that transform it into a CL peroxidase [84,85]; oxidized CL has much lower affinity for cyt *c*, which is subsequently released. Oxidized cardiolipin has also been linked to the formation of the mitochondrial permeability transition pore (MPTP), aiding in the escape of cyt *c* from the mitochondria. Pro-apoptotic members of the Bcl-2 family of proteins also bind CL on the mitochondrial surface [86,87].

CL provides support to carrier proteins that transport metabolites for energy metabolism from the cytosol into the mitochondrial matrix [72,88]. The adenine nucleotide transporter (ANT) and the phosphate carrier (PiC) are two members of the mitochondrial carrier family that must be

present in order for oxidative phosphorylation to take place. Together, the two provide the adenosine diphosphate (ADP) and free phosphate (Pi) required to make adenosine triphosphate (ATP). In yeast, ANT is surrounded by at least 6 CL molecules, believed to be required for its activation, although the exact mechanism by which CL activates ANT is still unclear [72,89]. PiC and the carnitine acylcarnitine translocase are other members of the mitochondrial carrier family that were shown to haven an essential requirement for CL [90,91]. These interactions intimately link CL to the transport of molecules into the mitochondria, which can serve as a rate-limiting step for oxidative phosphorylation. Biological therapies that result in CL remodeling and, consequently, improved mitochondrial function may lead to an efficacious treatment for BTHS.

1.3 Mouse Models of TAZ Deficiency

TAZ is a highly conserved gene and orthologs are present in a wide variety of model organisms, allowing study of TAZ function in organisms as diverse as yeast, drosophila and rodents. As TAZ FL is only found in primates, human TAZ Δ5 protein has the highest degree of homology to TAZs from other species. Two mouse models for BTHS have been developed – a doxycycline inducible TAZ knock-down (TAZ KD) mouse and, most recently, a TAZ knock out (TAZ KO) mouse [68,92,93].

Characterization of the TAZ KD mouse model revealed defects in cardiolipin remodeling and a reduction in oxidative capacity to various degrees as early as embryonic stage [94]. Cardiomyopathy, exercise intolerance, skeletal muscle dysfunction and neutropenia, on the other hand, hallmark perinatal symptoms in BTHS patients, manifest either late in life or not at all, in the case of neutropenia, in these mice. These mice do not demonstrate any appreciable cardiac dysfunction until the age of 8 months, and onset of skeletal muscle dysfunction was first demonstrated at 4 months of age.

Mass spectrometric analysis of cardiac and skeletal muscle from 2-month old mice shows a

redistribution of mature CL species, with more saturated species being more predominant in the TAZ KD tissues. These changes are accompanied by a reduction of L4CL and an increase in MLCL species, resulting in a significantly increased MLCL/CL ratio [68,95]. Electron micrograph examination of mitochondria in both these tissues revealed clustered aggregation of mitochondria, along with disorganized cristae and the presence of large vacuoles in the mitochondria. While these changes were obvious in skeletal muscle mitochondria from 2 month old mice, heart mitochondria appeared normal until 8 months of age [68]. Mitochondrial respiration in both primary neonatal cardiomyocytes and cardiac mitochondria of 2-month old mice is decreased, consistent with observations made in BTHS patient-derived cells [94,95].

Skeletal muscle function, tested by forced exercise on a treadmill, shows 4-month old TAZ KD mice are unable to keep up with WT littermates and closed circuit calorimetry assessments show an impairment in aerobic energy metabolism [94]. Echocardiographic measurements show development of left ventricular heart dysfunction, resulting in reduced EF and FS, at 8 months in TAZ KD mice [68].

While a useful research tool, this model is fundamentally different from the human disease in that a low level of protein is still being expressed; this could explain why mice develop pathology so late in life, whereas BTHS patients show pathology from early prenatal stages [14].

Efforts to develop a TAZ KO mouse, which would more accurately model the disease phenotype seen in patients with BTHS, have been largely unsuccessful due to infertility associated with TAZ deficiency in germ cells. Recently, however, the generation of an inducible TAZ KO mouse strain has been reported, but the degree to which it recapitulates the human phenoptype has not yet been reported [10,96]. An animal system that recapitulates the human phenotype will be useful for testing new therapeutic modalities for BTHS.

1.4 Cell Penetrating Peptides to Facilitate Intracellular Delivery of Recombinant TAZ

Intracellular delivery is crucial for many therapeutic molecules with targets inside the cell. For disorders caused by single enzyme deficiencies, such as BTHS, a recombinant protein replacement designed to easily enter cells would constitute a highly effective treatment modality. The ability to get a large molecule like TAZ across the plasma membrane, however, poses great challenges. Owing to reduced bioavailability *in vivo*, many promising candidates are not developed to their full therapeutic potential [97]. Thus, the need to find effective methods that enable the delivery of therapeutic compounds across the plasma membrane is urgent. Cell-penetrating peptides (CPPs), also referred to as protein-transduction domains (PTDs), have been widely used to facilitate the entry of proteins, small molecules, DNA and RNA into cells (reviewed in [98]). The first CPP was discovered serendipitously in the late 1980s when a group studying the human immunodeficiency virus (HIV) described the PTD of the trans-activator of transcription protein, Tat [99]. In the ensuing decades, CPPs attracted a great deal of interest for their potential in both biology research and therapy. They consist of short sequences of 8 to 30 amino acids in length that can facilitate entry of a variety of molecules into cells, including nucleic acids, proteins and synthetic drugs, usually with limited cell specificity. While multiple naturally derived sequences have been identified, a number of chimeric and synthetically designed peptides have also been generated, aiming to improve cellular uptake and provide more cellular and sub-cellular specificity. The peptides are usually classified according to their physical and chemical properties into cationic and amphipathic, or metabotropic, categories. The first two CPPs to be discovered, Tat and penetratin (a peptide derived from the drosophila homeobox protein, antennapedia, also referred to as Antp [100]), are highly cationic peptides [101]. Later work led to the discovery of peptides that carry a lower charge and are more hydrophobic in nature [102].

The ability of CPPs to deliver large cargo to the intracellular environment provides an opportunity to deliver intracellular, therapeutically active proteins, thus providing a novel platform for the development of medical treatments using molecules that had thus far been considered improbable for therapy. The work presented in this thesis is focuses on the use of CPPs to deliver recombinant TAZ intracellularly to address the need for an efficacious treatment of BTHS.

1.1.1 Mechanisms of Intracellular Delivery

The mechanisms by which CPPs promote uptake of associated molecules are influenced by the physico-chemical properties of the different penetrating peptides, the associated molecular cargo, and the variety of cells and tissues being treated. Two general models of uptake have been proposed: energy-independent direct translocation across the plasma membrane to the cytosolic compartment [103,104] and endocytosis [105,106]. Several types of endocytosis have been demonstrated for different peptides, including caveolar, clathrin-mediated and macropinocytosis[107–109]. In the case of endocytosis, the fate of the CPP-cargo complexes depends on their ability to escape the endosomal compartment before being delivered to lysosomes for degradation. It is important to note that this mechanism of cellular delivery can limit the effectiveness of CPP-based deliveries by decreasing the amount of cargo that is ultimately active and correctly targeted [110]. Results from studies conducted thus far, however, suggest that the mechanism of uptake is highly dependent on the type of cargo, making it difficult to predict which penetrating peptide should be selected in each case [111,112]. Strategies for increasing endosomolysis, thereby making more active cargo available, involve the use of pH-responsive elements, which are active in the acidic environment of endosomes without disrupting other organellar membranes. These include the addition of a short peptide derivative of the influenza virus protein hemagglutinin (INF) or the use of a synthetically designed peptide, GALA [113,114].

1.4.1 Toxicity of CPP Administration

In vitro studies on the cytotoxicity of CPPs show that cationic CPPs are less toxic and can be tolerated by the cells at much higher concentrations than amphipathic CPPs, such as transportan and model amphipathic peptide (MAP). Commonly used assays, such as cell viability, proliferation and leakage of lactate dehydrogenase (LDH) demonstrate virtually no toxic effects of Tat and penetratin. In contrast, MAP and transportan show an effect on cell viability and membrane integrity at relatively low concentrations, such as those used for intracellular delivery [115,116]. Similar results are found with more novel methods for assessing the effect of CPPs on cell function. A comprehensive metabolomics analysis comparing the effect of five different CPPs confirmed the low impact of cationic peptides, while showing that transportan can cause oxidative stress [66]. As with immunogenicity, the toxicity profile of a CPP is heavily influenced by the nature of its associated cargo, as well as the attachment site of the cargo. In the case of transportan, orthogonal attachment of cargo was shown to be significantly less toxic than N-terminal attachment [116]. This observation could be explained by a location-dependent alteration in the hydrophobicity or amphipathicity of the peptide.

Although comprehensive *in vivo* toxicity studies for CPPs are generally not available, a small number of published animal studies as well as the approval of several CPP formulations for use in clinical trials attest to the general safety of therapeutic CPP molecules at the doses studied [117–119]. One exception is a recent *in vivo* study using intravenously delivered nona-arginine (r_9), in which mice experienced immediate respiratory collapse and death [120]. At lower doses of peptide, however, mice did not develop observable long-term toxicity. In rats treated with twice-daily intranasal administration of insulin and penetratin for up to 30 days, no long-term toxicity was observed [121]. Histology studies of the nasal mucosa revealed healthy, intact membranes with no evidence of toxicity and no statistically significant evidence of increased LDH leakage. Interestingly,

when the CPPs were administered alone, there was a trend toward less leakage as when compared to co-administration with insulin. These findings support the notion that the safety of each CPP used for therapy should be determined individually, in conjunction with its associated cargo [121].

As recently noted by Verdurmen and Brock, several compounds involving CPPs have been tested in humans with no serious adverse effects [117]. KAI-9803 is a δ protein kinase C (δ PKC) inhibitor that was shown to reduce ischemia/reperfusion-related injury after myocardial infarction in animal models [122]. A subsequent clinical trial testing the safety and efficacy of the compound in humans after intracoronary administration found that the drug has an overall good safety profile, with no significant differences in clinical laboratory values between placebo and study drug and no serious adverse events, although the study was not powered sufficiently to demonstrate efficacy [123]. These studies demonstrate that it is possible to safely administer CPP constructs *in vivo* so long as careful consideration is given to potentially novel effects of conjugating a CPP to a previously untested cargo.

1.5 Enzyme Replacement Therapy for Inherited Metabolic Disorders

Congenital metabolic disorders are inherently difficult to treat, often requiring interventions that circumvent the biochemical pathway that is altered, with varying degrees of success. A class of emerging therapeutics introduces exogenous enzymes into cells deficient in those proteins. Enzyme replacement therapy (ERT) has the benefit of well-understood safety profiles when compared with gene therapies and also generally shows increased specificity compared with small molecule mimetics [124]. ERTs are commercially available for lysosomal storage diseases (LSDs) and several are in development for other inherited enzyme deficiency disorders that currently lack available treatments.

Effective ERT is already approved for some lysosomal storage disorders and this treatment modality has already been shown to reduce symptoms of Fabry's disease, through the use of agalsidase alpha and beta [125], Pompe disease, through the use of alglucosidase alpha, as well as

others. Recombinant enzyme-based therapies are also approved for use in a range of other classes of disorders, such as cystic fibrosis and collagen-based disorders [126].

Furthermore, ERTs in combination with CPPs have been successfully tested in pre-clinical models of various inherited enzyme deficiencies. Lawlor and co-workers showed that a small amount of exogenous myotubularin, a lipid phosphatase mutated in X-linked myotubular myopathy (XLMTM), linked to the 3E10Fv CPP and delivered intramuscularly, could significantly improve both local and distant muscle performance in a mouse model of XLMTM. Four intramuscular injections delivered over two weeks resulted in improvement in several parameters used to assess XLMTM, including excitation-contraction coupling and locomotion. The CPP used was thought to facilitate both local and systemic delivery when given intramuscularly [127].

Transducing cells with the CPP Hph-1 linked to an essential subunit of the phagocyte NADPH oxidase complex, which is mutated in chronic granulomatous disease (CGD), Honda and colleagues restored the ability to produce ROS in patient-derived neutrophils, a necessary function in these cells that facilitates clearing of bacterial infections [128]. Another inherited disorder with no available treatment is Friedrich's ataxia, caused by a deficiency in the mitochondrial protein, frataxin. Stemming from the deficiency is a loss of activity in iron–sulfur (Fe–S) cluster proteins that results in ataxia and lethal cardiomyopathy. Vyas *et al.* have reported on efforts to develop a frataxin-Tat enzyme replacement therapy with encouraging results in mice. *In vivo* delivery of frataxin-Taz to mice deficient in frataxin increased heart function and lifespan by significant amounts [129]. These data demonstrate that CPPs are an efficacious approach for delivering functional mitochondrial protein *in vivo* and present the possibility of protein replacement therapy for mitochondrial disorders.

Although increased expression of CL synthase (CLS) and ablation of phospholipase 2 (PLA2), which removes acyl chains from CL, were attempted as possible ways of circumventing the role of TAZ in the maturation of CL in TAZ deficient mice, these approaches were not successful in

rescuing the CL profile typically associated with deficiencies [130]. This finding underscores the importance of developing a TAZ-based treatment for Barth Syndrome. The mild phenotype of the TAZ KD mice, which still express ~5-10% of normal TAZ messenger RNA in most tissues, may reflect the minimal requirement for functional TAZ, making ERT a feasible option for BTHS.

1.6 Hypothesis and Specific Aims

Although a great deal of progress has been made in understanding the pathogenesis of BTHS, afflicted patients still succumb to this disease before middle age due to lack of an efficacious therapy. Recombinant TAZ enzyme replacement therapy that can be administered systemically, circulate and subsequently enter cells would address this unmet need for treatment in BTHS.

Hypothesis: Treatment of TAZ-deficient cells and mice will rescue the phenotypes associated with TAZ deficiency.

Aim 1: Engineer a TAZ protein sequence that includes cellular penetrating peptides (CPPs) that can enter cells and localize to mitochondria.

Aim 2: Identify the mitochondrial localization sequence for TAZ to aid in the development and optimization of enzyme therapy.

Aim 3: Characterize the effects of TAZ deficiency in tafazzin deficient models and assess the efficacy of recombinant TAZ proteins to rescue the TAZ deficiency-associated phenotypes in mammalian models of BTHS.

2 Methods

2.1 Cloning

2.1.1 Protein Expression Constructs

TAZ expression constructs were made in an N-terminal his-tag vector, pET16b (Novagen, Billerica, MA). To generate fusion proteins with cell penetrating peptides, pET16b-ANTP and pET16b-CTP vectors, 5′ phosphorylated complementary oligomers encoding a linker sequence and Antp (ESGGGGSRQIKIWFQNRRMKWKK) or CTP (SGGGSPGAPWHLSSQYSRT) motifs were synthesized (Sigma-Aldrich, St Louis, MO) [131,132]. The oligomers were annealed, then cloned into the pET16b vector at Xho I and BamHI sites. The open reading frame of mouse TAZ (mTAZ) was PCR amplified from mouse heart cDNA with primers 5′-GAACCACCTCcCCGTGCACAACAAGGAAGTG-3′ and 5′-TTCTCGAGTCTTCCAGGCTGGAAATG-3′ containing NdeI and XhoI sites.

The open reading frame of human TAZ (hTAZ) was PCR amplified from 293T cells cDNA with primers 5′- TTCATATGCCTCTGCACGTGAAGTG-3′ and 5′-TTGTCGACTCTCCCAGGCTGGAGGTG-3′ containing Nde I and Sal I restriction sites, respectively. The PCR products were cloned into either pET16b-ANTP or pET16b-CTP to generate pET16b-mTAZ-Antp, pET16b-mTAZ-CTP, pET16b-hTAZ-Antp and pET16b-hTAZ-CTP. The constructs were confirmed by sequencing (Eurofins, Louisville, KY).

2.1.2 CRISPR Constructs

To generate a plasmid for clustered, regularly interspaced, short palindromic repeat RNA-guided (CRISPR) targeting of TAZ in female rat cardiomyoblast H9c2 cells, two sets of primers for gRNA expression were used to target TAZ exon 3: 5'-TTTCAGGATCCCTACGAAAA-3' and 5'-

CTGAAGTTGATGCGTTGGTG-3' and were both cloned into pSQT1313 for the gRNA multiplex expression. Plasmid constructs were confirmed by sequencing (Eurofins, Louisville, KY).

2.1.3 EGFP-TAZ and TAZ-EGFP Constructs

The tdTomato open reading frame (ORF) was isolated by PCR from pCAG-ChromsonR-tdTomato (a gift from Edward Boyden, Addgene plasmid # 59169, [12]) and cloned into peGFP-N1 to replace the eGFP ORF. To construct expression plasmids encoding organelle-specific fluorescent markers that localize to lysosomes, peroxisomes, mitochondrial inner and outer membranes, the ORFs of LAMP2b (NP_054701.1), PXMP2 (NP_061133.1), TIMM23 (NP_006318.1), TOMM20 (NP_055580.1), and TAZ (isoform 1, NP_000107.1 and isoform 2, NP_851828.1), respectively, were isolated from 293T cell cDNA by PCR with corresponding primers. The ORFs of organelle-specific markers were cloned in-frame at the N-terminus of tdTomato at *Bgl* II and *Sal* I sites, driven by the CMV early promoter. The ORF of wild type TAZ was cloned into peGFP-N1 (Clontech, Mountain View, CA) at *Bgl* II and *Sal* I sites to generate the TAZ full length phTAZv1-eGFP and the TAZ Δ5 isoform 2 phTAZ-eGFP.

For constructing the N-terminal deletion series of human TAZ-eGFP fusion proteins, we selected endogenous codons encoding methionines as initiation codons to create in-frame fusions with eGFP at *Bgl* II and *Sal* I sites. The C-terminal TAZ deletion series were generated by PCR using hTAZ-eGFP as template and a reverse primer complementary to TAZ to create TAZ C-terminal mutations; the forward primer encoded a linker peptide (Gly- Gly-Gly) between the TAZ fragment and eGFP. The PCR products were isolated, digested with *Sal* I and ligated for transformation into STBL3 bacteria. For generating the single point mutations of hTAZ-eGFP, recombinant DNAs were generated by PCR of plasmid phTAZ- eGFP with the mutated nucleotides in primers according to the BTHS human TAZ gene variants database (Barth Syndrome

Foundation, available at http://www.barthsyndrome.org/english/ view.asp?x=1(Accessed July 15, 2017), [10]).

2.2 Cell Culture

H9c2 myoblasts and neonatal primary cardiac fibroblasts (cFB) were cultured in standard culture media: high-glucose DMEM (HyClone, SH30022.02) supplemented with 10% fetal bovine serum (FBS), 100 U/ml of penicillin and streptomycin. Cells were maintained at 37°C in a humidified atmosphere of 5% CO2. Medium was changed every 2–3 days, and cells were split once they reached 70–80% confluence.

2.2.1 H9c2 Differentiation

Differentiation of H9c2 cardiomyoblasts toward a cardiac lineage was initiated by changing the media to high-glucose DMEM with 1% FBS, supplemented with 1 μM retinoic acid (Sigma, R2625). Differentiation was continued for a period of 6 days, and the medium was changed every other day.

2.2.2 DNA Transfection

For fluorescence colocalization experiments, H9c2 cells were seeded at 25,000 cells/well on a 12 mm diameter coverslide in a 24-well plate and allowed to attach overnight. Equal amounts of plasmid DNAs, encoding mutated or full length hTAZ- eGFP and organelle-specific tdTomato, were used to transfect cells with Lipofectamine 3000 (ThermoFisher Scientific, Waltham, MA) according to the manufacturer's instructions. Cells were harvested and fixed with 4% paraformaldehyde/PBS and mounted with DAPI-Vectashield (Vector Laboratories, Burlingame, CA) or DAPI Fluoromount-G (Southern Biotech, Birmingham, AL).

2.3 CRISPR-mediated knock-out of TAZ

To generate TAZ knockout lines, a dimeric CRISPR RNA-guided FokI nuclease approach was used for genome editing [133]. In this strategy the dimerization-dependent FokI nuclease is fused to a catalytically inactive Cas9 (dCas9) to induce double stranded DNA breaks. This approach requires two separate guide RNAs in close proximity of each other on opposing strands of DNA, thereby greatly reducing the potential for off-target effects.

The H9c2 cells were plated in a 24-well plate at a density of 25,000 cells/well and transfected with 250 ng of the plasmid pSQT-rTAZ-exon3 and 750 ng of pSQT1601-FokI-dCAS9 to create indels, and co- transfected with 80 ng pIRES-hrGFP-Neo or with 120 ng pLKO-scramble for cell selection, using lipofectamine 3000 (ThermoFisher Scientific, Waltham, MA). Single colonies resistant to 500 μg/mL G418 for 7-days or 1 μg/mL puromycin for 2-days were screened by PCR with primers flanking rTAZ exon 3 in introns 2 and 3 (Table 1) which generated a 120 bp PCR product in wild type cells. To verify the TAZ alleles, the PCR products were resolved in 8% polyacrylamide (19:1 acrylamide:bisacrylaminde) in 0.5x TBE buffer. The PCR products from each colony were cloned into pJET1.2 (ThermoFisher Scientific, Waltham, MA) and

Table 2-1: Primers for CRISPR Off-Target in Rat Cardiomyocyte H9c2.

chr	Position	Off-target sequence	Primer
3	158982241	5'-CTGGAGTTGGTGTGTTGGTGAGG-3'	5'-ATCTGGGAGAAGATTTGCC-3' 5'-CAATCCAGTCATCATCCCC-3'
4	157813433	5'-TTTCAGGATGATTACGAAAAAAG-3'	5'-GCACACTTCCAGGTCTTG-3' 5'-TTCCTAGTCCTGGGGTTG-3'
4	159638475	5'-TTTCAGGATGATTACGAAAAAAG-3'	5'-GGAGGCAGAGATGTGCTC-3' 5'-GAAGTTGTGGCAGAAGG-3'
5	159545402	5'-CAGCAGCTGGTGCGTTGGTGGAG-3'	5'-GGCCCACCGGATTCCAG-3' 5'-GCGAATGTTTGCAAGACC-3'
5	170642529	5'-CTGAGGCTCATGCGTTGGTGTGG-3'	5'-CCCAGGCTCCACTTTTAG-3' 5'-GCTGGTACTCTGGGAGG-3'
7	27695381	5'-ATGAGGTGGATGTGTTGGTGAGG-3'	5'-TTATTGGCAACGTTTTAGGG-3' 5'-AGAACTCTCGATGGCCAC-3'
11	50427060	5'-TTGAAGGAAACCTACGAAAAAGG-3'	5'-AATGCAGTGCTAGCCAAG-3' 5'-CAGCAACATCATCTAGGG-3'
11	78928855	5'-TATCAGGATGCCTATGAAAAGGG-3'	5'-CAAGAACTTGACAAACATCAAC-3' 5'-CACAATTACATCTTTGAGG-3'
14	47547999	5'-TACCAAGATTCCTACGAAAATAG-3'	5'-AGATGTCATGATAATGGC-3' 5'-TTGATCCAAAATGCATAGTTG-3'
14	76188503	5'-TAGCAGGATACATACGAAAAGAG-3'	5'-TCTCCCACATCCCATGGTG-3' 5'-GCAAAGATTTGAACAGATAAATTG-3'

verified by sequencing (Eurofins, Louisville, KY). While there is no exact match for the guide RNAs used present in the rat genome, the candidate clones were further tested for the 10 most probable predicted off-targets (http://crispr.mit.edu) by PCR with 10 sets of primers (Table 2-1). All cell lines had wild type PCR products for all 10 off-target loci.

2.4 Protein Production, Purification, Concentration and Refolding

2.4.1 List of Buffers and Materials

Buffer A: 10 mM Tris, pH7.6, 1 mM EDTA

Buffer B: 50 mM Tris pH 8.0, 150 mM NaCl, 1 mM EDTA

Buffer F: 50 mM Na-PO_4, pH 8.0, 8 M Urea, 10 mM Imidazole, 2 mM TCEP

Buffer G: 50 mM Na-PO_4 pH 7.8, 6 M Guanidine-HCl, 500 mM NaCl, 2 mM TCEP

Buffer H: 50 mM Na-PO_4, pH 6.3, 8 M Urea, 20 mM Imidazole, 2 mM TCEP

Buffer E: 50 mM Na-PO_4, pH 8.0, 8 M Urea, 250 mM Imidazole, 2 mM TCEP

Buffer V: 10 mM Na-PO_4, pH 6, 0.2 M L-Arginine, 1 mM EDTA, 0.1 mM GSH, 0.01 mM GSSG, 5 mM TCEP

Lysozyme (Sigma, L-6876): 10 mg/mL in 10 mM Tris, pH 7, 1 mM EDTA

Tris(2-carboxyethyl)phosphine hydrochloride (TCEP) solution (Biosynth International, C-1818): 1 M TCEP in MilliQ water

2.4.2 Recombinant Protein Expression in E. coli

All proteins were expressed in E. coli *BL21(DE3)pLysS*, a bacterial expression strain with chloramphenicol resistance. The pET16b plasmid used to express TAZ carries an ampicillin resistance gene, so we inoculated frozen bacterial stocks in LB broth with 100 mg/l ampicillin and 32 mg/l chloroamphenicol for overnight culture. The following day, the bacterial culture was used in a ratio of 20 mL/liter to inoculate 4 – 6 L of LB with 100 mg/mL ampicillin shaking at 200 rpm, at 37 °C for 2 hours. After 2 hours, protein production was induced by adding IPTG to a final

concentration of 0.2 mM to the culture and allowed to shake at 200 rpm overnight at 20° C; this results in production of the protein in inclusion bodies (IBs).

The following day, bacteria were harvested by centrifugation at 5,000 rpm in a JA-10 rotor (Beckman-Coulter, Brea, CA) at room temperature for 10 minutes. Bacterial pellet was washed with PBS, then spun at 10,000 rpm in a JA-17 rotor (Beckman-Coulter, Brea, CA) at room temperature for 5 minutes. The bacterial pellet was weighed and resuspended in 5 ml of 5 M NaCl. Bacterial pellet was stored at -80 °C until the IB isolation.

2.4.3 Inclusion Body Isolation

Bacterial pellets were thawed on ice for 15 min, then lysed by the adding 20 ml of Buffer A, supplemented with 1 μg/ml lysozyme and allowed to incubate at room temperature for 10 minutes. DNA was sheared by sonication for four 30 second cycles, with output set to 3 on Sonic Dismembrator (Fisher, Waltham, MA). IBs were pelleted by centrifugation at 12,500 rpm at 4° C for 10 minutes (JA-17 rotor, Beckman-Coulter, Brea, CA). This step was repeated four more times. For steps 3-5, Buffer B was used and no lysozyme was added. After the final step, the supernatant was discarded and IBs were stored at - 80° C.

2.4.4 Denaturing Purification

IBs were thawed and re-suspended in 15 ml per liter of cultured bacteria in Guanidine Lysis Buffer. TCEP was added freshly to a final concentration to 2 mM. After incubating at RT for 15 min, the suspension was sonicated for 30-60 seconds, then centrifuged at 12,500 rpm, at room temperature for 10 min (JA-17 rotor, Beckman-Coulter, Brea, CA). The supernatant was filtered through a 0.45 μm low protein binding syringe filter (Millipore, Billerica, MA).

A 5 mL Cobalt resin (Pierce, Cat# 89965) column was equilibrated with 25 ml Buffer G, then the filtered protein lysate was loaded onto the column. Flow rate was set to 1 ml/min. Column was washed with 50 ml Buffer H and protein was subsequently eluted with 25 ml Buffer E. All buffers

were supplemented with 2 mM TCEP, added fresh. Eluted protein was collected in ~1.5 ml fractions. 5 µl from each fraction and mixed with 5 µl of 2x SDS sample buffer and ran on a 12% SDS-PAGE gel to determine the protein quality and quantity in each fraction. Alternatively, 1 µl of each sample was loaded onto a Nanodrop-1000 spectrophotometer (Thermo Fisher Scientific, Waltham, MA) and optical density at 280 nm (OD_{280}) was read. All protein fractions with $OD_{280} \geq 0.3$ were collected for refolding by rapid dilution at a ratio of 1:20 in Buffer V with freshly added 0.1 mM GSH, 0.01 mM GSSG and 5 mM TCEP. The protein fractions were pipetted drop-by-drop into the refolding buffer with a stir bar. Set the protein at 4 °C for overnight refolding.

2.4.5 Buffer Exchange

Amicon 30K centrifugal filters (Millipore, Billerica, MA) were equilibrated with 5 ml Buffer V. Refolded protein solution was concentrated by centrifugation in the Amicon filters at 4,000 rpm in a Sorvall Legend RT (Thermo Fisher Scientific, Waltham, MA) with a swing bucket rotor at 4° C to ~5 ml. PBS with 5 mM TCEP was then added to the protein solution and centrifuged as above until urea concentration in the solution was less than 5 mM. ¼ x volume of 100% glycerol was added to final protein solution before being aliquoted and stored at -80° C. 10 µl were used to measure protein concentration with a Bradford assay (Bio-Rad, Hercules, CA).

2.5 Crude Mitochondrial Isolation Western Blotting

H9c2 cells were cultured to confluency in 15 centimeter plates. Cells were then collected by scraping and centrifuged at 600 g for 5 minutes and the pellet resuspended in mitochondria isolation buffer (250 mM sucrose, 10 mM Tris pH 7.4, 0.1 mM EDTA). Cells were homogenized in a glass dounce homogenizer until 90% of cells showed trypan blue staining (70 strokes). Homogenates were then spun at 600 g for 10 minutes to pellet nuclei and cell debris and then at 7,600 g to pellet the crude mitochondrial fraction. The pellet was re-suspended in radioimmunoprecipitation assay

(RIPA) buffer (50 mM Tris, pH 7.4, 100 mM NaCl, 1% Triton X- 100, 0.25% SDS) with protease inhibitor cocktail (P8340, Sigma-Aldrich, St Louis, MO) added. Protein concentration was measured by Bradford assay (Bio-Rad, Hercules, CA) and 20 micrograms of protein from each sample were resolved by SDS-PAGE (10%).

Proteins were transferred onto nitrocellulose membranes, which were then probed with antibodies against succinate dehydrogenase (SDHA, MitoSciences, Cambridge, MA), ß-Tubulin (ß-Tub, Thermo Scientific, Cambridge, MA) and TAZ. For most experiments, commercially available TAZ from Sigma-Aldlrich (St Louis, MO) was used; for western blots comparing control and TAZ KO CRISPR lines, a TAZ antibody generously shared by S. M. Claypool was used [55]. The SDHA antibody was used at a dilution of 1:10,000, ß-Tub at 1:1,000, TAZ Sigma antibody was used at a dilution of 1:500 and TAZ from S.M. Claypool was used at 1:1,000. The membrane was then blotted with secondary antibodies horse anti-mouse and goat anti-rabbit IgG HRP-conjugates (Cell Signaling Technologies, both at 1:5,000 dilution). The membranes were incubated with enhanced chemiluminescence agents (Pierce) and analyzed by a ChemiDoc Image System (Bio-Rad, Hercules, CA).

2.6 Confocal Microscopy

Confocal images were taken with a 60x oil lens under a Nikon A1R confocal mounted on a Nikon TiE inverted microscope. The images are shown with maximal intensity projection of z-planes.

2.7 Mouse Models

TAZ KD mice were generated by inserting a vector containing TAZ specific shRNA under the control of the H1 of RNA polymerase III promoter and a tetracycline operator (tetO) into the *Gt(ROSA)26Sor* locus by homologous recombination. The vector also contained a constitutive

expression cassette encoding the tet repressor CAGGS-itetR. Transcription of the H1 RNA polymerase III promoter is blocked in cells expressing itetR and can only proceed in the presence of a tetracycline. The transgenic mice were initially developed on a B6D2F1 background, then backcrossed to C57BL/6J for at least 8 generations. Heterozygous *Gt(ROSA)26Sor*$^{tm37(H1/tetO\text{-}RNAi:Taz)Arte}$ (TAZ KD) mice were purchased from The Jackson Laboratory (stock # 014648).

Animals were housed at the University of Washington, which is an Association for the Assessment and Accreditation of Laboratory Animal Care approved facility, and all experiments were performed with approval University of Washington Institutional Animal Care and Use Committee.

Breeding pairs were maintained without doxycycline to maintain fertility. For experimental animals, females were started on 625 mg/kg doxycycline chow (Harlan Teklad, Indianapolis, IN) after timed mating and maintained on the chow until pups were weaned. Upon weaning, the pups were maintained on the medicated chow.

2.7.1 Genotyping

Animals were genotyped by PCR with the 5′-CCATGGAATTCGAACGCTGACGTC-3′ and 3′-TATGGGCTATGAACTAATGACCC-5′ primers to confirm presence of the the *TAZ* shRNA transgene, which yield a 381-bp product.

2.7.2 Recombinant Protein Treatment

40 or 100 μg of recombinant protein solution, or an equivalent volume of vehicle solution, were injected retro-orbitally in TAZ KD mice and WT littermates. For short protocols, mice were injected daily for 8 days and sacrificed on the 9th day. For long term protocols, mice were injected weekly, for 12 consecutive weeks.

2.7.3 Necropsy

Mice were euthanized by CO_2 asphyxiation followed by necropsy. Tissues were collected for bioenergetic assays, lipid isolation and muscle contractility assessments. Tissues collected included: heart, lungs, liver, kidneys and skeletal muscle.

For bioenergetics assays of heart, tissue was collected, weighed and homogenized immediately in respiration buffer (RB, recipe below). Typically, 4 – 5 milligrams of tissue from one heart were homogenized in 200 μl RB. For skeletal muscle, a whole soleus muscle was harvested with tendons still intact and bathed in RB while the muscle fibers were manually separated. Experiments then proceeded as detailed in the oxygraph section.

For myography experiments, whole soleus or EDL muscles with tendons still intact were collected and immediately loaded into a pre-warmed chamber. Experiments proceeded as detailed in the myography section.

2.7.4 Cardiac Fibroblast (cFB) Isolation and Treatment

TAZ KD mouse hearts from P0 pups were harvested, minced into small pieces and plated on tissue culture dishes with standard culture media supplemented with 1 μg/ml of doxycycline, to ensure continued knockdown. Fibroblasts were allowed to migrate out for 6 days, then trypsinized and each plate (containing cells from an individual heart) divided into 2-4 plates. The day after splitting, cells were treated with 5 μg/ml of recombinant TAZ protein or vehicle directly in cell culture media for 6 days, refreshing media with protein treatment and doxycycline every other day. For lipid isolation, at the end of the treatment period cells were harvested, rinsed with PBS, then resuspend in 500 ul H2O and stored at -80° C. For Seahorse mitochondrial respiration assays, after 6 days of treatment cells were trypsinized, plated on a Seahorse plate and cultured overnight with no further treatment.

2.8 Myography

Mice were euthanized immediately prior to excising the muscles, which were then introduced into the myograph chamber. Maximal length was first determined prior to assessing the optimal voltage and in turn the maximum isometric twitch force. Pulses were 450ms, with 2 min breaks in between. The maximal isometric twitch force for the extensor digitorum longus (EDL) was achieved at 120Hz and at 100Hz for the soleus. Finally the specific force for EDL and soleus muscles was calculated by normalizing to each muscle's cross-sectional area [134].

2.9 Lipid Extraction

Glass tubes and glass serological/Pasteur pipettes were used for all lipid extraction procedures. For tissue extraction, frozen tissue was immediately homogenized in 1 ml H_2O using a Dounce homogenizer (~40 strokes). For cardiac fibroblasts, frozen vials of cells were directly resuspended in 1 ml H_2O. Tetramyristoyl CL was added to all samples as an internal standard (IS) and 500 μg protein from each sample were used for lipid extraction, using a modified Folch method [135,136]. A mixture of chloroform:methanol 2:1 was added to each sample and vortexed until an emulsion formed. Separation of organic and water phase was achieved by centrifugation for 10 min at 1,000 g (RT). The lipid containing chloroform phase was extracted with a Pasteur pipette and aliquoted into a separate tube. The pellet was re-extracted and the two chloroform phases were combined and mixed with 1 ml chloroform:methanol:H_2O 1:46:47, vortexed and centrifuged for 10 min at 1,000 g (RT). Chlororform phase (bottom) was extracted, aliquoted to a clean tube and dried under a N_2 stream. Lipids were then resuspended in 50 μl chloroform:methanol 1:1 and analyzed by mass spectrometry (MS).

Table 2-2: LC protocol for mass spectrometric analysis of CL.

Time (min)	Flow rate (mL/min)	% Mobile Phase A (Methanol+ 0.1% NH_4OH)	% Mobile Phase B (Chloroform + 0.1% NH_4OH)
initial	0.2	10	90
5	0.2	10	90
15	0.2	37	63
16	0.2	37	63
16.1	0.2	100	0
17.0	0.2	100	0
17.1	0.2	10	90
25	0.2	10	90

2.10 Mass Spectrometry

Lipids were analyzed by liquid chromatography mass spectrometry (LC-MS) on an Orbitrap mass analyzer (Thermo Fisher Scientific, Cambridge, MA), using an Acquity ultra performance liquid chromatography (UPLC) pump (Waters, Milford, MA).

LC was performed on a 250mm Synchronis (Thermo Scientific, Cambridge, MA) column with a 2.1 mm diameter and 5 μm particle size using a normal phase protocol. Lists the chromatography protocol used, along with the mobile phases. Spectra were acquired in negative ion mode using selected ion monitoring (SIM) of select species.

2.11 Mitochondrial Oxygen Consumption Measurements

2.11.1 Seahorse Extracellular Flux Assays

For cardiac fibroblast respiration measurements, assay were done in a 96-well Flux Analyzer (Seahorse Biosciences, Agilent Technologies, USA). Fibroblasts treated as detailed above were trypsinized the day before an experiment and plated in a 96-well Seahorse plate at a density of 15,000 cells/well and cultured overnight. For TAZ KO H9c2 cells, assays were performed in a 24-well Flux Analyzer and cells were plated at a density of 25,000 cells/well.

The day of the experiment, plates were rinsed with assay media (XF base medium, Seahorse Biosciences, 102353–100) supplemented with 1 g/L glucose, 1 mM sodium pyruvate and 2 mM

glutamine (Sigma-Adlrich, St. Louis, MO) and placed in a 37°C incubator without CO_2 to degas for one hour before running the assay. Three different compounds, Oligomycin (final concentration 2 μM), FCCP (final concentration 1 μM for cFBs and 3 μM for H9c2s) and a cocktail of rotenone (1 μM) and Antimycin A (1 μM) were injected sequentially. Three OCR measurements were taken after each injection.

Substrate/Inhibitor	Final Conc. in Chamber	Value Recorded
Malate	2 mM	-
Pyruvate	5 mM	-
Glutamate	10 mM	LEAK
ADP	2.5 mM	Com I, Pre Cyt C
Cytochrome C	10 μM	Com I
Succinate	10 mM	Com I and II
CCCP	0.6 μl steps	Max Respiration
Rotenone	0.1 μM	Com II
Antimycin A	2.5 μM	Non Mito. Resp.

Table 2-3: SUIT protocol of oxygraph masurements of oxygen consumption.

2.11.2 Oroboros Oxygraph Assays

For hearts, 50 μl of tissue homogenized in RB buffer was directly added to the metabolic chambers, pre-warmed to 25° C.. For soleus, following manual separation of the muscle fibers, the whole muscle was incubated in permeabilization buffer (IB with 50 μg/ml saponin) for 45 while shaking, then washed with RB and added to the pre-warmed metabolic chambers, proceeding with the substrate-uncoupler-inhibitor titration (SUIT) protocol detailed below. Oxygen was added to the medium in the chambers and maintained between 300-500 nmol/ml for the duration of the experiment. Fluxes were recorded after stabilization, following the addition of each substance. The values were normalized to mg of protein per chamber and for data analysis non-mitochondrial respiration values, obtained after the addition of antimycin A, were subtracted from all other values.

Isolation Buffer (IB): 20 mM CaK_2EGTA (pH 7), 20 mM K_2EGTA (pH 7), 50 mM MES, 5.8 mM Na_2ATP, 6.6 mM $MgCl_2$-6H2O, 20 mM Taurine, 15 mM Na_2-Phosphocreatine, 20 mM Imidazole, 0.5 mM DTT

Respiration Buffer (RB): 10 mM KH_2PO_4, 20 mM HEPES, 60 mM K-MES, 3 mM $MgCL_2$-$6H_2O$, 110 mM Sucrose, 1 g/L Mannitol, 1 g/L bovine serum albumin (BSA), 20 mM Taurine, 1.5 mM EGTA

2.12 Echocardiography

Cardiac muscle function in mice was assessed using echocardiography, as previously described [137]. Mice were anesthetized using 0.5% isoflurane anesthesia and heart size and function were assessed using a VEVO 770 system (Visual Sonics, Toronto, Canada). M-mode views were analyzed for anterior and posterior LV wall thickness as well as LV internal diameter at diastole and systole. Percentage ejection fraction (%EF) and LV Mass were calculated from Visual Sonics Standard Measurements and Calculations. Fractional shortening was calculated as the difference between internal chamber sizes during systole and diastole, divided by value of diastolic chamber size.

2.13 Treadmill Running

The exercise capacity of the TAZ-deficient mice was assessed by subjecting them to a graded treadmill exercise protocol before and after tafazzin injection. All mice started by running on a treadmill for 15 minutes per day at 5-15 m/min for 3 days prior to beginning assessments. Mice then had a baseline study in which they underwent graded exercise challenge beginning at 5 m/min for 5 minutes, increasing by 5 m/min to a speed of 15 m/min, which was then held for 50 minutes, at which point a final step brought the speed to 20 m/min. The mice were kept on the treadmill until reaching exhaustion, which was defined as failure to run when prompted by a puff of air or touched with a brush. A brush was used to keep mice from going off the treadmill. After administration of recombinant TAZ (as described above), the mice underwent the graded exercise challenge again.

3 Engineering and Characterization of Recombinant Tafazzin Enzyme

TAZ is the gene responsible for Barth Syndrome and its protein product is a monotopic membrane protein. Due to the hydrophobic nature of membrane proteins, it can be difficult to purify them in significant quantities due to their tendency to form aggregates and precipitate out of solution. Several attempts have been made at purifying TAZ protein and the only successes involved either the addition of a large tag, such as maltose binding protein (MBP), the use of detergents, or a combination thereof [61,62]. Both of these methods could interfere with downstream applications. MBP protein is larger than TAZ and could interfere with its substrate interactions or activity. Detergents are difficult to remove once added to a protein solution and their presence in *in vitro* reactions could interfere with both the substrate's ability to bind TAZ and TAZ's enzymatic activity. In addition, treatment with purified TAZ of cultured cells or live animals could also be hampered by the presence of detergent. It is therefore crucial to be able to purify TAZ without the presence of a large tag or detergents in the purification process.

3.1 Development of a Novel Protocol for Recombinant TAZ Protein Induction and Purification

TAZ Δ5 is the isoform with the greatest degree of homology between humans and other species and was therefore a clear choice for expression. E. *coli* bacteria was selected as an expression system as it is an inexpensive and efficient means of producing protein.

3.1.1 TAZ Recombinant Proteins Are Engineered with C-terminal CPPs

Human and mouse wild type TAZ proteins (hTAZ and mTAZ) were cloned into a bacterial expression vector (pET16b) containing a 10-histidine (His) tag in the N-terminus of the expression construct. The His tag allows binding of the recombinant protein to a cobalt (Co) column for affinity purification. A cell penetrating peptide, either Antp or CTP, was cloned in the C-terminus of

TAZ, for both human and mouse versions of the protein. A TAZ protein with no CPP was designed as a control.

A version of TAZ that included a one amino acid substitution in the most commonly mutated residue in BTHS patients, arginine 94 to serine (R94S), was also cloned into the pET16b vector with a CTP in its C-terminus [57,138]. This mutation has been shown to render TAZ catalytically null, while still being able to localize to mitochondria [57]. This protein serves as an intracellular protein control and also informs us to any potentially dominant negative effects TAZ might have in wild type cells.

3.1.2 Optimization of TAZ Protein Induction and Purification

Protein production was achieved in BL21 (DE3) bacteria, using IPTG to induce expression. Cells were harvested by centrifugation and stored at -80° C until purification, achieved using a standard affinity chromatography protocol, as described in Chapter II. The cells were lysed using lysozyme following osmotic shock with hypo- and hypertonic solution, then centrifuged to remove cell debris. The lysate, containing the His-tagged protein was loaded onto a Co resin column. The resin was washed with a buffer containing a low concentration of 20 mM of imidazole to remove non-specifically bound proteins and the recombinant protein was eluted with a high concentration of 250 mM imidazole. The eluate was collected in 1.5 ml fractions which were then resolved on an SDS-PAGE gel. This determined the purity of the obtained protein, as well as the quantity of protein in each fraction. The fractions containing the highest amount of protein were then rapidly diluted in a ratio of 1:20 in refolding buffer, then concentrated and buffer exchanged to PBS with 20% glycerol, in order to eliminate denaturing reagents and imidazole from the final protein solution. Protein concentration was measured in the final solution using the Bradford assay.

Initial attempts at inducing soluble recombinant protein in *E. coli* and performing native purification did not result in a measurable protein yield, indicating the protein was likely forming

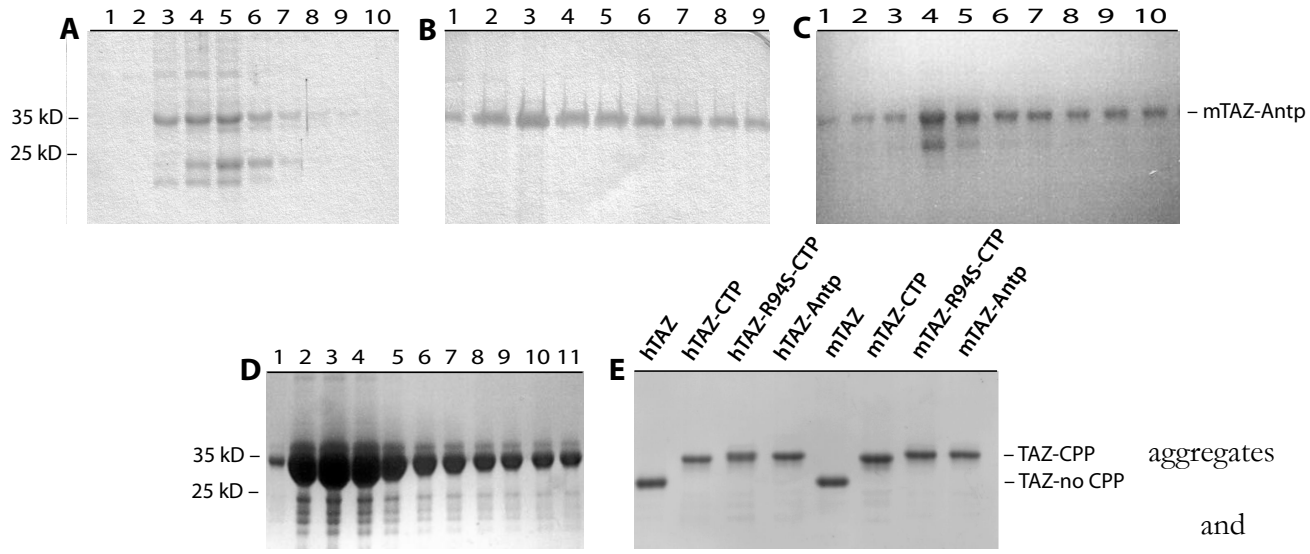

Figure 3-1: TAZ protein is prone to forming aggregates and induction in inclusion bodies results in the highest yield of protein. **(A-D)** Elution fractions of affinity chromatography purified TAZ, using different protocols for purification, as described in the text. **(E)** Equal amounts of purified mouse and human TAZ protein with different CPPs.

precipitating out of solution. To overcome this, urea was added to the lysis buffer as a denaturing agent. While denaturation kept some of the protein soluble, it still resulted in a very small yield of protein (Figure 3-1, A). In an attempt to keep the protein from aggregating, different induction protocols, as well as detergents and reducing agents were used.

A change in the amount of IPTG used for bacterial protein induction, from 1 mM to 0.5 mM for 2 hours at room temperature (RT) led to a small increase in yield of purified protein (data not shown), which suggested that inducing large quantities of this membrane protein in a relatively short amount of time is likely toxic to bacteria. To further improve yield, 10% TritonX-100 and 10 mM DTT were added during the lysis process, which resulted in better yield and purity (Figure 3-1, B). Switching from 8 M urea to 6 M guanidine as a denaturing reagent improved protein yield, but only incrementally (Figure 3-1, C). Addition of sodium chloride or substitution of different detergents generally resulted in a slight decrease in the amount of purified protein (data not shown).

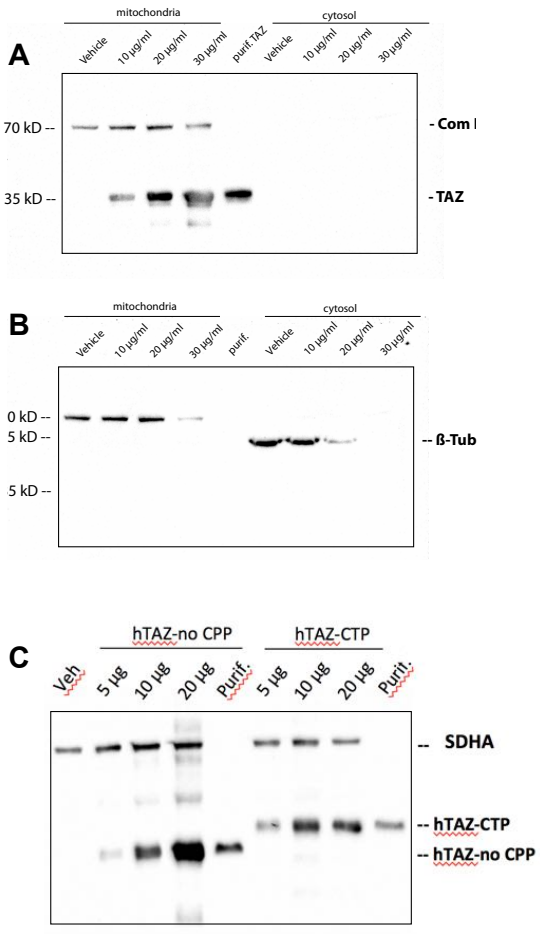

Figure 3-2: CTP promotes cellular uptake of TAZ protein. **(A)** Immunoblot of mitochondrial and cytosolic fractions isolated from H9c2 cells treated with vehicle or 3 doses of hTAZ-CTP. Membrane was probed with antibodies against SDHA and TAZ. **(B)** Same immunoblot as in (A), re-probed with antibody against ß-tubulin. **(C)** Blot of mitochondrial fractions from cells treated with vehicle or 3 doses of hTAZ or hTAZ-CTP. Probed with antibodies against SDHA and TAZ.

As the previously described conditions are quite harsh and likely to dissociate most protein aggregates, this indicated that the protein induction step might be the limiting factor in the final protein yield. To address that, a protocol for induction of protein in inclusion bodies was developed, as this would limit the level of toxicity the overexpressed protein has on the bacteria. This was done using low amounts of IPGT (0.2 M) and inducing overnight at 20° C. After osmotic shock lysis of the cells, inclusion bodies were purified by sequential sonication, centrifugation and wash steps, as detailed in the Methods section. Finally, the purified inclusion bodies were solubilized with a 6 M guanidine buffer and purification proceeded with affinity chromatography. Additionally, TCEP, a reducing agent that is more stable than DTT, is active over a wider pH range and does not interact with cobalt in the resin, was substituted for DTT during purification and refolding. These changes led to a significant increase in protein yield (Figure 3-1, D). Bradford assay quantification revealed final concentrations in the 2 – 3 mg/ml range, whereas previous protocols yielded a maximum of 0.1 – 0.3 mg/ml. Although developed using

mTAZ-Antp, this purification protocol resulted in successful purification of significant protein amounts of all the recombinant proteins we designed (Figure 3-1, E).

3.2 Cellular Uptake and Mitochondrial Localization of Recombinant TAZ

Previous studies have shown that CPPs are able to promote entry of proteins into cells, however this ability is cargo specific. The ability of Antp and CTP to facilitate uptake into cells of purified TAZ recombinant protein was, therefore, tested in cultured myoblasts. Cells were treated with protein by administration of the protein solution directly into the standard cell culture media.

3.2.1 Dose Response and Subcellular Localization of Recombinant TAZ

To verify that recombinant TAZ containing a CPP undergoes cellular uptake and localizes to mitochondria, H9c2 cardiomyoblasts were treated with 3 different doses of hTAZ-CTP or vehicle for 48 hours. Cells were then harvested and cellular fractionation was performed, as described in Chapter II. As a control condition, cells were similarly treated with hTAZ with no CPP.

Crude mitochondrial and cytosolic fractions, along with purified TAZ protein, were analyzed by SDS-PAGE and subsequently immunobloted, then probed with antibodies against TAZ, as well as SDHA and ß-Tub, mitochondrial and cytosolic markers, respectively. A 35 kD band corersponding to hTAZ-CTP was detectable in mitochondrial, but not cytosolic fractions after 48 hours of continuous treatment (Figure 3-2, A and B). An increase in TAZ signal was seen with increasing doses of purified protein treatment, indicating dose-dependent uptake. A 70 kD band was evident in the mitochondrial fraction, which corresponds to SDHA, a part of ETC Complex II (ComII). A 55 kD band corresponding to ß-Tub was not detectable in the mitochondrial fraction, but was detected in the cytosolic fractions, as expected.

Surprisingly, H9c2 cells treated with hTAZ protein containing no CPP also demonstrated uptake of the protein in a dose dependent fashion, as evidenced by a 28 kD band on the immunoblot (Figure 3-2, C), suggesting that hTAZ may contain an intrinsic CPP.

3.2.2 Time Course of Treatment

To determine an optimal length of treatment, a time course was performed by treating cells with 10 μg/ml of hTAZ-CTP for various lengths of time, ranging from 0 to 48 hours. Cells were treated at the same time and then harvested at different time points, followed by cellular fractionation and analysis by SDS-PAGE and WB. No uptake was evident at 0 hour, a control condition where cells were harvested immediately after protein administration, but TAZ protein was detected as early as 2 hours after treatment (Figure 3-3, A). Under these conditions, protein uptake peaked at 12 hours of treatment, but further fine-tuning revealed an increase in uptake up to 16 hours of treatment (Figure 3-3, B). Despite continuous treatment, levels of TAZ in mitochondria decline by the 48 hours time point.

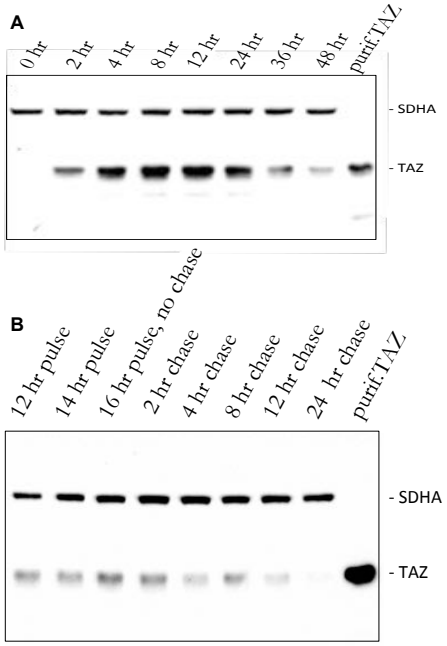

Figure 3-3: Protein uptake kinetics in H9c2 cells. **(A)** Blot of mitochondrial fractions from cells treated with 10 μg/ml hTAZ-CTP for different pulse times. **(B)** Immunoblot of mitochondrial fractions from cells pulsed with 10 μg/ml hTAZ-CTP for 12, 14 and 16 hours and then chased for 0-24 hours. Both blots probed with antibodies against SDHA and TAZ.

3.2.3 Time Course of Degradation

To determine how long protein persists in the cells after the removal of treatment, a pulse-chase experiment was performed. H9c2 cells were treated with 10 μg/ml of hTAZ-CTP for 16 hours, after which the protein containing media was replaced with fresh media. Cells were returned to the incubator and harvested at different time points, followed by immediate cellular fractionation. Immunoblot analysis of the mitochondrial fractions shows that recombinant TAZ starts diminishing by 4 hours post removal of treatment and is almost undetectable at 24 hours (Figure 3-3, B).

3.2.4 Conclusions and Discussion

The results in this chapter detail a new protocol for purifying TAZ with only a His-tag in the N-terminus and demonstrate the ability of the recombinant TAZ to enter cells.

Previous work from other groups has shown that TAZ is a membrane protein prone to aggregation rendering it difficult to purify to homogeneity without bulky attachments.

A commonly encountered problem with membrane proteins is that overexpression can be toxic for the host cells, because the proteins need to insert into membranes, however the availability of these structures is limited. Bacteria can circumvent this problem by packaging the overexpressed protein in dense aggregates known as inclusion bodies. Recombinant TAZ expression in inclusion bodies resulted in a significant increase in the amount of induced protein compared to soluble expression.

Recombinant TAZ was designed to contain a cellular penetrating peptide in the C-terminus, in order to facilitate cellular uptake. Unexpectedly, however, TAZ without a CPP also exhibited uptake into cells. One explanation would be that TAZ contains an endogenous CPP and its mitochondrial localization signal is one candidate. Another possibility is that the His tag in the N-terminus of the recombinant protein is facilitating uptake. Both mitochondrial targeting sequences and His tags are positively charged and share similar motifs to CPPs [101].

hTAZ-CTP is detectable in mitochondria 2 hours after treating cells and peaks after 16 hours of continuous treatment. Interestingly, although the protein is still detectable after 48 hours of continuous treatment, the levels detectable in mitochondria are lower than at 16 hours. Removing recombinant protein from the cell culture media results in rapid loss of signal with only small amounts of protein detectable 24 hours after removing treatment. As protein is still detectable after 48 hours of continuous treatment, it is unlikely the recombinant TAZ is subject to degradation in the media. The loss in signal in both cases may be a sign that mitochondria are rapidly degrading the

exogenous TAZ in an attempt to remove excess protein, which correlates with reports that TAZ half-life is much shorter than that of other mitochondrial proteins (approximately 3 hours) [58]. It should be noted that the published report measured degradation of endogenously expressed protein, while the present study measured the degradation of exogenously administered purified TAZ, which may explain the difference in observed values. It is unclear why TAZ half-life is considerably shorter than that of other mitochondrial proteins, but it tempting to speculate that high levels of the protein could be deleterious for cells. When over-expressed in insect cells, TAZ formed homodimers, a behavior not observed at endogenous levels. The protein was also shown to associate with multiple protein complexes in a relatively non-specific manner. Overexpression altered the distribution of the protein, from larger complexes towards smaller ones, lending credit to the idea that unregulated levels of TAZ may negatively impact its role in mitochondria [58].

4 Identification of Novel Mitochondrial Localization Signals in Human Tafazzin

It has been postulated that TAZ activity is promiscuous and the observed specificity of its action is conferred by the restraints of the membrane space where it is most active [62]. As CL is only synthesized in mitochondria, correct targeting of TAZ is critical in order for CL to undergo its final step of remodeling. Previous work in yeast has identified a 28 amino acid peptide in the C-terminus of the TAZ is necessary for mitochondrial targeting. However, the exact mitochondrial targeting sequence for human TAZ is yet unknown [139].

This chapter investigates the internal sequences that are responsible for targeting TAZ to the mitochondria. Using various regions of TAZ fused with eGFP, two distinct fragments were identified that were capable of localizing to mitochondria independently, but only with eGFP placed at the C-terminus. TAZ (84-95) confers exclusive targeting to mitochondria of eGFP, while TAZ (185-220) results in partial targeting, along with other subcellular compartments.

4.1 TAZ Fusion Constructs Expressing eGFP in the N-terminus Fail to Localize to Mitochondria

To locate TAZ's mitochondrial localization signal, constructs containing TAZ fragments spanning the length of the protein fused to eGFP were designed (detailed in schematic in Figure 4-1, A). The fragments were designed taking into account the predicted function of the different domains of TAZ [51]. In order to ensure uniform expression, eGFP was first cloned in the N-terminus of TAZ and expression was verified in HEK 293 cells. Lysates of cells transfected with eGFP-TAZ fragment constructs were analyzed by SDS-PAGE and immunoblot and subsequently probed with antibodies against GFP and TAZ. All the constructs were expressed and showed the expected molecular weight when probed with an antibody against GFP. eGFP with hTAZ Δ5, designed as a control construct, showed lower expression than the others, but showed a robust signal when the blot was probed with an antibody against TAZ (Figure 4-1, B).

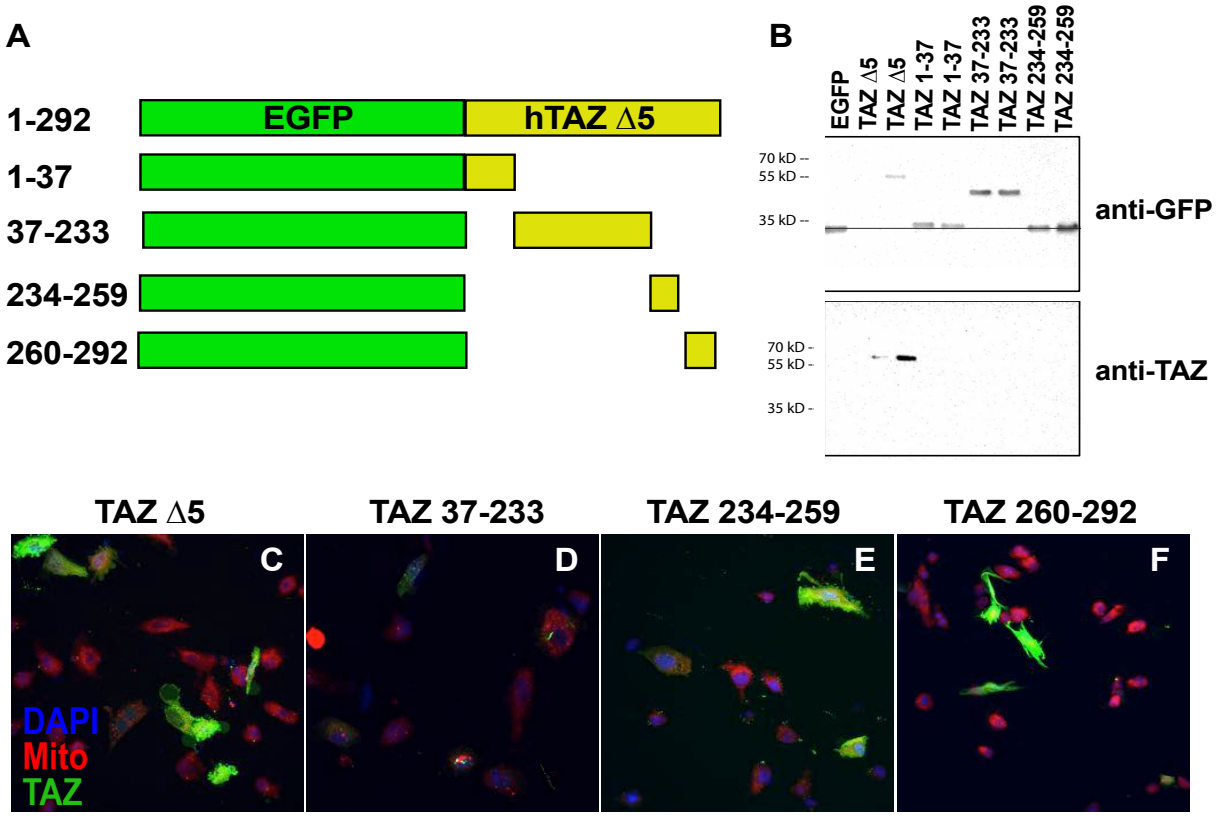

Figure 4-1: eGFP-TAZ constructs do not localize to mitochondria. **(A)** Schematic of eGFP-TAZ constructs, listing the amino acids of TAZ expressed in each construct. **(B)** Immunoblots of HEK 293 cells transfected with eGFP-TAZ constructs. WBs were probed with antibodies against GFP (top panel) and TAZ (bottom panel). **(C)** Confocal images of H9c2 cells transfected with eGFP-TAZ constructs. Blue – DAPI nuclear stain, Red - the mitochondrial dye, MitoTracker Red, Green – antibody against TAZ.

To determine the ability of TAZ with an N-terminus eGFP protein to localize to mitochondria, H9c2 cells were transfected with the fusion constructs, stained with an antibody against TAZ and colocalization with the mitochondrial dye Mitotracker Red was ascertained by confocal microscopy. Wild type TAZ with an eGFP protein in its N-terminus was not able to correctly localize to mitochondria and appeared to have a cytosolic distribution instead (Figure 4-1, C). Unsurprisingly, none of the other fusion constructs tested localized to mitochondria (Figure 4-1, D-F). These data indicate eGFP can interfere with the mitochondrial localization signal of TAZ when cloned in the N-terminus.

4.2 Full Length TAZ with C-terminus eGFP Localizes to Mitochondria

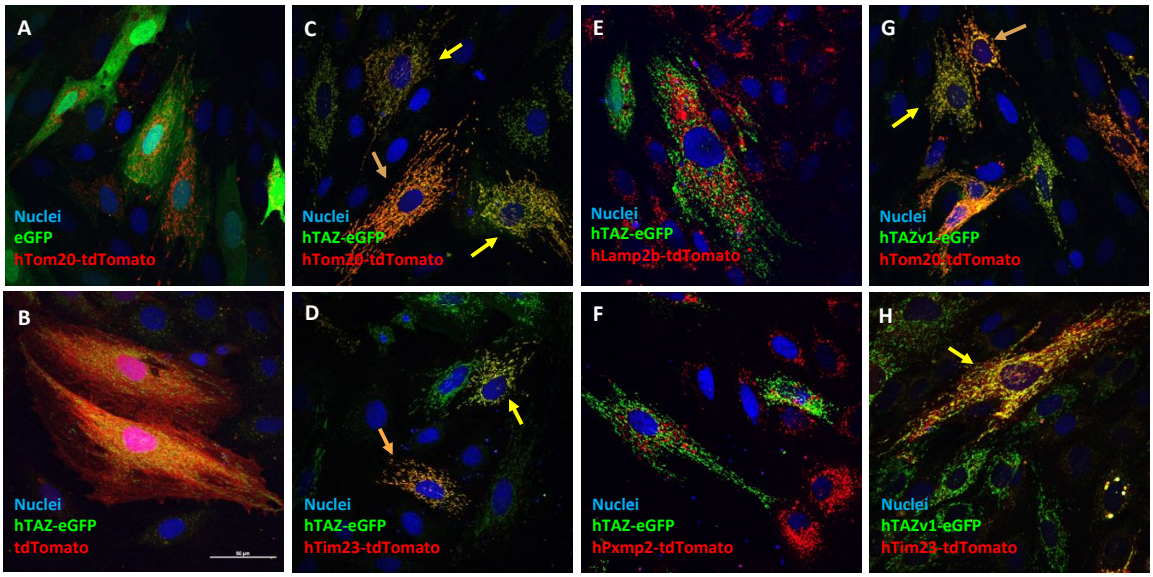

Figure 4-2: Mitochondrial localization of human tafazzin isoforms in rat cardiomyoblast H9c2 cells. The H9c2 cells were transfected with eGFP and tdTomato native and fusion protein expression plasmids and fixed with 4% paraformaldehyde 24 hours after transfection and photographed with a confocal microscope with a 60x oil objective lens. The maximal intensity projection of z-stack images are shown for the co-expression of hTAZ isoform 1 and 2 with organelle markers. A. eGFP and mitochondrial outer membrane marker hTom20-tdTomato, B. TAZ isoform 2 hTAZ-eGFP and tdTomato, C. hTAZ-eGFP and mitochondrial outer membrane hTom20-tdTomato, D. hTAZ-eGFP and hTim23-tdTomato, E. hTAZ-eGFP and lysosomal hLamp2b-tdTomato, F. hTAZ-eGFP and peroxisome hPxmp2-tdTomato, G. TAZ isoform 1 hTAZv1-eGFP and hTom20-tdTomato, H. hTAZv1-eGFP and hTim23-tdTomato. Cells showing mitochondrial localization of hTAZ-eGFP with mitochondrial markers are indicated by yellow arrows and cells in which tdTomato is more strongly expressed are indicated by orange arrows. All images were taken with a 60 x oil lens and the white bar in panel B represents 50 μm.

Initial efforts to colocalize TAZ-eGFP fusion proteins with MitoTracker Red dye were unsatisfactory, due to bleeding of red signal into other organelles that likely resulted from toxicity (data not shown). To investigate further the TAZ mitochondrial localization signal, organellar marker-tdTomato fusion proteins and TAZ-eGFP fusion protein were co-expressed. Control studies with

eGFP or tdTomato alone did not affect Tom20 or TAZ-eGFP fusion protein localization to mitochondria (Figure 4-2, A and B). A previous study reports that TAZ protein is embedded in mitochondrial membranes, facing the intermembrane space [14]. Both TAZ isoforms tested, the 292 amino acid TAZ full length isoform 1 and the 262 amino acid TAZ Δ5 (isoform 2), localized to

mitochondria when co-expressed with the fusion proteins Tim23-tdTomato and Tom20- tdTomato, mitochondrial markers of the inner or outer membrane, respectively (Figure 4-2, C, D, G and H). These data are consistent with a previous report using HA-tagged TAZ [49]. Neither TAZ variant-eGFP fusion protein colocalized with peroxisomes or lysosomes when co- expressed with the organelle-specific markers PXMP2- and LAMP2b-tdTomato fusion proteins, respectively (Figure 4-2, E and F, data not shown). In agreement with previous studies, exon 5 does not affect the mitochondrial localization of TAZ [49]. We therefore used isoform 2 to investigate the amino acid sequences necessary for mitochondrial localization, however, amino acid numbers and mutation

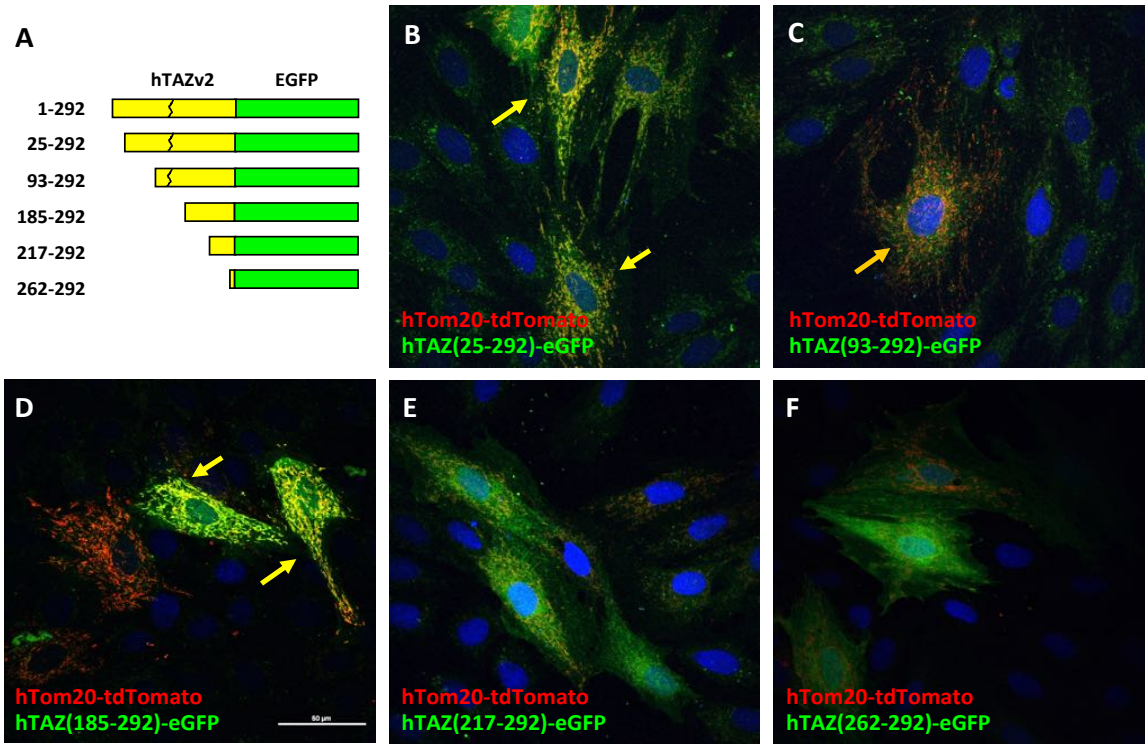

Figure 4-3: Mitochondrial localization of hTAZ isoform 2 serial N'-terminal deletion mutants. **(A)** Schematic diagram of hTAZ isoform 2 serial N'-terminal deletion mutants, which have no exon 5 encoding amino acids 124-154 (broken line). The amino acid numbers assigned by the full length hTAZ isoform 1 are listed on the left of each mutated TAZ fusion protein. The endogenous methionines in hTAZ were selected as initiation codons to create in-frame fusion proteins with eGFP. The maximal intensity projection of z-stack confocal images are shown for the mitochondrial outer membrane marker hTom20- tdTomato with hTAZ mutants **(B)** hTAZ(25-292), **(C)** hTAZ(93-292), **(D)** hTAZ(185-292), **(E)** hTAZ(217-292), and **(F)** hTAZ(262- 292). All images were taken with a 60x oil lens and the white bar in panel D represents 50 µm

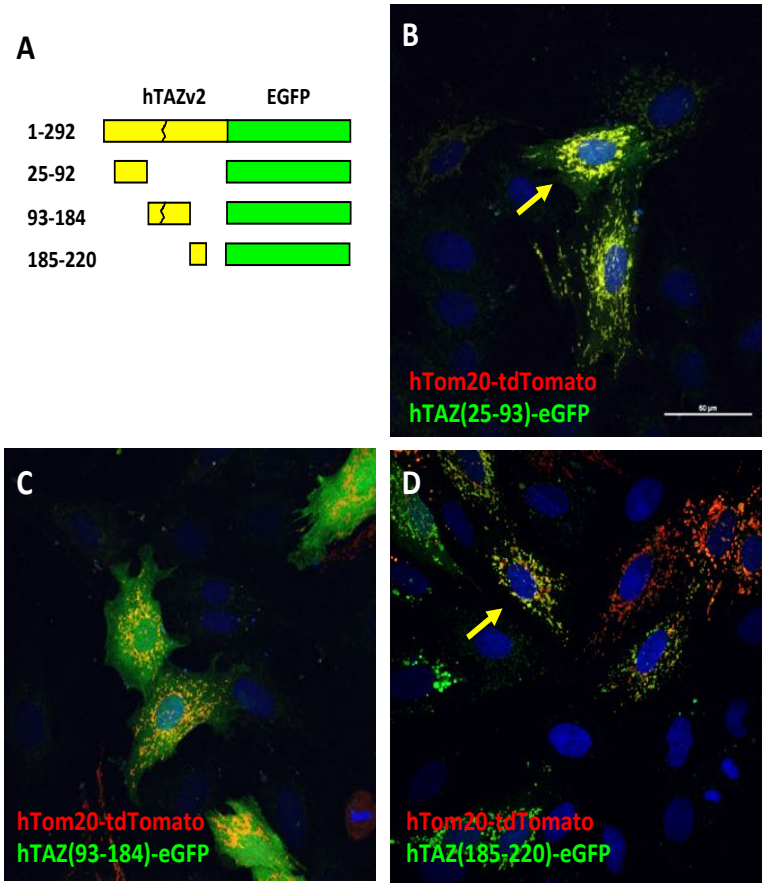

Figure 4-4: Mitochondrial localization of hTAZ isoform 2 subfragments. **(A)** Schematic diagram of hTAZ isoform 2 subfragments fused to eGFP. The peptide sequence gly-gly- gly was inserted as a linker at the C'-terminal TAZ deletion site when needed to create an in-frame fusion protein with eGFP. The maximal intensity projection of z-stack (0.2 mm x 6 slices) confocal images are shown for the mitochondrial outer membrane marker hTom20-tdTomato with hTAZ mutants **(B)** hTAZ(25-92), **(C)** hTAZ(93-184), and **(D)** hTAZ(185-220). All images were taken with a 60 x oil lens and the white bar in panel B represents 50 µm

positions are in accordance with isoform 1 length, as described in the BTHS human TAZ gene variants database (Barth Syndrome Foundation, available at http://www.barthsyndrome.org/english/ view.asp?x=1(Accessed July 15, 2017), [10]).

4.3 Mitochondrial Localization of N- and C-terminus truncated TAZ fragments

To identify TAZ mitochondrial localization peptides, we made a series of N- and C-terminus deletions of TAZ, in-frame with eGFP at the C-terminus. For N-terminus deletions, the TAZ mutants were translated from endogenous methionines at M25, M93, M185, M217, and M262 as start codons (Figure 4-3, A). The N-terminus deletion mutants TAZ (25-292) and TAZ (93-292) showed strong mitochondrial localization (Figure 4-3, B and C), whereas TAZ (185-292) showed partial mitochondrial signal, along with some cytosolic signal (Figure 4-3, D). Both TAZ (217-292) and TAZ (262-292) showed cytosolic signal only (Figure 4-3, E and F), suggesting a potential mitochondrial targeting sequence between amino acids 185 and 217.

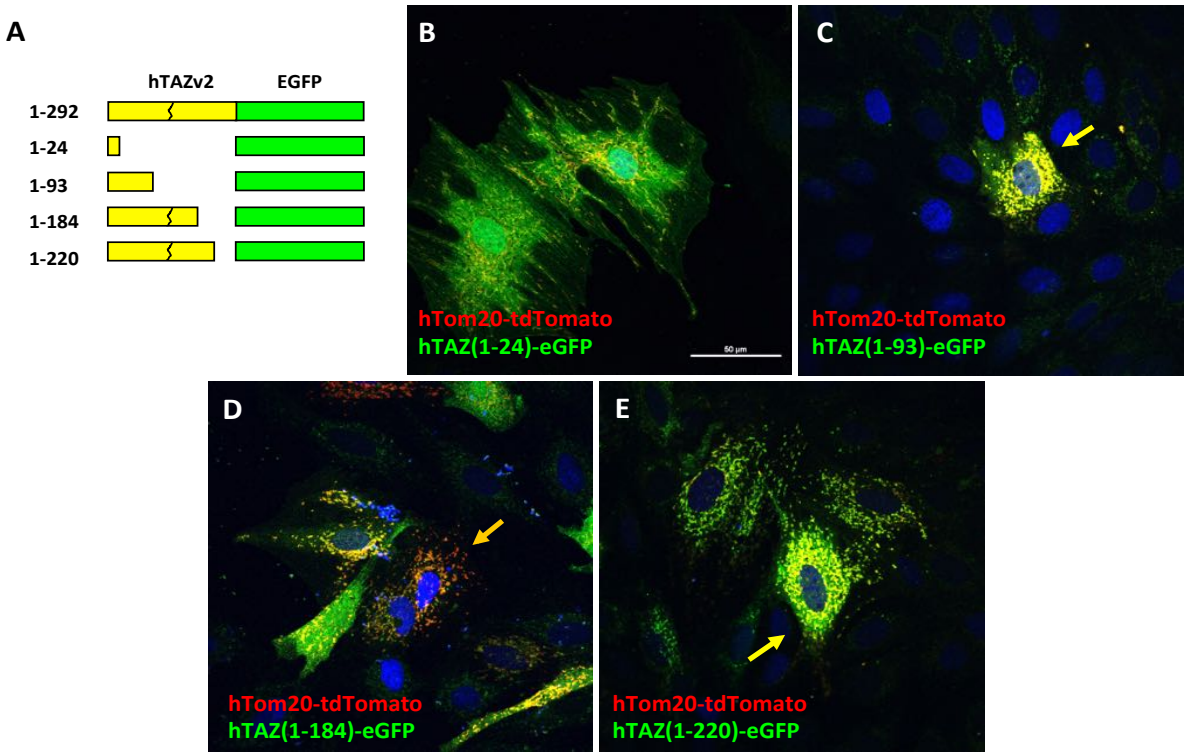

Figure 4-5: Mitochondrial localization of hTAZ isoform 2 serial C'-terminal deletion mutants. **(A)** Schematic diagram of hTAZ isoform 2 serial C'-terminal deletion mutants, which have no exon 5 encoding amino acids 124-154 (broken line). The amino acid numbers assigned by the full length hTAZ isoform 1 are listed on the left of each mutated TAZ. The peptide sequence gly- gly-gly was inserted as a linker at the C'-terminal TAZ deletion site in each clone to create an in-frame fusion protein with eGFP. The maximal intensity projection of z-stack confocal images were are shown for the mitochondrial outer membrane marker hTom20-tdTomato with hTAZ mutants **(B)** hTAZ(1-24), **(C)** hTAZ(1-93), **(D)** hTAZ(1-184), and **(E)** hTAZ(1-220). All images were taken with a 60 x oil lens and the white bar in panel B represents 50 µm.

We also investigated four TAZ C-terminus deletions (Figure 4-5, A). TAZ (1-24) showed cytosolic eGFP signal (Figure 4-5, B), whereas both TAZ (1-93) and (1-220) showed mitochondrial localization (Figure 4-5, C and E). TAZ (1-184) showed some mitochondrial localization, but also significant cytosolic signal (Figure 4-5, D). These results indicated that a TAZ mitochondrial localization signal lies between amino acids 25 and 220. Since both TAZ (1-93) and TAZ (185- 292) showed some mitochondrial localization, we investigated whether TAZ contains two mitochondrial localization signals: one in between amino acids 25-93 and the other between amino acids 185-220.

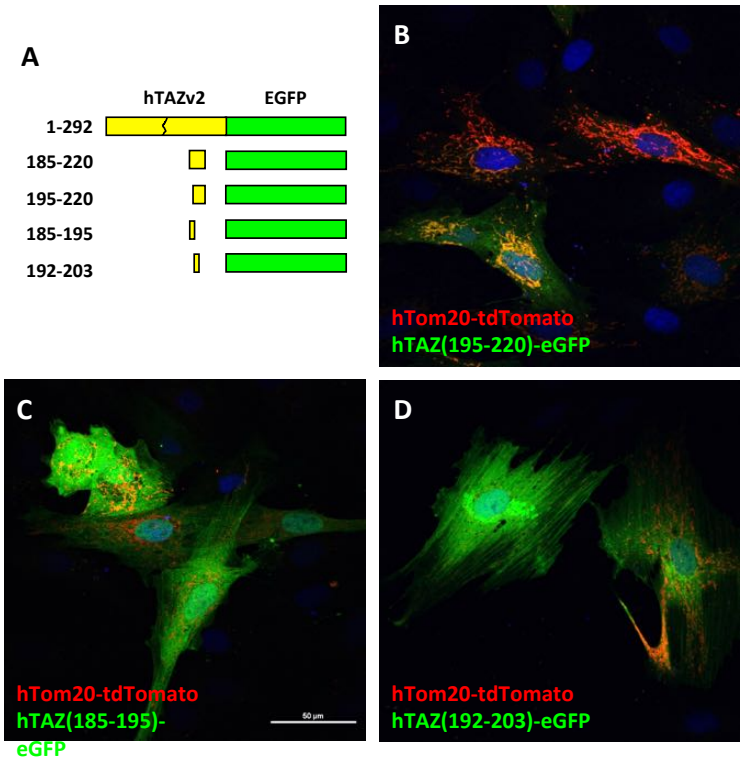

Figure 4-6: Mitochondrial localization of hTAZ isoform 2 subfragments derived from hTAZ(185-220). **(A)** Schematic diagram of hTAZ isoform 2 subfragments derived from hTAZ(185-220) fused to eGFP, which contain amino acids encoded from part of exon 7 (185-194) and entire exon 8 (195-215) and part of exon 9 (216-220). The peptide sequence gly- gly-gly was inserted as a linker at the C'-terminal TAZ deletion site to create an in-frame fusion protein with eGFP. The maximal intensity projection of z-stack (0.2 mm x 6 slices) confocal images are shown for the mitochondrial outer membrane marker hTom20-tdTomato with hTAZ mutants **(B)** hTAZ(195-220), **(C)** hTAZ(185-195), and **(D)** hTAZ(192-203). All images were taken with a 60 x oil lens and the white bar in panel C represent 50 μm.

4.4 TAZ contains two distinct and independent mitochondrial targeting peptides

To identify the possible mitochondrial localization signals in TAZ, we isolated the fragments encoding amino acids 25-92, 93-184, and 185-220 to generate plasmids encoding fusion proteins with eGFP (Figure 4-4, A) and co-transfected these plasmids with the hTom20-tdTomato plasmid into H9c2 cells. Both TAZ (25-93) and TAZ (185-220) showed mitochondrial localization, with some cytosolic signal (Figure 4-4, B and D). TAZ (93-184) localization is primarily cytosolic with a small fraction of signal present in mitochondria (Figure 4-4, C). These results indicated that TAZ possesses two mitochondrial localization signals and each can function independently.

4.5 Fine mapping of essential TAZ fragments that confer mitochondrial localization

We further dissected the TAZ (185-220) into three smaller fragments: 185-195, 195-220 and 192-203 and generated eGFP fusion proteins (Figure 4-6, A). Interestingly, all of these smaller

fragments were unable to direct the fusion protein to the mitochondria and were found only in the cytosol (Figure 4-6, B, C, and D). These results indicated that the amino acids 185-220 are undividable and necessary for mitochondrial localization.

To narrow down the essential amino acid sequence required for mitochondrial localization, the TAZ (25-93) fragment was divided into smaller fragments (**Figure 4-7**, A). Co-localization of hTom20-tdTomato and mutated TAZ fragment–eGFP proteins were analyzed in H9c2 cells by confocal microscopy. The N-terminus of this TAZ fragment, amino acids 37-80, which is encoded by exon 2, was mostly in the cytosol (**Figure 4-7**, B). A computer predicted helix structure [51] spanning amino acids 46-57 within this fragment does not confer mitochondrial localization (**Figure 4-7**, C). In contrast, the other computer predicted helix (GOR4) at the C-terminus of this fragment, spanning amino acids 80-95, clearly possesses a mitochondrial targeting peptide (**Figure 4-7**, D). To shorten the minimal amino acid sequence required to lead to mitochondrial localization of eGFP, we further narrowed down the sequence to: 82-95, 84-95 and 80-92. All three of these fragments still directed eGFP to mitochondria (**Figure 4-7**, E, F, and G). We attempted to further reduce the fragment, however, amino acid sequence 82-92 was unable to localize to mitochondria (**Figure 4-7**, H). Taken together, our results indicate that this region of TAZ contains an independent peptide responsible for mitochondrial localization, but the borders of this peptide appear to be inexact, which may be explained by secondary structure requirements. A basic local alignment search tool analysis against known proteins in the National Center for Biotechnology Information database (BLASTP) for the peptide sequence encompassing amino acids 80-95 revealed no homology to any known proteins other than tafazzin, demonstrating the novelty of this mitochondrial localization sequence (data not shown).

4.6 Mitochondrial localization of TAZ-eGFP fusion proteins containing Barth Syndrome missense mutations

Barth Syndrome missense mutations are located throughout the TAZ gene. To investigate whether known missense mutations in the identified localization peptides encoded by exon 3 or exon 8 would affect TAZ localization, we engineered selected TAZ mutations into the mitochondrially localizing eGFP fusion proteins and assessed their localization. We investigated the TAZ Barth Syndrome mutations located in exon 8 by introducing these mutations into the full length hTAZ-eGFP fusion protein (**Figure 4-8**, A). One of the hot spots for TAZ mutations is at G197. However, TAZG197R mutation does not affect mitochondrial localization. Similarly, the other mutations in exon 8, I209N, L210R, L212P, and H214R, also do not affect mitochondrial

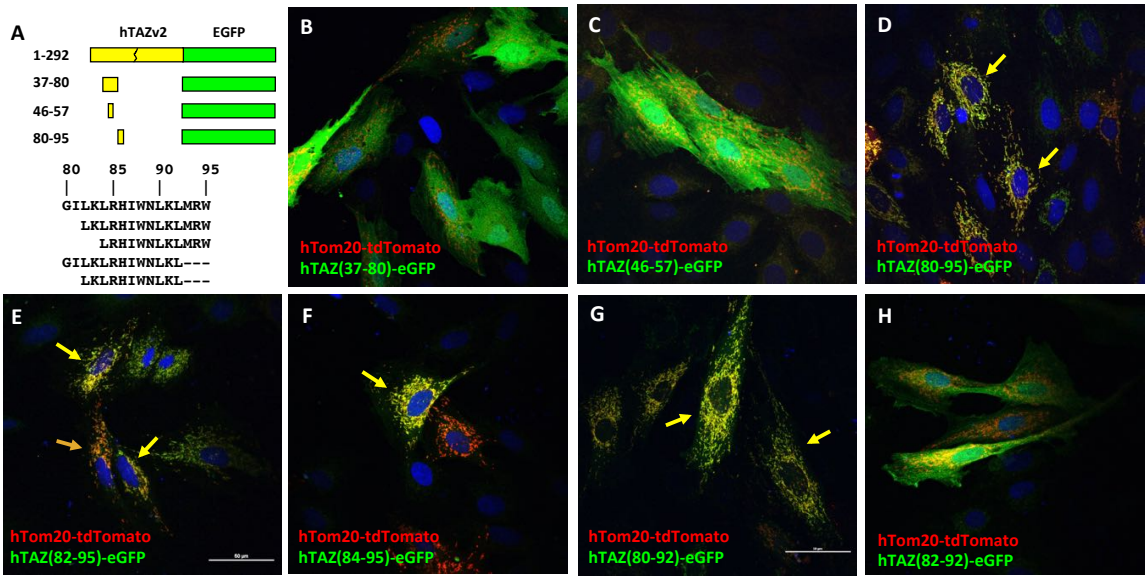

Figure 4-7: Mitochondrial localization of hTAZ isoform 2 subfragments derived from hTAZ(25-92).. **(A)** Schematic diagram of hTAZ isoform 2 subfragments derived from hTAZ(25-92) fused to eGFP, which contain amino acids encoded from part of exon 1, exon 2 (37-80) and exon 3 (80-93). The amino acid sequence of hTAZ exon 3 is also shown. The splicing junction encodes the amino acid R94, which is a site of common missense mutations in Barth syndrome patients. The W95 residue encoded in exon 4 is indicated (red letter). The peptide sequence gly-gly-gly was inserted as a linker at the C'-terminal TAZ deletion sites to create an in-frame fusion protein with eGFP. The maximal intensity projection of z-stack (0.2 mm x 6 slices) confocal images are shown for the mitochondrial outer membrane marker hTom20-tdTomato with hTAZ mutants **(B)** hTAZ(37-80), **(C)** hTAZ(46- 57), **(D)** hTAZ(80-95), **(E)** hTAZ(82-95),**(F)**hTAZ(84-95), G. hTAZ(80-92), **(H)** hTAZ(82-92). All images were taken with a 60 x oil lens and the white bar in panel E represents 50

localization (**Figure 4-8**, B, C, D, E, and F).

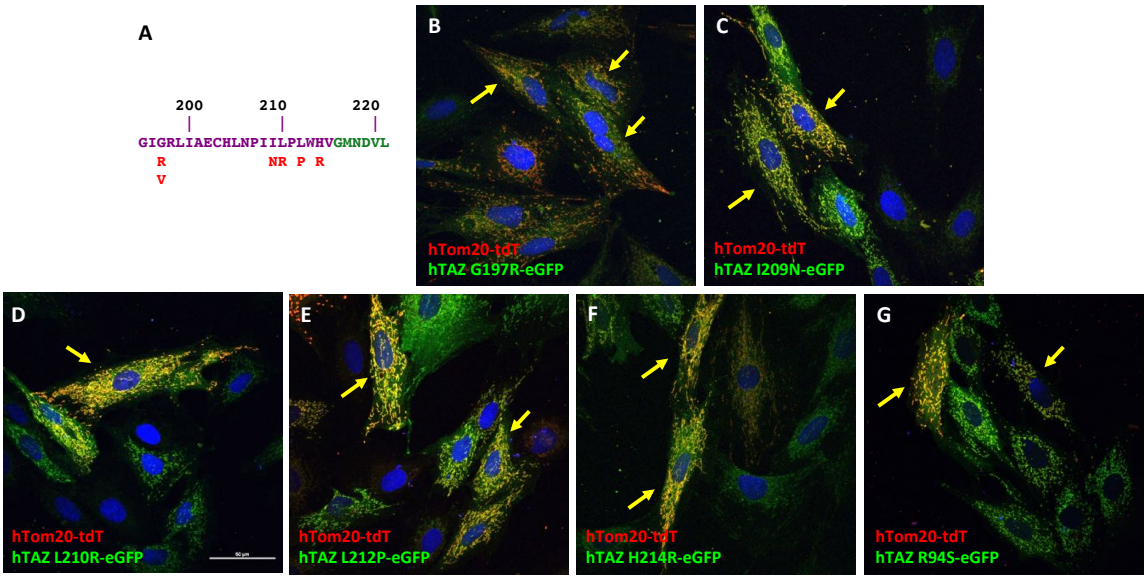

Figure 4-8: Mitochondrial localization of hTAZ-eGFP proteins containing Barth syndrome missense mutations. **(A)** Amino acid sequence of hTAZ exon 8 (purple letters) and 9 (green letters). The TAZ missense mutations in Barth syndrome are labeled in red letters. Confocal images of of TAZ mutants are shown: **(B)** G197R, **(C)** I209N, **(D)** L210R, **(E)** L212P, **(F)** H214R, and, **(G)** R94S (located in exon 3). All images were taken with a 60 x oil lens and the white bar in panel D represents 50 μm.

Another hot spot for mutation, R94, is located at the end of exon 3. Although mutations in the first or second nucleotides in the codon do not affect RNA splicing, the known mutated amino acids are relatively diverse and include cysteine, serine, histidine, leucine, or glycine. TAZ with the R94S mutation is still able to localize to mitochondria (**Figure 4-8**, G).

4.7 Localization of TAZ-eGFP in TAZ knockout H9C2 cells

The exact mechanism by which TAZ is imported into mitochondria is still unknown. To exclude the possibility of homodimerization, whereby the TAZ fragment-eGFP fusion proteins are carried into the mitochondria by normal, endogenously expressed TAZ interacting with the fusion protein, we verified localization of the previous constructs in TAZ knockout (KO) H9c2 cells. As we found exon 3 to be responsible for mitochondrial localization, we targeted it for deletion in the myoblasts using CRISPR/Cas9 technology (**Figure 4-9**, A). We selected three separate lines: one line, CR38, does not contain a TAZ mutation and two lines that contain TAZ deletions that were verified

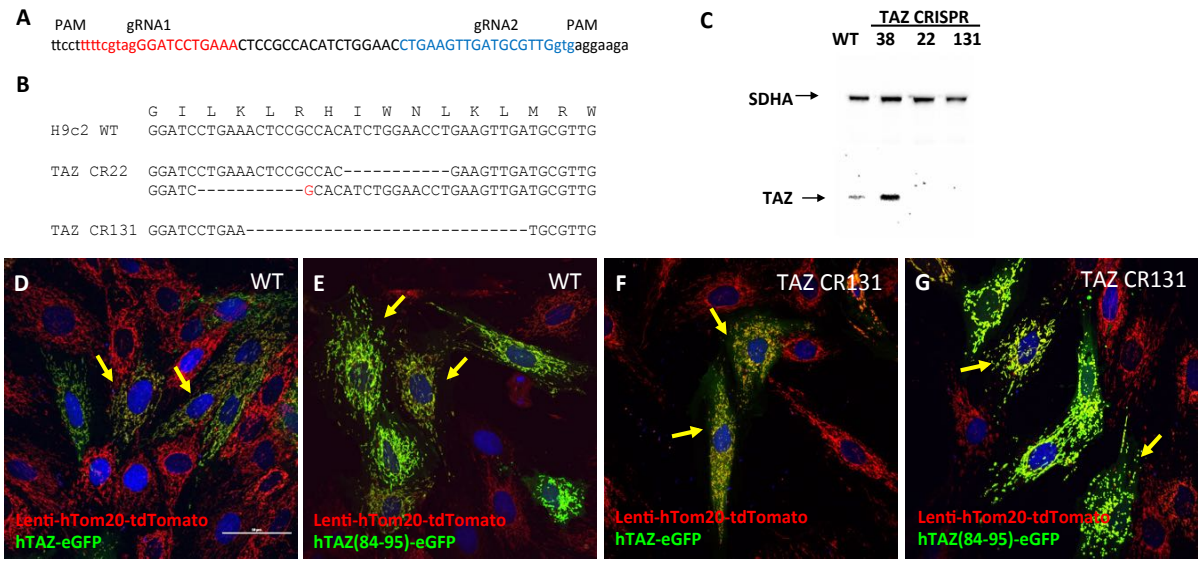

Figure 4-9: TAZ-eGFP mitochondrial localization in H9c2 TAZ Knockout cells. **(A)** Strategy of TAZ knockout in H9c2 by two tracer-gRNAs. Anti-sense (red letters) and sense (blue letters) guide RNAs target the 5'- and 3'-end of exon 3, respectively. **(B)** Sequence alignment of TAZ CRISPR mutations in targeted H9c2 cell lines derived from single colonies. The exon 3 encoded amino acids are indicated above the WT DNA sequence. Clone CR22 has deletions (dashed line) in both alleles: one with an 11 nt deletion and the other with a 12 nt deletion combined with a single nucleotide insertion (red letter). CR131 has a 29 nt deletion. Both KO clones contain out-of-frame nonsense mutations. **(C)** TAZ western blot of WT H9c2 and H9c2- derived TAZ CRISPR knockout cells. Antibodies were used to detect TAZ and also the mitochondrial complex 2 marker SDHA. **(D-G)** Mitochondrial localization of TAZ-eGFP proteins in WT and TAZ-KO cells containing a stable lentiviral-hTom20- tdtomato marker. D. hTAZ-eGFP in WT cells. E. hTAZ(84-95)-eGFP in WT cells. F. hTAZ-eGFP in KO cells, and G. hTAZ(84-95)-eGFP in KO cells. All images were taken with a 60 x oil lens and the white bar in panel D represents 50 μm.

by sequencing. The sequence alignments revealed that both deletion cell lines, CR22 and CR131, contain TAZ nonsense mutations by deletion of 11 and 29 nucleotides of exon 3, respectively (**Figure 4-9**, B). To further confirm the protein expression in both cell lines, western blot analyses showed that TAZ proteins were detectable in the wild type and CR38 lines, but not in the nonsense clones CR22 and CR131 (**Figure 4-9**, C).

To investigate whether TAZ isoform 2 or TAZ(84-95) targeting to mitochondria is mediated by endogenous wild type TAZ, we created cell lines derived from H9c2 wild type, CR22 and CR131 that constitutively expressed hTom20-tdTomato by lentivirus infection. Using these cell lines, we found that TAZ-eGFP and TAZ (84-95)-eGFP are still able to localize to mitochondria in both the TAZ KO lines and the WT myoblasts (**Figure 4-9**, D, E, F, and G). We observed similar results with

TAZ(185-220)-eGFP (data not shown). These data suggest that the short mitochondrial targeting sequences in TAZ are sufficient to target proteins to mitochondria in the absence of full length TAZ.

4.8 Discussion

The acyltransferase TAZ is responsible for cardiolipin maturation in the mitochondrial inner membrane. TAZ is encoded in the nucleus and then targeted to the mitochondrial inner membrane, where its substrate is exclusively remodeled. Therefore, mislocalization of this protein, even if fully enzymatically active, could have severe implications for CL remodeling. It is thus critical to understand how TAZ is targeted to mitochondria. Targeting of proteins to mitochondria can be achieved with different types of targeting sequences, depending on the final destination and function of the protein. Whereas matrix proteins contain a cleavable N- terminal presequence that is recognized by the translocase of the outer membrane 20 (Tom20) complex, membrane and intermembrane space (IMS) proteins typically contain non-cleavable internal targeting sequences that are recognized by the Tom70/71 complexes [140]. A subgroup of IMS and inner mitochondrial membrane (IMM) proteins are targeted to their correct location by further interactions with the mitochondrial intermembrane space assembly (MIA) complex, via a characteristic double cysteine (C) motif (typically in the form of CxnC) [141,142]. Mutations in these internal sequences could lead to aberrant sorting within the mitochondria, as well as failure to be targeted to the mitochondria at all. Human tafazzin contains one Cx_3C motif located downstream of the 80-95 localization domain.

In this report, we determined the mitochondrial localization sequences for TAZ and found that there are two discrete regions that can target it to the mitochondria. The two sequences, TAZ (84-95) and TAZ (185-220), are located in exons 3 and 7/8, respectively. While the exon 3 sequence targets TAZ exclusively to mitochondria, the exon 7/8 sequence does not confer precise localization. Both of these sequences are able to direct eGFP to mitochondria in the absence of wild

type TAZ, in TAZ deficient cells. Although several BTHS-causing point mutations are located within these two regions, our data shows that many of these mutations do not disrupt mitochondrial localization of the protein. This is in accordance with previous studies that modeled BTHS point mutations in yeast [55,57].

4.8.1 TAZ contains two distinct mitochondria targeting regions

As the two mitochondrial localization sequences are able to independently target TAZ to the mitochondria, this suggests a redundant role for one of the peptides. TAZ (84-95) confers exclusive mitochondrial localization, indistinguishable from wild type TAZ, whereas TAZ (185- 220) targets other sub-cellular compartments as well. The former sequence is unique and does not share homology with any other known proteins or mitochondrial localization sequences. The latter sequence may interact with other domains of the protein in the wild type molecule to form an exclusive mitochondrial targeting signal, or may be a remnant of an evolutionarily older signal. Of the four TAZ isoforms documented in humans, two lack exon 7, which encodes amino acids 181-195, part of the TAZ (185-220) peptide. Studies in 293 cells show these two isoforms are still able to localize to mitochondria, suggesting a redundant role for this peptide [49].

Our studies utilize confocal microscopy to determine co-localization with mitochondrial markers, however this technique cannot distinguish between different sub-mitochondrial compartments. It is possible that TAZ(80-95)-eGFP could localize to a different mitochondrial compartment than the IMM. Overexpression might cause the TAZ(80–95)-eGFP, hTOM20-tdTomato or hTIM23-tdTomato constructs to localize to both membranes and possibly the mitochondrial matrix, and thus may also confound the results. Future studies using super resolution microscopy, when available, will likely be informative

4.8.2 Exon 3 of TAZ plays an important role in mitochondrial localization

TAZ (84-95), the peptide responsible for exclusive mitochondrial localization, encompasses a large part of exon 3 of the TAZ gene. Recent *in-silico* prediction of TAZ structure showed that most of this region is found on an exposed part of the globular protein structure and contains part of a patch of positive residues that help anchor it to the IMM in conjunction with the actual membrane insertion domain, predicted to reside in exon 1 [51]. R94, one of the sites most commonly found to have single point mutations leading to BTHS, is one of the residues that helps anchor TAZ to the membrane. This led us to surmise a mutation in this spot could lead to de-stabilization and mislocalization of the protein. In our experiments, however, the TAZ R94S mutation did not affect mitochondrial localization of eGFP. This finding correlates with the ability of the TAZ (80-92) peptide to direct eGFP to the mitochondria. It is possible that TAZ R94S can still localize to mitochondria, but has difficulty remaining anchored to the IMM, where it needs to locate in order to interact with its substrate.

Intriguingly, both TAZ (80-92) and TAZ (84-95) are able to localize to the mitochondria, however, the core overlapping sequence of 82-92 does not. The former two peptides contain a similar number of positively charged and hydrophobic amino acids. It has been proposed that mitochondrial targeting sequences consist of alpha helices enriched in positively charged and hydrophobic amino acids that bind the outer membrane translocases [141,143]. It is therefore tempting to speculate that structure in the form of a minimal length amphipathic helix is also required, in addition to a specific amino acid sequence. This would explain why TAZ (82-92) is not able to localize eGFP to mitochondria, while the other two peptides are sufficient. It is also possible that the added amino acids provide essential post-translational modifications, which are not present in the shortened sequences.

4.8.3 In-silico modeling of human TAZ structure

Although the bulk of exon 3 is exposed, the *in-silico* model locates the G80 and L82 residues in a secondary structure within the core of the protein. While it could be intuitively expected that a mitochondrial targeting sequence would need to be exposed to the surface of the protein for interaction with the TOM complex, a large number of proteins have been shown to enter mitochondria in an incompletely folded state, accompanied by chaperones on the cytosolic side [144]. It is therefore possible that a region normally buried within the core of the protein can serve as an organellar localization domain. Similarly, I209, L210, L212, H214 and G216, part of the TAZ (185-220) peptide, are also predicted to locate in the core of the protein. Therefore, the predicted model of TAZ structure represents an enzymatic steady state, rather than a dynamic, structure-shifting, mitochondrial targeting state.

4.8.4 Correlation of human and yeast TAZ mitochondrial localization studies

Yeast studies have previously identified the membrane insertion domain to reside between amino acids 215-232 in Taz1p, corresponding to 201-219 in human TAZ [139]. This domain, in conjunction with an N-terminus flanking sequence, 204-232 in Taz1p (192-219 in human TAZ) was proposed to facilitate mitochondrial import. In agreement with the yeast TAZ study, we found that TAZ (185-220) is able to partially target eGFP to mitochondria. Any attempts to shorten this sequence, however, using either TAZ (185-195), TAZ (192-203), or TAZ (195-220), completely abolished mitochondrial targeting. Whereas in this study exon 3 of TAZ more precisely targets mitochondria, in the yeast studies, mitochondrial targeting of Taz1p lacking the 204-232 peptide, but containing exon 3 was completely abolished. These results indicate that Taz1p and human TAZ differ in their mitochondrial targeting mechanisms and lend support to the speculation that the 185-220 peptide in human TAZ may be a remnant of an evolutionarily older signal. It is unclear, evolutionarily, at what point the switch may have occurred, however, alignment of tafazzins from

various species (human, mouse, frog, zebrafish, fruit fly and yeast) reveals that the 185-220 peptide shows a higher degree of conservation than the 84-95 peptide. Among the vertebrates, the 185-220 peptide is 81% conserved, while the 84-95 peptide is 75% conserved [51]. In fruit flies, the former is 73% conserved, while yeast it is 59% conserved, and the latter is only 50% conserved in both organisms [54]. Interestingly, experimental data shows that Drosophila-specific N-terminal sequences, not contained in any of the higher organisms, may impact tafazzin's mitochondrial targeting. Flies express 3 isoforms of TAZ, which differ solely in the N-terminal sequences. Although they are upstream of both potential mitochondria targeting peptides, the length of the sequences can influence the precise mitochondrial targeting of the protein [49]. These data suggest that the 84-95 peptide became more important in higher organisms, although factors outside of the these two peptides can play a role in the protein's localization in different organisms. More detailed evolutionary analysis of TAZ genes from different model organisms could shed light on important differences in their protein targeting mechanism to mitochondria.

Several other BTHS missense mutations (G197R, I209N, L210R, L212P, and H214R) are located within the TAZ (185-220) peptide. We investigated the role these mutations might play in the localization of the protein, however, none of these mutations affected mitochondrial localization of TAZ. This is unsurprising, as our experiments have shown that the TAZ (84-95) peptide is able to independently confer mitochondrial localization. In previous experiments, where I209, L210 and L212 mutations were modeled in yeast, they were shown to localize to the mitochondrial matrix rather than the IMM or OMM. Our data does not distinguish between these two submitochondrial compartments, and we cannot rule out the possibility that this occurs with human TAZ. Failure to localize to the IMM is expected to prevent proper remodeling of MLCL and thus affect membrane curvature and respiratory complex assembly [62,68].

Herndon et al. reported that Taz1p does not require a membrane potential to translocate into mitochondria, as most inner membrane proteins do [139]. They found it requires both TOM20 and 70 receptors on the surface, but likely does not require TIM22 or 23. Taz1p seems to interact with Tim10p instead. Although, human TAZ contains the recognition motif (Cx_3C) for the MIA complex, it is further away from the identified mitochondrial targeting signals than in other MIA substrate proteins, suggesting it may not be functional. Recent studies have found that overexpression of mitochondrial translocation proteins can affect mitochondrial protein import, thereby it is possible that overexpression of TOM20-tdTomato in our experiments could interfere with the proper localization of TAZ [27, 28]. Another caveat with our study is that the eGFP moiety may also prevent complete translocation to the IMM. The use of human proteins in a rat cell line may also lead to subtle differences in mitochondrial localization due to variations in protein sequence.

4.8.5 TAZ-eGFP does not co-localize with peroxisomes or lysosomes

A great deal of evidence has accumulated demonstrating the dynamic interplay between different organelles in the cell. The connection between mitochondria and endoplasmic reticulum (ER) has long been established, but more recently mitochondria derived vesicles (MDVs) have been shown to mediate transport from mitochondria to both peroxisomes and lysosomes [23]. Peroxisomes are arguably closely related to mitochondria; these two organelles not only share biogenesis and division markers, but recent studies have shown that mitochondria are required for *de novo* synthesis of peroxisomes [145]. It has been postulated that MDVs populate newly formed peroxisomes with proteins and lipid products derived from mitochondria, in addition to facilitating transport of fatty acids and oxidized products [24]. CL, which is synthesized in the mitochondria, but has been detected in the peroxisomes of yeast, could be one such candidate [146]. Functionally, both organelles perform β-oxidation of fatty acids and neutralize oxidized products [145].

Our result that TAZ-eGFP was not detected in peroxisomes indicates that it is unlikely to be carried over to the peroxisomes via MDVs. TAZ is not normally detected in peroxisomes, despite MDVs having been shown to bud off regions of both inner and outer mitochondrial membranes for delivery to peroxisomes. It is possible that the domains of mitochondrial membrane targeted for peroxisomes are not those where TAZ tends to be enriched, or that TAZ is endogenously present in such low amounts it cannot be detected.

Lysosomes are responsible for degrading molecules taken up by the cell by endocytosis, as well as cytoplasmic proteins and organelles (such as mitochondria) via auto/mitophagy [147]. In addition, MDVs have been shown to bud off damaged sections of mitochondria and transport them to lysosomes, thereby avoiding the more costly mitophagy. Overexpression of a membrane protein such as TAZ (or parts of it) could lead to the formation of aggregates, which would make our TAZ-eGFP a target for lysosomal degradation. In addition, the over-expression of TAZ-eGFP could affect mitochondrial health, therefore, making these organelles targets for autophagy. However, we did not observe any TAZ-eGFP signal localized in lysosomes.

4.8.6 Conclusions and implications

Recent studies have found that overexpression of mitochondrial translocation proteins can affect mitochondrial protein import [148,149]. Identification of minimal, non-functional protein domains that promote mitochondrial targeting but do not affect mitochondrial import is useful for localization studies and for development of targeted mitochondrial therapies. In this study, we have demonstrated that a short 12 amino acid fragment of TAZ (84-95) is sufficient to target eGFP to mitochondria and thus can be used for such an application. The IMM in particular is the site of oxidative phosphorylation and location of many important components of the electron transport apparatus, many of which have been implicated in mitochondrial dysfunction in human disease [150]. Development of a peptide reagent that facilitates the delivery of therapeutic molecules to the

IMM may lead to development of novel therapies for mitochondrial diseases that result from respiratory dysfunction.

5 Characterization of Barth Syndrome Models

Numerous studies have demonstrated that TAZ deficiency leads to decreased mitochondrial respiration and muscle dysfunction in organisms ranging from Drosophila, to zebrafish, to mice. These defects are the result of a failure to remodel CL, a phospholipid that plays an integral role in mitochondrial function [8]. Previous studies seeking to more precisely dissect the mitochondrial defects, however, report varying, and at times contradicting, mechanisms of dysfunction [94,151]. These efforts may be complicated by the mild phenotype displayed by TAZ knockdown models, which still express 5 up to 20% levels of wild type levels of TAZ, depending on the tissue, emphasizing the need for a knockout model [93]. A number of attempts have been made to create TAZ KO models, both at the cellular and mouse level with very little success until recently [81,96]. This chapter characterizes the effects of TAZ deficiency in the TAZ KD mouse model, as well as a novel TAZ KO cardiomyoblast cell line.

5.1 Effects of shRNA Knockdown in Mammalian Models

TAZ KD mice were generated commercially by the Barth Syndrome Foundation through the insertion of a tetracycline-inducible cassette controlling expression of a TAZ-specific shRNA in the *ROSA26* locus. The shRNA is only expressed in the presence of a tetracycline. Feeding doxycycline chow to these mice leads to degradation of the TAZ mRNA via

Table 5-1: Molecular composition of CL and MLCL species monitored by LC-MS.

CL or MLCL	m/z^{2-}	C atoms:double bonds	Fatty Acyl Chains
MLCL	581.3	52:3	(16:1)(18:1)(18:1)
MLCL	582.3	52:2	(16:0)(18:1)(18:1)
MLCL	594.3	54:3	(18:1)(18:1)(18:1)
CL	619.4	56:0	(14:0)(14:0)(14:0)(14:0)
CL	700.4	68:4	(16:0)(16:1)(18:1)(18:2)
CL	713.4	70:5	(16:1)(18:1)(18:1)(18:2)
CL	723.4	72:8	(18:2)(18:2)(18:2)(18:2)
CL	724.4	72:7	(18:2)(18:2)(18:2)(18:1)
CL	725.4	72:6	(18:1)(18:1)(18:2)(18:2)
CL	747.5	76:12	(18:2)(18:2)(18:2)(22:6)

the RNA interference pathway and results in 90-95% knockdown of TAZ in heart and skeletal muscles [93]. The shRNA cassette is maintained on a heterozygous background as homozygous mice do not survive over 3 weeks of age.

5.1.1 Knock-down in Cardiac Fibroblasts leads to Altered Lipid Profile with Normal Mitochondrial Respiration

To investigate the effect of TAZ KD at the cellular level, cardiac fibroblasts were isolated from neonate TAZ KD and WT littermate mice and continuously treated with Doxycycline in culture to maintain shRNA production. While TAZ KD homozygous mice are not able to survive to adulthood, we found that it is possible to obtain neonates with this genotype. We therefore isolated fibroblasts from both homozygous and heterozygous TAZ KD pups; dams carrying the pups were maintained on doxycycline chow throughout gestation.

5.1.1.1 Lipid Profile of Cardiac Fibroblasts

Increases in the levels of MLCL and decrease in total CL are the hallmark biochemical signs of BTHS. To determine whether neonatal cardiac fibroblasts have an altered CL profile in the absence of TAZ, cells were isolated from WT, heterozygous and homozygous TAZ KD neonates. Lipids were extracted using a modified Folch method and analyzed using mass spectrometry. As the levels of CL are relatively low among cellular lipids, the abundance of CL and MLCL species was measured in the fibroblast lipid samples by selected ion monitoring (SIM) mass spectrometry. The most abundant CL species were monitored and Table 5-1 lists these species and their fatty acid composition. Some of the species (CL 68:4, CL 70:5 and MLCL 52:3) were present in very low amounts leading to unreliable quantification, therefore they were excluded from further analyses. Mass spectrometric analysis showed the most abundant mature CL species in cardiac fibroblasts isolated from both WT and KD mice is CL 76:12 (25% vs 21% CL 72:8), which contains three linoleic acids and one docosahexanoic (DHA). Previous reports differ on this account, with both CL

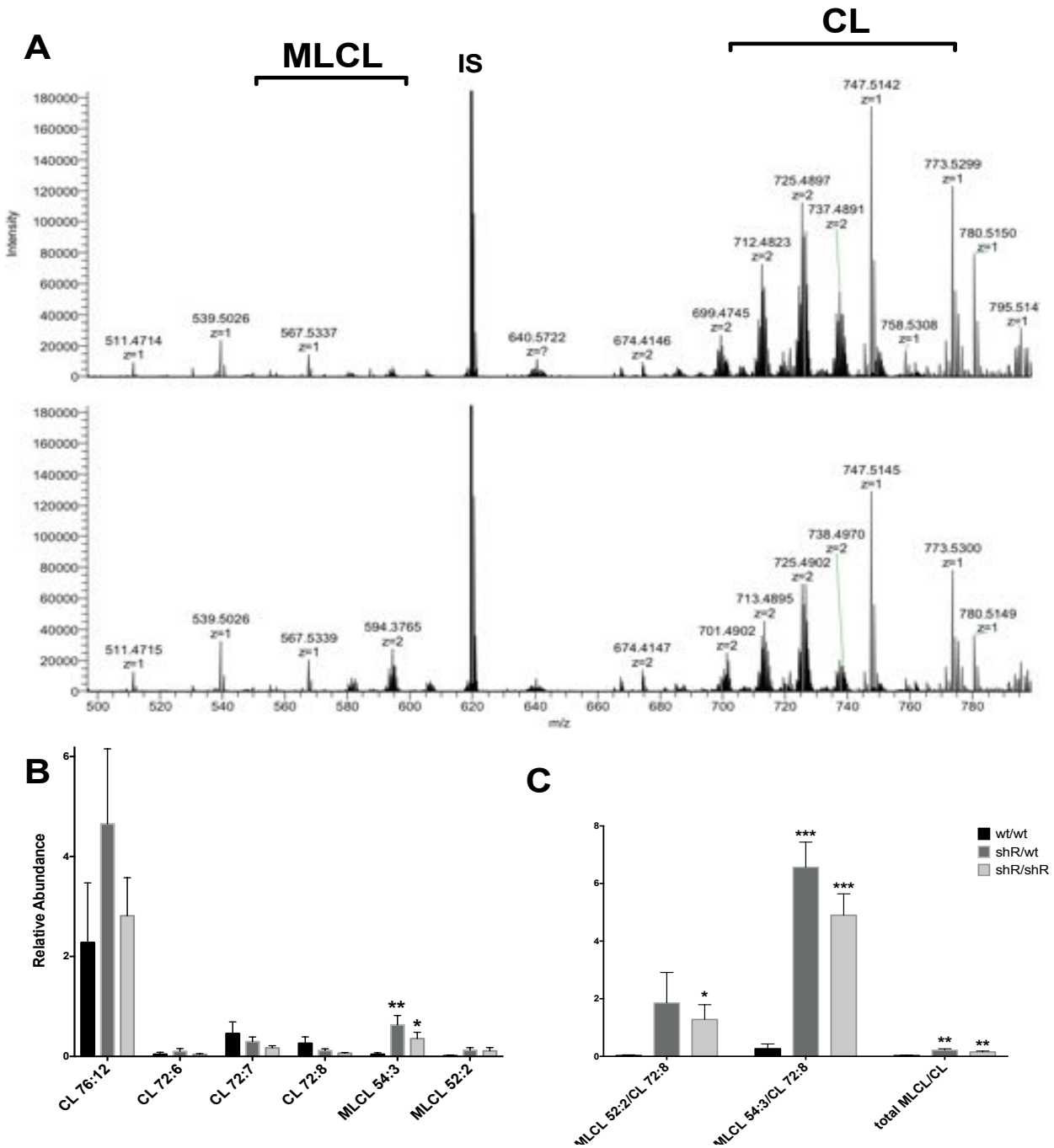

Figure 5-1: LC-MS analysis of cardiolipin in primary cardiac fibroblasts. **(A)** Representative spectra obtained from WT (top panel) and heterozygous TAZ KD (bottom panel) cells. **(B)** CL and MLCL species monitored by SIM LC-MS in WT, heterozygous and homozygous TAZ KD cells. MLCL 54:3 was significantly higher in both homozygous and heterozygous TAZ KD cells than in WT cells (n=3 for wt/wt and n=7 for shR/wt and shR/shR, Welch's t-test, *p<0.05, **p<0.01). **(C)** Different MLCL/CL ratios (using the values in B) for WT, heterozygous and homozygous TAZ KD cells. MLCL 54:3/CL 72:8 was the most sensitive in distinguishing TAZ deficiency in these cells (Welch's t-test, *p<0.05, **p<0.01, ***p<0.001).

72:8 and 76:12 being noted as the most abundant species in mouse heart, potentially an effect of the particular mouse strain used [65,95,152]. In humans, CL 72:8 is the most abundant species in both

cardiac and skeletal muscles [153]. Although it did not reach significance, the mature CL species that decreased the most between WT and TAZ KD cells was CL 72:8. Both MLCL species examined, 52:2 and 54:3, were increased in TAZ KD fibroblasts, although only MLCL 54:3 reached statistical significance (Figure 5-1, B).

Previous case studies in BTHS patients have reported that it is possible to detect normal total CL levels in a patient with BTHS and the ratio of MLCL to CL 72:8 is the most sensitive measurement of the disease phenotype [154]. As it was unclear which CL and MLCL species would be most sensitive in mouse cardiac fibroblasts, different ratios were investigated. Consistent with literature, wild type fibroblasts had very low MLCL levels, resulting in a very small MLCL/CL ratio regardless of the species investigated. Both heterozygous and homozygous TAZ KD cells had a significantly increased total MLCL/CL and MLCL 54:3/CL 72:8 ratios compared to WT cells, but only homozygous cells had a significantly higher MLCL 52:2/CL 72:8 ratio (Figure 5-1, C).

5.1.1.2 Mitochondrial Respiration in Cardiac Fibroblasts

Decreased mitochondrial respiration has been reported in both neonatal cardiomyocytes from TAZ KD mice, as well as fibroblasts from BTHS patients. Given the increased MLCL/CL ratio in cardiac fibroblasts, it would be expected that it results in decreased respiration. Oxygen consumption rates (OCRs) in intact WT and heterozygous KD fibroblasts was analyzed using a 96-well Seahorse Extra-cellular Flux Analyzer. During the experiment, a basal rate was first determined, followed by inhibition of the ATP synthase using oligomycin. The observed decrease in oxygen consumption after oligomycin addition

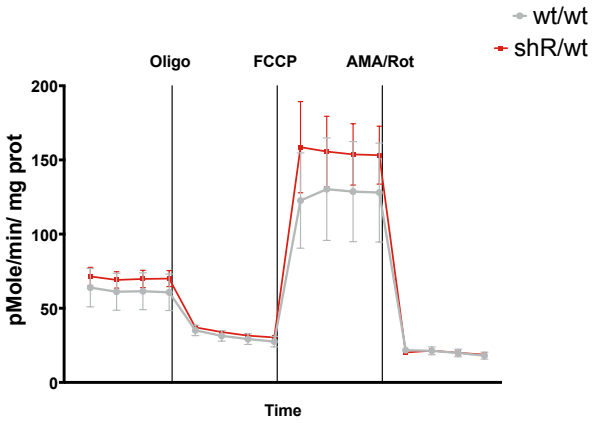

Figure 5-2: Oxygen consumption rates in neonatal cardiac fibroblasts isolated from WT and heterozygous TAZ KD mouse hearts (n=3 for each). Vertical bars represent SEMs.

is the result of coupling between the respiratory chain and the ATP synthase by the membrane potential; a failure to decrease oxygen consumption at this stage would indicate a proton leak in the IMM. The membrane is subsequently depolarized with FCCP, which uncouples the respiratory chain from ATP synthesis and reveals the maximal respiratory capacity. To measure non-mitochondrial O_2 consumption of the cell, complexes I and III were inhibited with rotenone and antimycin A, respectively. In contrast to neonatal cardiac myocytes derived from TAZ KD mice [94], no difference was observed between WT and heterozygous KD neonatal cardiac fibroblasts (Figure 5-2). While homozygous KD mice had shown a greater degree of lipid species alterations, which may have resulted in lower mitochondrial respiration, only a very limited number of those pups was available due to their problems in survival. Unlike in BTHS patients, the heterozygous TAZ KD mice do not manifest a profound disease phenotype perinatally and their MLCL 52:2/CL 72:8 is not as drastically different from normal TAZ-expressing mice [14]. While a useful research tool, this mouse model may have limited applicability.

5.1.2 TAZ KD in 10 Week Old Mice Leads to Distinct Effects in Cardiac and Skeletal Muscles

5.1.2.1 CL Profile is Altered in Mouse Hearts in Response to TAZ Deficiency

Although TAZ KD mice do not display organ level dysfunction until later in life, examination of CL speciation in 2-month-old mice revealed CL remodeling defects in both heart and skeletal muscle. We therefore expected to find similar effects. To determine the CL profile of heterozygous TAZ KD and WT mouse hearts, the organs were homogenized and lipids were extracted with a modified Folch method [135,155]. As it was unclear whether sex would have an effect, male and female samples were compared separately. In contrast to the fibroblasts, no difference was detected between CL 76:12 and the other CL species in WT tissues, however it was significantly higher than CL 72:8 in female TAZ KD heart tissues (Figure 5-3, A). In males this difference did not reach

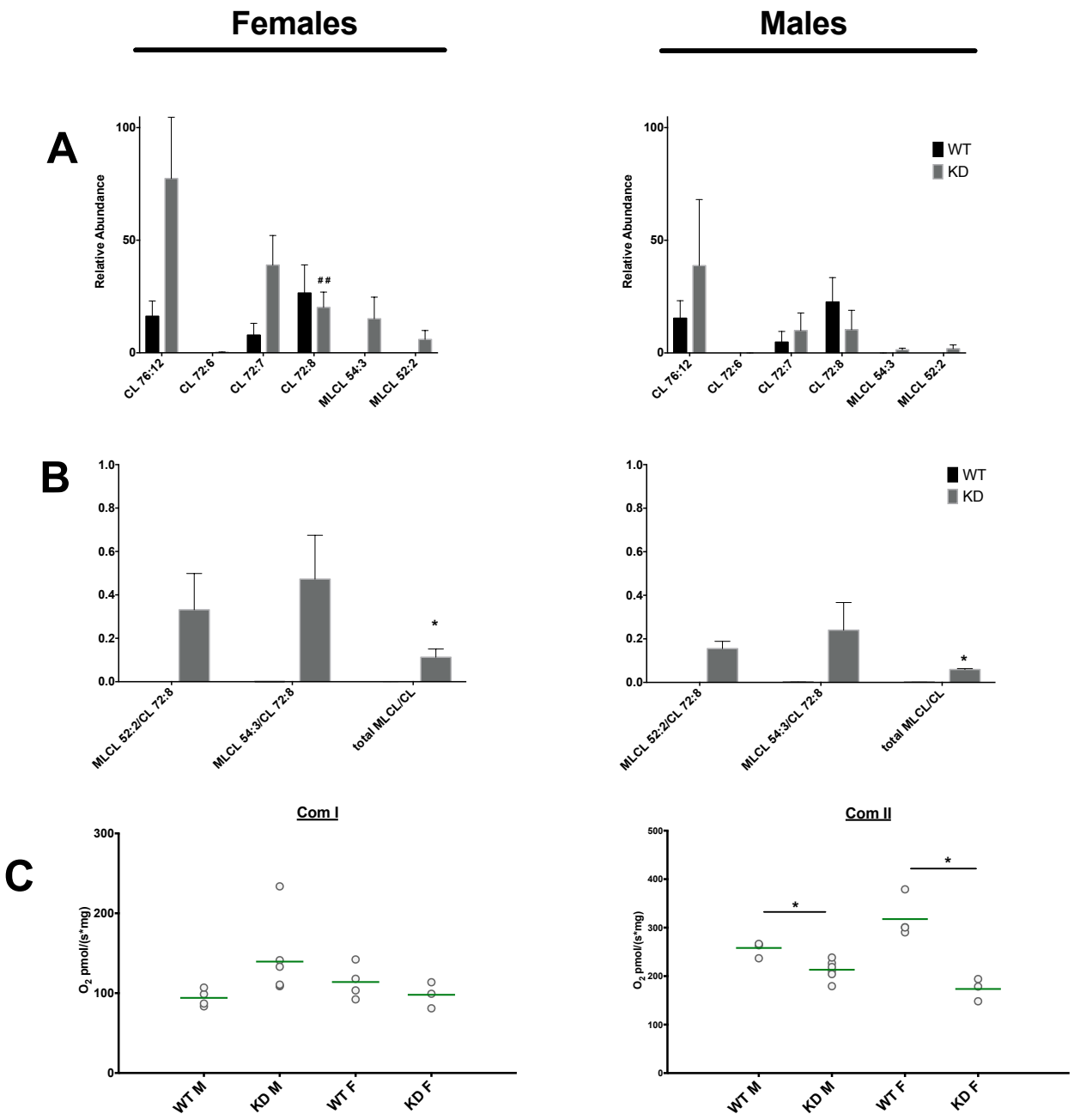

Figure 5-3: CL species composition and mitochondrial respiration in 10-week-old mouse hearts. **(A)** CL and MLCL species monitored by SIM LC-MS in WT and heterozygous TAZ KD mouse heart samples. CL 72:8 is significantly lower than CL 76:12 in TAZ KD females (n=5 for WT fem, n=6 for KD fem, n=2 for both genotypes males, ANOVA with Dunnett's multiple comparisons, ## $p<0.01$). **(B)** Different MLCL/CL ratios (using the values in A). Total MLCL/CL was significantly different between WT and TAZ KD tissues (Welch's t-test, *$p<0.05$). **(C)** Oxygraph measurements of oxygen consumption rates in homogenized hearts. TAZ KD rates were significantly lower than wild type when utilizing complex II, but not complex I substrates (multiple comparison t-test with Holm-Sidak correction, *$p<0.05$). Error bars indicate SEM (An and B) and horizontal bars indicate means (C, green).

significance. This indicates that in addition to an accumulation in MLCL, mature CL species steady

states are different in TAZ KD compared to WT mice, with a change in overall distribution of the mature CL species changes in the absence of TAZ. As expected, TAZ KD heart tissues had a significantly increased total MLCL/CL ratio, although comparison of MLCL 54:3/CL 72:8 and MLCL 52:2/CL 72:8 ratios did not reach significance (Figure 5-3, B). This is in contrast to what has been observed in hearts from BTHS patients, where the MLCL 52:2/CL 72:8, and not just total MLCL/CL, ratios are significantly different from the healthy population [156].

5.1.2.2 Mitochondrial Respiration in Heart Homogenates

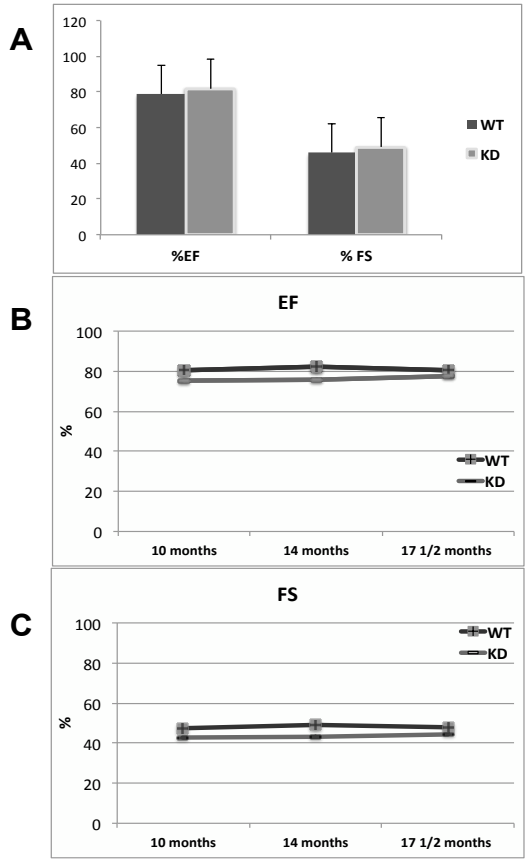

Figure 5-4: LV functional measurements by echocardiography. **(A)** EF and FS measured in 2 month old WT and TAZ KD mice (n=3 for both WT and KD). **(B)** EF and **(C)** FS measurements in 10-17 ½ month old mice (n=1 for each genotype). Means (A-C) and SEM (A) are represented.

Preservation of mitochondrial respiration plays a major role in cardiac energy metabolism. Based on alterations in the CL profile of two month old TAZ KD mouse hearts, it would be expected that respiration would be consequently decrease. OCRs in 10-week-old hearts were measured using an Oroboros oxygraph. Freshly harvested hearts were homogenized, then immediately loaded into the metabolic chambers of the oxygraph. Glutamate and pyruvate were used as substrates for complex I and succinate was used as a substrate for complex II. Similarly to previous studies, a significant decrease in oxygen consumption rates was seen in complex II enabled respiration for both male and female TAZ KD mice compared to WT mice [151]. With complex I substrates, however, no significant difference was detected in either males or females (Figure 5-3, C). These data indicate that a loss of

tafazzin function leads to a selective succinate dehydrogenase impairment in the cardiac tissue, which is consistent with observations by Dudek *et al* who reported a decrease in both SDH protein amounts and enzymatic activity. Similar defects were recapitulated in cardiomyocytes derived from BTHS patient induced pluripotent stem cells [151].

5.1.2.3 LV Function Remains Normal in TAZ KD Old Mice

In contrast to BTHS patients, TAZ KD mice are reported to have normal heart function for the first 7-8 months of life, at which point they develop ventricular dysfunction, with reduced EF and FS [68]. Echocardiographic assessment was performed on 2 month old mice, revealing normal EF and FS (Figure 5-4, A), as previously reported [68]. Unexpectedly, however, when tested at ages older than 8 and up to 18 months, TAZ KD mice still had normal EF and FS values, comparable to their wild type littermates (Figure 5-4, B and C). This indicates the phenotype in these mice is highly variable and the bioenergetics and biochemical defects detected are not always sufficient to drive organ level dysfunction in the adult mouse.

5.1.2.4 Contractile Function is Decreased in Soleus, but Not in EDL Skeletal Muscle of TAZ KD Mice

A hallmark symptom of BTHS patients is skeletal muscle weakness and we expected to find a similar phenotype in TAZ KD mice. Skeletal muscle function was interrogated in 10 week old WT and TAZ KD mice using *ex vivo* isometric force-frequency measurements in lower limb muscles. The maximal isometric twitch force for the extensor digitorum longus (EDL) was achieved at 120Hz and the specific force was calculated by normalizing to the muscle's cross-sectional area [134]. No difference was observed between TAZ KD and WT animals in EDL function. The EDL muscle, however, is abundant in fast glycolytic fibers, with few mitochondria, which may explain a lack of impairment. We, therefore, sought to compare function between WT and KD mice in a muscle with higher mitochondrial content. The soleus contains more slow-twitch oxidative fibers and is rich with

mitochondria [157]. Maximal isometric twitch force was achieved at 100Hz for the soleus. Specific force for this muscle function, was significantly reduced in TAZ KD mice compared to WT mice (Figure 5-5, A), consistent with reports by Soustek *et al* [93].

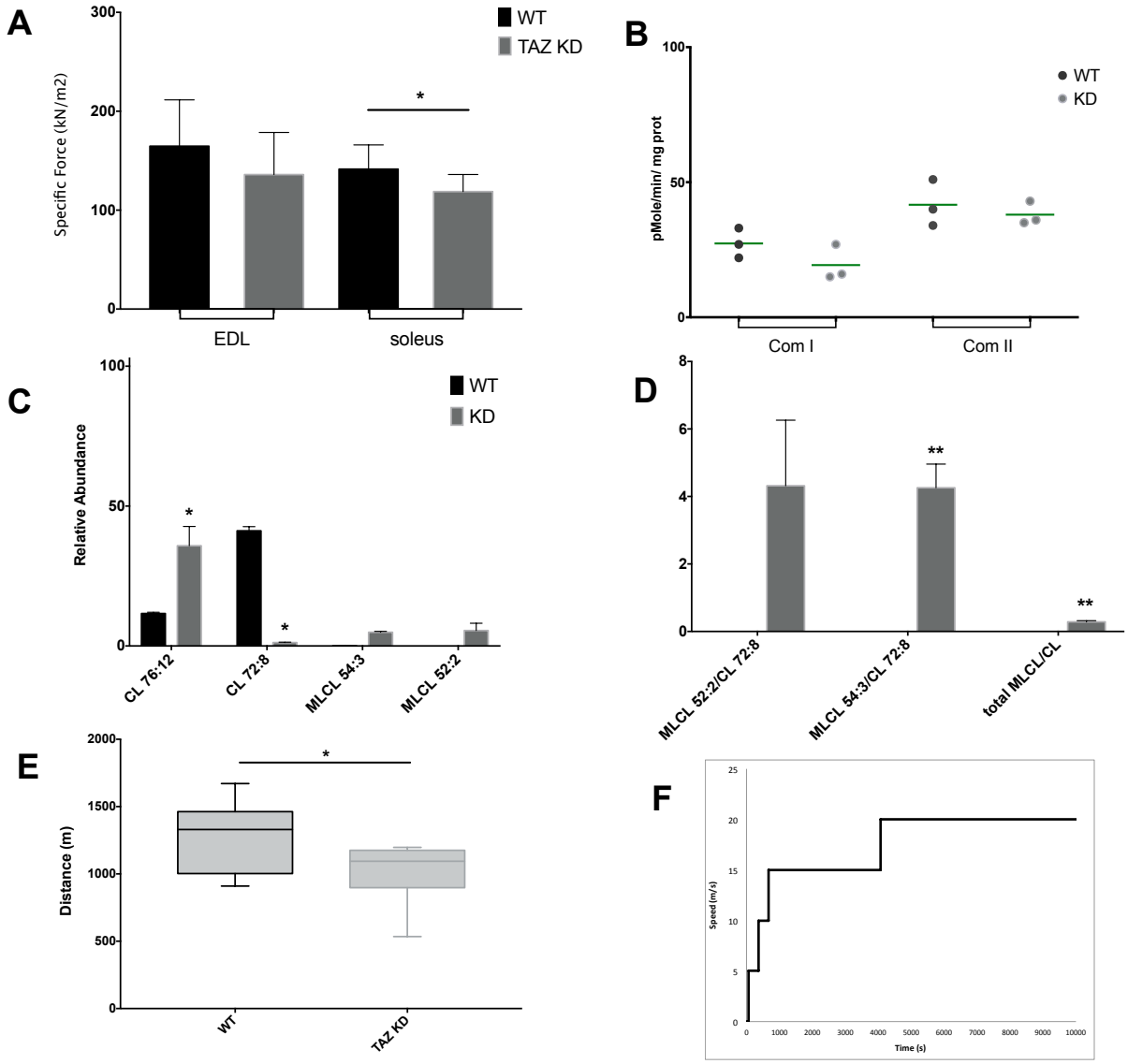

Figure 5-5: Lipidomic and bioenergetic analysis of 10 week old WT and TAZ KD mouse skeletal muscle. **(A)** Specific force measurements in EDL and soleus skeletal muscles from 2 month old mice (n=6 for both genotypes, for both muscles). Soleus of TAZ KD mice has significantly lower specific force compared to WT littermates. **(B)** Oxygen consumption rates in homogenized heart tissue from 2 month old TAZ KD mice are similar to WT mice. **(C)** CL molecular species measured in soleus muscles (n=2 for WT and n=4 for TAZ KD). **(D)** MLCL/CL ratios calculated from values in (C). **(E)** TAZ KD mice reach exhaustion much faster than their WT littermates in a forced exercise paradigm (n=8 for WT and n=9 for TAZ KD, t-test with a Holm-Sidak correction, *$p<0.05$). **(F)** Schematic of the treadmill running protocol used for experiments in (E). Error bars indicate SEM and horizontal bars indicate means (B, green) and median in (E).

5.1.2.5 TAZ KD Results in CL Profile Alteration in Skeletal Muscle

Similarly to heart tissue, the most abundant CL species in human skeletal muscle is CL 72:8, which is significantly reduced in BTHS patients. Consistent with these observations, assessment of the CL profile in the soleus muscle of TAZ KD mice revealed a significant decrease in CL 72:8 species accompanied by a drastic increase in CL 76:12 (Figure 5-5, C). Consequently, MLCL/CL ratios were highly increased in tafazzin deficient mice compared to WT (Figure 5-5, D), as expected.

5.1.2.6 Bioenergetic Function is Not Compromised in Soleus Muscle

Soleus muscle contains oxidative fibers abundant in mitochondria and we expected its demonstrated contractile impairment in TAZ KD mice likely results from impairments in mitochondrial respiration. To test this hypotheis, oxygen consumption measurements were conducted in permeabilized soleus muscles. Intact muscles were dissected from euthanized mice and the individual muscle fibers were manually separated. The muscle was then permeabilized with saponin and loaded into the metabolic chamber of the oxygraph.

Despite impaired contractile function and the drastic alteration seen in the lipid profile, bioenergetics assessment revealed no difference in oxygen consumption rates between WT and TAZ KD soleus muscles (Figure 5-5, B). This held true for measurements done with both complex I and complex II substrates. These data are in contrast to reports from BTHS patients, whose skeletal muscles demonstrate O_2 extraction impairments during exercise [31].

5.1.2.7 Treadmill Running Capacity Is Impaired by TAZ KD

In agreement with BTHS patients' inability to sustain physical activity, Powers *et al* subjected 4 month old mice to forced exercise on a treadmill and found that TAZ KD mice were unable to sustain the exercise at a speed of 20 meters/minute (m/min) with a 10% incline. The mice were able to complete the 36 minute running session with a 5% incline. Calorimetry measurements during the exercise session revealed that TAZ KD mice are likely unable to switch from carbohydrate sources

to mixed substrate utilization. During the first 60 minutes of endurance exercise, skeletal muscle is still undergoing significant changes in substrate utilization and reliance on fatty acid oxidation (FAO), the preferred substrate for both heart and skeletal muscle mitochondria, is still exponentially increasing during this time [158]. We tested the ability of TAZ deficient animals to sustain physical exercise and expected them to show an impairment compared to their WT littermates, particularly when challenged to utilize FAs rather than glucose. We therefore sought to design a treadmill running protocol that would test the ability of skeletal muscle mitochondria to utilize FAs. The protocol was conducted with a 5% incline and started with a 5 m/min speed. Speed was increased step-wise by 5 m/min every 5 min to a speed of 15 m/min, which was then held for 50 minutes, at which point a final step brought the speed to 20 m/min (see Figure 5-5, F for a schematic). Mice were run to exhaustion and total distance traveled was recorded. TAZ KD mice ran significantly lower distances than their WT littermates (Figure 5-5, E). The fact that most KD mice were able to run 1,000 m or more (over 60 minutes) and reached exhaustion as skeletal muscle FAO reliance is reported to sharply increase, suggests an impaired ability to switch to fatty acids as substrates, consistent with previous reports [95].

5.2 Knock out Models

5.2.1 CRISPR-Mediated Knock-out of TAZ in H9C2

Given the results obtained with the knock down models, it was clear that even a small amount of residual protein could ameliorate defects associated with TAZ deficiency and a complete knock out model may be necessary for a consistent system.

TAZ KO H9c2 cell lines were generated as described in Chapters II and III. Examination of the CL profile of the CR22 TAZ KO line using mass spectrometry revealed MLCL species were drastically increased in the KO line compared with WT H9c2, while the mature CL species decreased, indicating a lack of remodeling by TAZ (Figure 5-6, A).

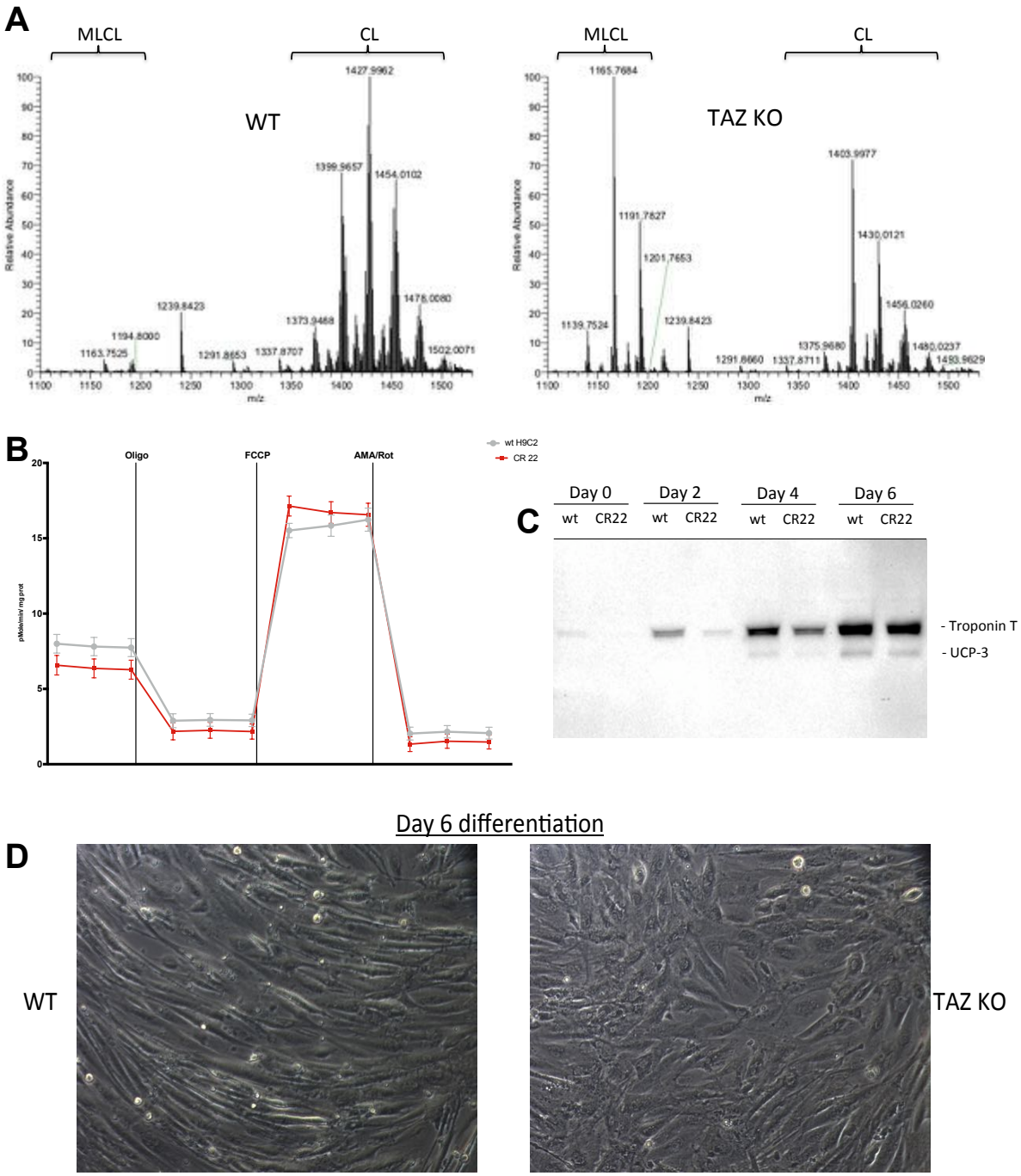

Figure 5-6: Defects in CL profile, mitochondrial respiration and differentiation associated with TAZ KO in H9c2 cardiomyoblasts. **(A)** Mass spectra for WT and TAZ KO myoblasts. **(B)** OCRs measured using Seahorse Flux Analyzer in WT and TAZ KO myoblasts (n=3 for each). Vertical bars represent SEM. **(D)** Immunoblot of cell lysates from WT and TAZ KO cells at various stages of differentiation. **(D)** Light microscopy of WT and TAZ KO cells after 6 days of differentiation.

Given these results we expected these cells to have decreased mitochondrial respiration compared to WT cells, surprisingly, however, the KO cells did not demonstrate a decrease in oxygen

consumption, as measured with a 24-well Seahorse Extracellular Flux Analyzer (Figure 5-6, B). This is reminiscent of the results seen in skeletal muscle of the TAZ KD mouse and suggests other factors may compensate for CL species alterations in myoblasts and muscle cells.

As mitochondrial susceptibility to TAZ deficiency changes during development [159], the ability of the TAZ KO myoblasts to differentiate was interrogated. Treatment with *trans*-retinoic acid, along with low levels of FBS, drives H9c2 myoblasts toward a cardiac lineage differentiation. The myoblasts fuse, forming aligned myotubes, and start expressing more cardiac markers. Cardiac troponin T is a protein involved in sarcomeric contraction in cardiac myocytes and it is expressed in very low amounts in myoblasts, but it is abundant in differentiated H9c2s [160]. TAZ KO cells show reduced elongation and fusion after 6 days of treatment and do not express the same level of cardiac Troponin T as WT cells, although its expression is induced significantly in both types of cells. As the myoblasts differentiate, their mitochondria become more mature and the cells start expressing more mitochondrial markers. Unsurprisingly, TAZ KO cells had lower levels of mitochondrial uncoupling protein 3 (UCP-3) than WT cells (Figure 5-6, C and D). These data indicate TAZ plays a role during cellular development and differentiation, but is not essential in this model.

5.3 Conclusions and Discussion

This chapter describes the defects associated with TAZ deficiency observed in the TAZ KD mice acquired by our lab and in our newly generated TAZ KO cardiomyoblast line, H9c2.

TAZ KD mouse tissues and cells demonstrate an alteration in their lipid profiles with varying degrees of severity. Surprisingly, however, this did not always correlate with a defect in mitochondrial respiration. Previous studies by Dudek *et* al report that mitochondria isolated from 2 month old TAZ KD mouse hearts show the highest degree of impairment (40% decrease) when using succinate as a substrate, which transfers electrons into the ETC via complex II, and a smaller decrease (30%) when utilizing pyruvate, a complex I specific substrate. In contrast, Kiebish *et al*

found no difference between WT and KD mice when using pyruvate, or pyruvate and succinate combined, although they do report a 15% decrease in respiration with pyruvate and glutamate combined. The data presented here show a significant decrease in respiration when using succinate as a substrate. No difference is detected when using only a pyruvate/glutamate combination as substrates. These discrepancies suggest an inherent variability in this mouse model, potentially owing to the residual low, but biologically significant, amount of TAZ expression. Another possibility is that the mouse background may differ to a certain extent between different groups, arising from differences in breeding procedures and mouse colonies. In our own TAZ KD colony we found one gene recently reported to influence mitochondrial redox homeostasis, nicotinamide nucleotide transhydrogenase (Nnt), in a small cohort of mice [161]. This gene is deleted in C57BL6/J mice and its presence in our colony is likely a remnant from the ES cells used to generate KD mice. This may also be the reason for the reported difference in heart function. As in the present study, Cadalbert *et al* found no evidence of decrease in LV function using echocardiographic assessment of 8 month old mice [96], while others reported a decrease in EF and FS starting with 7 months of age in TAZ KD mice [94,162].

In agreement with previous studies, interrogation of skeletal muscle function showed exercise intolerance and decreased *ex vivo* contractile function in the soleus muscle. No contractile defect was apparent in the EDL muscle. These data are in line with the oxidative capacity of these two muscles. Whereas the EDL is a fast twitch muscle with predominantly glycolytic fibres, the soleus contains a higher proportion of oxidative fibres, with a higher mitochondrial content [157]. Despite these differences and an altered biochemical profile, however, the soleus did not demonstrate a decrease in oxygen consumption rates. We are not aware of previous reports examining the oxidative capacity of permeabilized skeletal muscle in TAZ KD mice, however, these results could be explained by the fact that OCR in these tissues was assessed after the mice underwent the treadmill running protocol.

Recent studies in both TAZ KD mice and patients with BTHS report improvement in mitochondrial function following exercise training and a reduction in respiration rates in the soleus may be masked by exercise-derived improvements [163,164].

Characterization of a new H9c2 cardiomyoblast TAZ KO cell line revealed severely impaired CL remodeling, as well as defects in differentiation, with normal oxygen consumption. A report from Acehan *et al* examining the impact of cell differentiation state indicates that mitochondria of undifferentiated cells are not as severely impacted by tafazzin deficiency as differentiated cells, likely due to less reliance on aerobic metabolism [159]. H9c2s are still in a myoblast stage and are probably more reliant on anaerobic metabolism. Assessment of mitochondrial respiration after differentiation could lead to different results.

6 Effects of Recombinant Tafazzin Enzyme on Abnormalities Associated with TAZ Deficiency

Numerous efforts have been made to counteract the effects of TAZ deficiency with various strategies circumventing the TAZ CL remodeling pathway. Blocking the activity of PLA2, a calcium independent phospholipase that de-acylates CL into MLCL, partially restored the MLCL/CL ratio, however the CL in this case did not contain the typical steady state species that are seen after remodeling by TAZ, which could impact its function in mitochondria [130]. Treatment of TAZ-deficient HL-60 cells, a cellular model of human myeloid dysfunction, with mature CL solubilized in nanodisk complexes, successfully ameliorated the apoptotic phenotype reported in BTHS-derived neutrophils [165]. While this could be a potentially exciting treatment avenue, it does not address the variable CL composition seen in different tissues, or other potential non-CL related aspects of BTHS.

Attempts to prevent development of LV dysfunction in TAZ KD mice with the mitochondrial biogenesis activator bezafibrate showed some success in preventing a decrease in heart function seen with isoproterenol treatment, a ß-adrenergic stressor, in TAZ KD mice. This treatment, however, lead to the formation of aberrant CL species and an even further increase in the MLCL/CL ratio [162]. Given these conditions, it is unclear whether treatment with bezafibrate would be able to ameliorate LV dysfunction.

A need for a curative treatment for BTHS is still essential and administration of exogenous TAZ protein would address all aspects of the BTHS phenotype. This chapter examines the effects of TAZ recombinant protein treatment on the defects associated with TAZ deficiency.

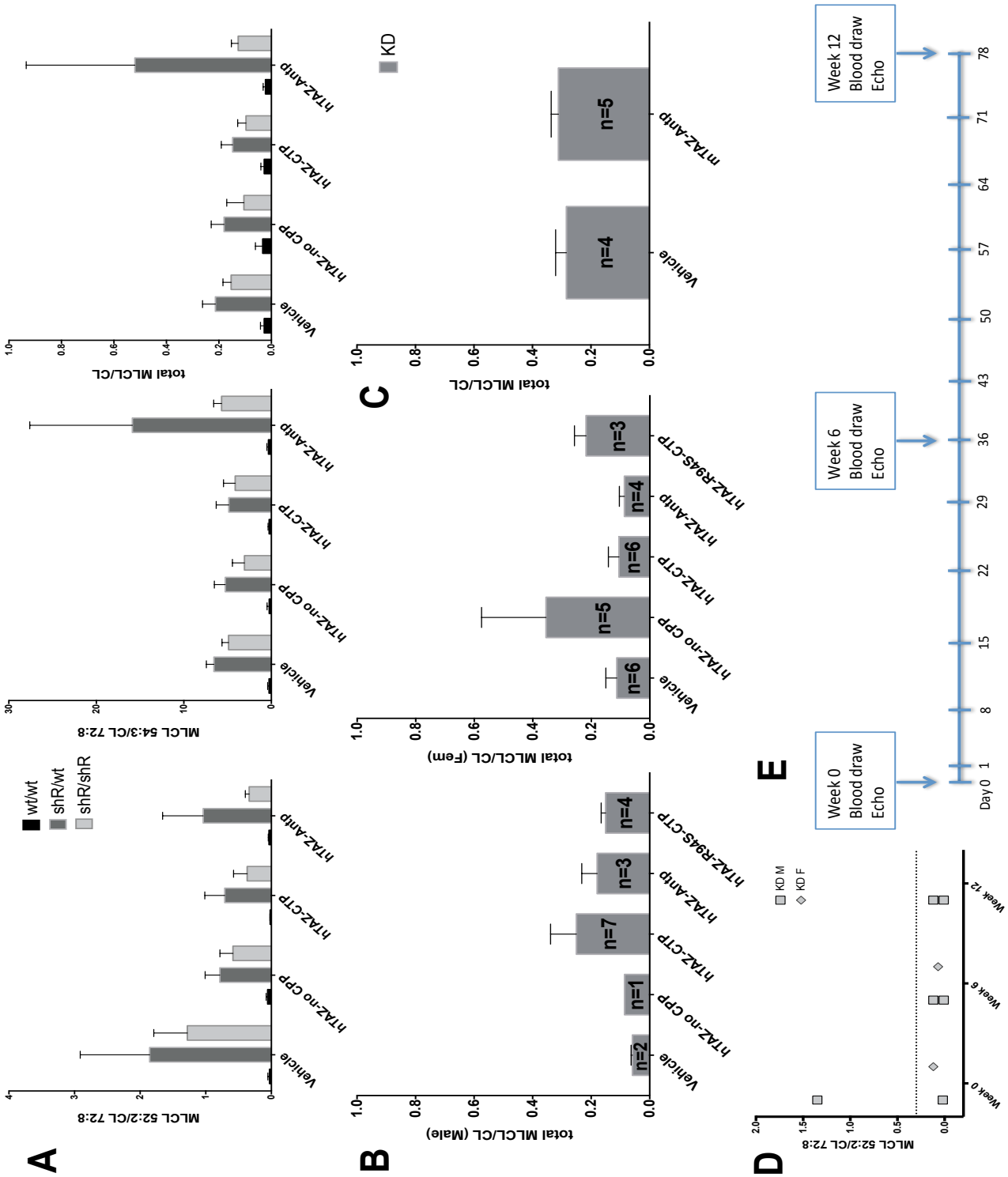

Figure 6-1: Mass spectrometric analysis of lipids in TAZ KD mouse tissues after treatment with recombinant TAZ. **(A)** MLCL 52:2/CL 72:8, MLCL 54:3/CL 72:8 and total MLCL/total CL ratios (left, middle and right panels, respectively) in neonatal cardiac fibroblasts treated with vehicle or a recombinant protein (n=3 for wt/wt and n=7 for shR/wt and shR/shR, except for hTAZ, where n=2 for wt and n=3 for shR/shR). No difference was observed between vehicle and any of the protein treated cells. Total MLCL/total CL ratio of 10 week old male (left panel) and female (right panel) heart muscle (B) and soleus muscle (C) from TAZ KD mice treated with vehicle or a recombinant protein. There was no statistically significant difference between any of the treatment conditions. (D) Bloodspot assay of TAZ KD mouse blood from mice treated with vehicle or hTAZ-CTP according to the treatment schematic in (F). Statistical significance was determined with Welch's t-test ($p<0.05$) and error bars indicate SEM values.

6.1 Effect of recombinant TAZ treatment on Cardiolipin Profile Following Treatment with Recombinant TAZ

6.1.1 CL Species in TAZ KO Cardiomyoblasts Remain Unchanged

TAZ KO H9c2 cells demonstrated a severe defect in CL remodeling, consistent with the complete lack of TAZ protein in these cells. An experiment treating TAZ KO cells in culture for 16 days continuously with hTAZ-CTP did not significantly reduce the MLCL/CL ratio compared to vehicle treated cells (data not shown).

6.1.2 TAZ Treatment May Ameliorate CL Defects in Cardiac Fibroblasts

Cardiac fibroblasts demonstrated significant impairment in CL remodeling. To determine whether exogenous protein treatment can correct the CL defects associated with TAZ deficiency, WT and heterozygous and homozygous TAZ KD cardiac fibroblasts were treated with vehicle or 5 μg/ml of recombinant hTAZ protein for 6 days. hTAZ contained either one of two cell penetrating peptides, CTP and Antp, or no CPP at all. The protein was delivered directly in the culture media, which was refreshed every 48 hours. Both hTAZ-CTP and hTAZ-Antp appeared to reduce the MLCL 52:2/CL 72:8 ratio in homozygous KD cells, however, this effect did not reach statistical significance (Figure 6-1, A). Treatment with hTAZ appeared to slightly reduce the MLCL/CL ratios, but did not lead to any measurable changes. No difference was seen in the MLCL/CL ratios of WT cells after being treated with exogenous TAZ.

6.1.3 Examination of Heart and Soleus CL Species Following Treatment with TAZ

The total MLCL/CL ratio in TAZ KD mouse hearts was higher than that in WT counterparts, although CL remodeling defects were not as severe as seen with the cultured fibroblasts. To determine whether treatment with exogenous TAZ could improve CL remodeling, 9-week-old mice were treated with vehicle or 100 μg of hTAZ-CTP or hTAZ-Antp protein daily, for 8 days. Mice treated with hTAZ containing no CPP were also examined. Data from cultured cells

showed hTAZ is able to enter cells, however it is unclear whether the same holds true in tissues as the available antibodies are not able to detect TAZ in mouse samples.

Treatment with hTAZ with no CPP did not lead to any improvement. Although *in vitro* experiments show uptake of hTAZ in cultured cells, this may not necessarily occur *in vivo* as well. In females, treatment with hTAZ-Antp had a small impact on the ratio of MLCL/CL compared to vehicle, however, no significant differences were evident among the different groups (Figure 6-1, B). Treatment with hTAZ-R94S-CTP, a TAZ containing a mutation predicted to result in catalytic inactivity, did not have an impact on CL profiles.

Similarly, no differences were observed in CL content in soleus muscles following treatment with mTAZ-Antp (Figure 6-1, C).

6.1.4 Investigation of CL Remodeling by Bloodspot Assay After Long Term Treatment with TAZ

Given the previous results, we reasoned it is possible that 8 days are not a sufficient amount of time for CL remodeling to occur to a noticeable degree *in vivo*. A long-term protein treatment protocol was therefore designed, with multiple assessment points, to interrogate the kinetics of TAZ CL remodeling. TAZ mice were treated with 40 μg hTAZ-CTP, weekly, for 12 weeks (schematic in Figure 6-1, E). Blood samples were acquired before the start of treatment (baseline), after 6 weeks and after 12 weeks of treatment. CL species were measured using a well established bloodspot mass spectrometry protocol, developed to determine the CL composition in patients suspected of BTHS [156]. Of the three mice being treated, one was sacrificed after 6 weeks, as it was exhibiting severe breathing impairments.

Only one of the three animals had a significantly elevated MLCL/CL ratio, while the other two, including the mouse that had to be sacrificed early, had ratios similar to WT mouse levels.

MLCL/CL ratio in the mouse with a high baseline normalized after treatment with hTAZ-CTP. The other two mice continued to show very low ratios (Figure 6-1, D).

6.2 TAZ Treatment Increases OCR in 10-Week Old Female Mice

TAZ KD male and female hearts from 10-week-old mice showed significantly lower OCR compared to their wild type littermates when utilizing complex II substrates. To determine the ability of recombinant TAZ to rescue this respiration defect, mice were treated retro-orbitally with vehicle or 100 μg protein (hTAZ, hTAZ-Antp, hTAZ-CTP or hTAZ-R94S-CTP) every day for 8 days. Mice were then sacrificed and the hearts were harvested, homogenized and mitochondrial respiration was tested using glutamate, pyruvate and succinate as substrates.

TAZ protein administration did not affect OCR in the male homogenized hearts, however it did reduce rates in WT females when using complex II substrates. hTAZ containing no CPP, hTAZ-CTP, hTAZ-Antp and the point mutant hTAZ-R94S-CTP all significantly reduced OCR in this cohort. In contrast, treatment with both hTAZ-CTP and hTAZ-Antp, but not hTAZ, seemed to positively impact OCR in KD females when utilizing complex II substrate, although not significantly so (Figure 6-2, B). Similarly, both hTAZ-Antp and hTAZ-CTP tended to increase OCR in TAZ KD females when utilizing complex I substrates, which had not shown an appreciable decrease in TAZ KD mice (Figure 6-2, A). No difference was observed in males between the different treatment groups.

Assessment of mitochondrial respiration in permeabilized soleus muscle showed similar OCR levels between WT and TAZ KD samples. Unsurprisingly, exogenous TAZ treatment did not significantly affect OCR (Figure 6-2, C-D).

6.3 Training Increases Exercise Capacity in the TAZ KD mouse

To assess recombinant TAZ's ability to ameliorate exercise capacity impairments, TAZ KD and WT littermates were treated retro-orbitally with vehicle or 100 μg mTAZ-Antp every day for 8 days, then tested on a treadmill. The maximal distance the mice could run before becoming exhausted was assessed both prior to and after the treatment period. At baseline, TAZ KD mice reached exhaustion much sooner than WT mice. Upon re-testing after the treatment period, both WT and TAZ KD mice showed noticeable increases in running distance, likely an effect of increased familiarity with the task. No difference in running distance was noted, however, between vehicle and protein treated animals. Moreover, there was no longer a significant difference between WT and TAZ KD mice treated with vehicle.

6.4 Conclusions and Discussion

This chapter examines the effects of exogenous TAZ protein treatment on the phenotypes associated with TAZ deficiency. While differences in CL remodeling between WT and KD animals were seen at baseline, approximately one week of treatment with recombinant TAZ, with either CTP or Antp, did not result in significant remodeling of the defective CL species. A small reduction in the MLCL/CL ratio was noted when treating fibroblasts, possibly due to more direct access of the protein to its target. This accentuates the need to develop a treatment protocol based on protein kinetics *in vivo*, which has been challenging, as the commercially available antibodies do not detect endogenous or exogenous TAZ in mouse tissues [93]. To circumvent this, we attempted to measure exogenous protein levels in tissues by mass spectrometry and were able to detect a peptide unique to human TAZ in mouse serum (data not shown), however the amount present was below the limit of quantification. As endogenous TAZ is low enough to go undetected by antibodies, it stood to reason that it is possible to achieve therapeutic doses in mice that are not detectable by WB and that treatment could be optimized by the important biochemical read out of CL remodeling status.

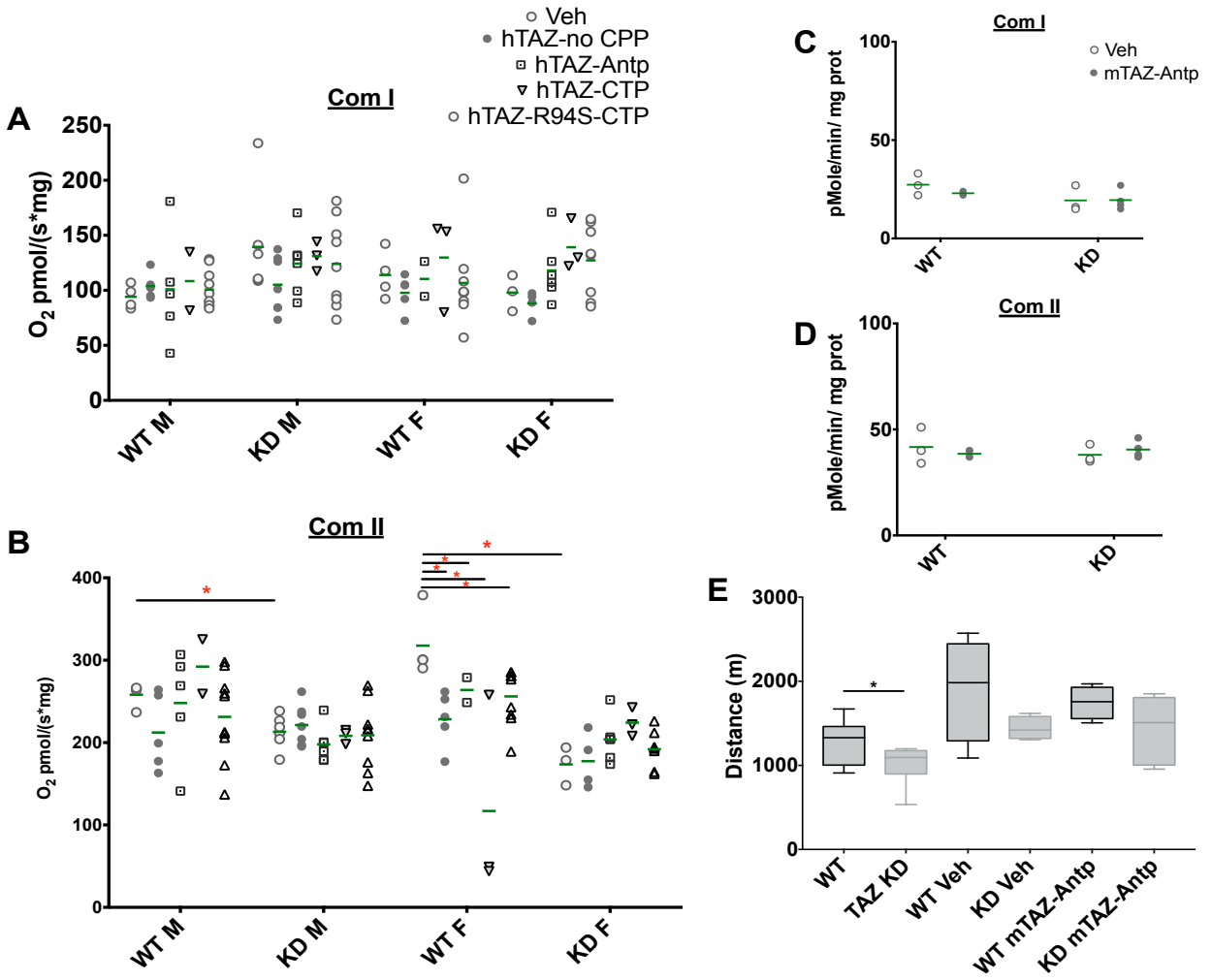

Figure 6-2: Mitochondrial respiration and treadmill performance in mice treated with recombinant protein. **(A-B)** OCR in heart homogenates from 10 week old mice treated with vehicle or a recombinant protein, using substrates for complex I (A) and complex II (B). Vehicle treated TAZ KD males and females had significantly lower OCR with complex II substrates and WT females experienced a significant reduction in OCR with all protein treatments. **(C-D)** OCR in permeabilized soleus muscle from 2 month old mice treated with vehicle or mTAZ-Antp. **(E)** Treadmill running distances for mice treated with either vehicle or mTAZ-Antp. No difference was observed between vehicle and protein treated mice in (B) and (C). Statistical significance was determined using t-test with a Holm-Sidak correction (n=4 for all, except KD with mTAZ-Antp, where n=5, *$p<0.05$). Horizontal bars indicate means (A and B, green) and median in (C).

A long-term treatment regimen was designed, with a new protocol for measuring CL in bloodspots, which allowed for multiple sampling from the same mouse without requiring sacrifice of the animal. Data from biochemical experiments with TAZ uptake in cell culture suggested that TAZ levels in mitochondria are highly regulated and excess protein is rapidly removed (Chapter III). To avoid oversaturating the mitochondria with exogenous TAZ during a long treatment period, mice

were treated with a lower dose of TAZ than they had been for the 8-day experiments and on a more infrequent basis. This regimen more closely resembles dosing seen with approved infused ERTs, such as elosulphase and ß-algasidase [166]. Mass spectrometric analysis of baseline bloodspots showed only one of the mice had an elevated MLCL/CL ratio, which is reminiscent of the mild CL phenotype seen with heart tissue. Prolonged treatment with TAZ over 6-12 weeks led to a drastic reduction of the MLCL/CL ratio in this mouse, however, it is unclear if this is a true effect of TAZ treatment or the result of an inherent variation in the CL phenotype. A higher number of animals will need to be tested before any conclusions can be drawn.

Recombinant protein treatment seemed to have opposing effects on respiration in WT versus TAZ KD homogenized hearts. WT females experienced a decrease in OCR following protein administration, including the control protein, hTAZ, and the mutant hTAZ-R94-CTP. Since every protein administered had the same effect in these tissues, this points to a general sensitivity to protein administration, rather than a specific TAZ response. It is also possible that the small number of vehicle treated animals represents a skewed subpopulation of WT animals, resulting in an artificial difference between this and the protein treatment conditions.

TAZ KD mice undergoing forced running treadmill tests showed exercise impairment at baseline, but no significant difference when re-tested after protein treatment. Both WT and KD mice had increases in running distances between baseline and the second assessment. This is likely an effect of increased familiarity with the task. These data indicate that the small degree of muscle dysfunction seen in TAZ KD mice at this age can be masked by modest improvements due to extraneous factors.

7 Discussion and Future Directions

Development of a curative therapy for BTHS is a critical need for patients suffering from this devastating disorder. Enzyme replacement therapy is an attractive alternative to gene therapy, as it does not face the same regulatory hurdles. In the absence of a crystal structure, understanding the function of the different domains of TAZ through biochemical and fluorescence studies is crucial for the optimization of an ERT. In the work described here, a novel method for the purification of TAZ, an important step in the study of the protein's structure, is described, and the mitochondrial localization signal for TAZ is elucidated. Along with characterization of existing and new models of TAZ deficiency, evidence is provided for potentially therapeutic effects of hTAZ linked to intracellular delivery cell penetrating peptides.

In Chapter V, evidence is presented of a disconnection between CL levels and mitochondrial function in myoblastic cells lacking TAZ. Work done in stem cells suggests they have poorly developed cristae and mitochondrial networks. This correlates with their demonstrated glycolytic metabolism [167] and the heavy reliance of neonatal hearts on glycolysis, along with low oxidation of both glucose and fatty acids [168]. These findings illustrate the decreased reliance of differentiating cells on mitochondrial respiration and oxidative phosphorylation, potentially obviating a dependence on tetralinoleoyl CL, which was shown to play an important role in cristae morphology [169]. Data presented in Chapter V shows that TAZ KO myoblasts have decreased levels of mature CL compared to WT myoblasts, yet still achieve OCRs similar to WT cells. It is therefore possible that H9C2 myoblasts, both WT and TAZ KO, are reliant on glycolysis for obtaining ATP and the oxidative phosphorylation capacity of these cells is not yet fully developed. In such a scenario, decreased levels of tetralinoleoyl CL would have a minimal impact on respiration. Despite this, TAZ deficiency in the embryonic stages has a clear, negative and profound impact on development, suggesting TAZ may play different roles in proliferating versus quiescent cells [14,59].

The question arises here as to exactly what role does TAZ play in highly proliferative stem cells? A recent study uncovered a new role for TAZ in the suppression of endogenous retrotransposons during germ cell meiosis, although it is unclear whether this was achieved through a direct role of TAZ or through a downstream effect [96]. Others found that TAZ KD in neonatal rat cardiomyocytes and fibroblasts interfered with cell cycle progression, with different effects depending on the cell type [170,171]. It is possible that delivering recombinant TAZ to myoblasts and neonatal fibroblasts could lead to improvements in aspects other than mitochondrial respiration. In the future, measurements of cell proliferation, multiple nucleation and total protein content may reveal beneficial effects of recombinant TAZ administration at a proliferative cellular stage. Given the respiration defects seen in BTHS patient cells, however, the need for an *in vitro* model that demonstrates reduced oxygen utilization to test potential therapeutic agents is clear. Assessment of respiration in differentiated H9c2 TAZ KO cells could expose a defect not seen with undifferentiated myoblasts. Alternatively, given the reduced oxygen consumption documented in patient blood cells [9,172], TAZ KO in HL-60 cells, a promyeloblast cell line, may prove to be a useful model [22].

Cellular uptake of recombinant TAZ was achieved by cloning a cell penetrating peptide in the C-terminus of TAZ, which likely results in endocytosis of the protein. Despite *in vitro* evidence of uptake into cells, isolation of the crude mitochondrial fractions does not rule out the possibility that recombinant TAZ may have reduced lysosomal escape, resulting in its degradation rather than delivery to mitochondrial compartments. The acidic environment within lysosomes could also lead to reduced enzyme activity for the protein that does escape. Measurements of enzyme activity *in vitro* and in mitochondrial extracts from cells treated with recombinant TAZ would be important indicators of the preservation of function.

TAZ deficiency in adults has a demonstrable impact on oxidative phosphorylation, through its effects on CL speciation [6]. In BTHS patients this results in life-threatening cardiomyopathy and skeletal muscle defects, which manifest themselves in the first year of life [13,66]. TAZ KD mice, on the other hand, have been shown to develop skeletal and cardiac muscle defects much later in life, at 2 and 8 months, respectively [68]. Taken together, these data indicate that the presence of a small amount TAZ protein can significantly ameliorate organ dysfunction resultant from TAZ deficiency, making ERT a promising therapy. It is important to note, however, that not having a reliable direct method for quantification of the amount of endogenous or exogenous protein in the tissues of treated TAZ KD mice, it is difficult to ascertain whether the amount of therapeutic protein delivered surpasses the endogenous protein still present. This could be a reason why a stronger effect of ERT in the TAZ KD mouse model is not observed. Development of more sensitive mass spectrometry methods for quantification of endogenous and exogenous TAZ in the tissues of treated animals could shed light on this.

Previous studies assessing mitochondrial respiration in the hearts of TAZ KD mice did so by measuring oxygen consumption in isolated heart mitochondria [95,151]. In the experiments presented in Chapter VI, measurements were done with crude homogenates, which may have affected the assays. Assessment of oxygen consumption in isolated mitochondria from mice treated with protein could lead to different results, as it would equalize the amount of mitochondria between the two genotypes.

While the TAZ KD mouse shares some features with symptoms documented in BTHS patients, this model fundamentally differs from the human disease both in severity and progression of symptoms. The poor ability to mimic human disorder and the variability of phenoptype seen in this mouse make it hard to assess the therapeutic efficacy of recombinant TAZ. Rescue experiments in a complete TAZ KO mouse, which has recently been developed, may prove much more

efficacious. In addition, examination of the effects of long term recombinant TAZ administration, with different doses of protein, would more clearly establish a therapeutic window for the ERT.

Significant work remains to be done, however, the groundwork to develop an ERT for the devastating cardiomyopathic disorder, Barth Syndrome, has been laid out. We are hopeful that optimization of therapeutic windows and doses, along with a true KO mouse model (generously shared by Douglas Strathdee from the Transgenic Technology Laboratory, Beatson Institute, UK) will lead to the successful development of a recombinant TAZ therapeutic.

8 References

1. Barth PG.; Scholte HR.; Berden JA.; Van der Klei-Van Moorsel JM.; Luyt-Houwen IE.; Van 't Veer-Korthof ET.; et al. An X-linked mitochondrial disease affecting cardiac muscle, skeletal muscle and neutrophil leucocytes. *J. Neurol. Sci.,* **1983**, 62, 327–55.
2. Barth PG.; Valianpour F.; Bowen VM.; Lam J.; Duran M.; Vaz FM.; et al. X-linked cardioskeletal myopathy and neutropenia (Barth syndrome): an update. *Am. J. Med. Genet. A,* **2004**, 126A, 349–54. doi: 10.1002/ajmg.a.20660
3. Jefferies JL. Barth syndrome. *Am. J. Med. Genet. C. Semin. Med. Genet.,* **2013**, 163C, 198–205. doi: 10.1002/ajmg.c.31372
4. Bione S.; D'Adamo P.; Maestrini E.; Gedeon AK.; Bolhuis PA.; and Toniolo D. A novel X-linked gene, G4.5. is responsible for Barth syndrome. *Nat. Genet.,* **1996**, 12, 385–9. doi: 10.1038/ng0496-385
5. Aprikyan A a.; and Khuchua Z. Advances in the understanding of Barth syndrome. *Br. J. Haematol.,* **2013**, 161, 330–8. doi: 10.1111/bjh.12271
6. Houtkooper RH.; Turkenburg M.; Poll-The BT.; Karall D.; Pérez-Cerdá C.; Morrone A.; et al. The enigmatic role of tafazzin in cardiolipin metabolism. *Biochim. Biophys. Acta - Biomembr.,* **2009**, 1788, 2003–14.
7. Hauff KD.; and Hatch GM. Cardiolipin metabolism and Barth Syndrome. *Prog. Lipid Res.,* **2006**, 45, 91–101. doi: 10.1016/j.plipres.2005.12.001
8. Dudek J.; Cheng I-F.; Balleininger M.; Vaz FMFM.; Streckfuss-Bömeke K.; Hübscher D.; et al. Cardiolipin deficiency affects respiratory chain function and organization in an induced pluripotent stem cell model of Barth syndrome. *Stem Cell Res.,* Elsevier B.V.; **2013**, 11, 806–19. doi: 10.1016/j.scr.2013.05.005
9. Gonzalvez F.; D'Aurelio M.; Boutant M.; Moustapha A.; Puech J-P.; Landes T.; et al. Barth syndrome: cellular compensation of mitochondrial dysfunction and apoptosis inhibition due to changes in cardiolipin remodeling linked to tafazzin (TAZ) gene mutation. *Biochim. Biophys. Acta,* Elsevier B.V.; **2013**, 1832, 1194–206. doi: 10.1016/j.bbadis.2013.03.005
10. Barth Syndrome Foundation. FAQs [Internet]. [cited 2017 Sep 1].
11. Rigaud C.; Lebre A-S.; Touraine R.; Beaupain B.; Ottolenghi C.; Chabli A.; et al. Natural history of Barth syndrome: a national cohort study of 22 patients. *Orphanet J. Rare Dis.,* **2013**, 8, 70. doi: 10.1186/1750-1172-8-70
12. Cantlay AM.; Shokrollahi K.; Allen JT.; Lunt PW.; Newbury-Ecob RA.; and Steward CG. Genetic analysis of the G4.5 gene in families with suspected Barth syndrome. *J. Pediatr.,* **1999**, 135, 311–5. doi: 10.1016/s0022-3476(99)70126-5
13. Clarke SLN.; Bowron A.; Gonzalez IL.; Groves SJ.; Newbury-Ecob R.; Clayton N.; et al. Barth syndrome. *Orphanet J. Rare Dis.,* **2013**, 8, 23. doi: 10.1186/1750-1172-8-23
14. Steward CG.; Newbury-Ecob RA.; Hastings R.; Smithson SF.; Tsai-Goodman B.; Quarrell OW.; et al. Barth syndrome: an X-linked cause of fetal cardiomyopathy and stillbirth. *Prenat. Diagn.,* **2010**, 30, 970–6. doi: 10.1002/pd.2599
15. Spencer CT.; Bryant RM.; Day J.; Gonzalez IL.; Colan SD.; Thompson WR.; et al. Cardiac and clinical phenotype in Barth syndrome. *Pediatrics,* **2006**, 118, e337–46. doi: 10.1542/peds.2005-2667
16. Roberts AE.; Nixon C.; Steward CG.; Gauvreau K.; Maisenbacher M.; Fletcher M.; et al. The Barth Syndrome Registry: Distinguishing disease characteristics and growth data from a longitudinal study. *Am. J. Med. Genet. Part A,* Wiley Subscription Services, Inc., A Wiley Company; **2012**, 158A, 2726–32. doi: 10.1002/ajmg.a.35609
17. Kang S-L.; Forsey J.; Dudley D.; Steward CG.; and Tsai-Goodman B. Clinical Characteristics

and Outcomes of Cardiomyopathy in Barth Syndrome: The UK Experience. *Pediatr. Cardiol.,* Springer US; **2016**, 37, 167–76. doi: 10.1007/s00246-015-1260-z
18. D'Adamo P.; Fassone L.; Gedeon A.; Janssen EAM.; Bione S.; Bolhuis PA.; et al. The X-Linked Gene G4.5 Is Responsible for Different Infantile Dilated Cardiomyopathies. *Am. J. Hum. Genet.,* **1997**, 61, 862–7. doi: 10.1086/514886
19. Yancy CW.; Jessup M.; Bozkurt B.; Butler J.; Casey DE.; Drazner MH.; et al. 2013 ACCF/AHA guideline for the management of heart failure: a report of the American College of Cardiology Foundation/American Heart Association Task Force on practice guidelines. *Circulation,* American Heart Association, Inc.; **2013**, 128, e240-327. doi: 10.1161/cir.0b013e31829e8776
20. Adès LC.; Gedeon AK.; Wilson MJ.; Latham M.; Partington MW.; Mulley JC.; et al. Barth syndrome: Clinical features and confirmation of gene localisation to distal Xq28. *Am. J. Med. Genet.,* Wiley Subscription Services, Inc., A Wiley Company; **1993**, 45, 327–34. doi: 10.1002/ajmg.1320450309
21. Neustein HB.; Lurie PR.; Dahms B.; and Takahashi M. An X-linked recessive cardiomyopathy with abnormal mitochondria. ***Pediatrics.,*** 1979. p. 24–9.
22. Saric A.; Andreau K.; Armand A-S.; Møller IM.; and Petit PX. Barth Syndrome: From Mitochondrial Dysfunctions Associated with Aberrant Production of Reactive Oxygen Species to Pluripotent Stem Cell Studies. *Front. Genet.,* Frontiers Media SA; **2015**, 6, 359. doi: 10.3389/fgene.2015.00359
23. Finsterer J.; Stöllberger C.; and Towbin JA. Left ventricular noncompaction cardiomyopathy: cardiac, neuromuscular, and genetic factors. *Nat. Publ. Gr.,* **2017**, 14, doi: 10.1038/nrcardio.2016.207
24. Pignatelli RH.; McMahon CJ.; Dreyer WJ.; Denfield SW.; Price J.; Belmont JW.; et al. Clinical Characterization of Left Ventricular Noncompaction in Children. *Circulation,* **2003**, 108,
25. Hanke SP.; Gardner AB.; Lombardi JP.; Manning PB.; Nelson DP.; Towbin JA.; et al. Left Ventricular Noncompaction Cardiomyopathy in Barth Syndrome: An Example of an Undulating Cardiac Phenotype Necessitating Mechanical Circulatory Support as a Bridge to Transplantation. *Pediatr. Cardiol.,* Springer-Verlag; **2012**, 33, 1430–4. doi: 10.1007/s00246-012-0258-z
26. Weber KT.; and Brilla CG. Pathological hypertrophy and cardiac interstitium. Fibrosis and renin-angiotensin-aldosterone system. *Circulation,* American Heart Association, Inc.; **1991**, 83, 1849–65. doi: 10.1161/01.cir.83.6.1849
27. GOFFART S.; VONKLEISTRETZOW J.; and WIESNER R. Regulation of mitochondrial proliferation in the heart: power-plant failure contributes to cardiac failure in hypertrophy. *Cardiovasc. Res.,* Oxford University Press; **2004**, 64, 198–207. doi: 10.1016/j.cardiores.2004.06.030
28. Thomas JD.; and Popović ZB. Assessment of Left Ventricular Function by Cardiac Ultrasound. *J. Am. Coll. Cardiol.,* Journal of the American College of Cardiology; **2006**, 48, 2012–25. doi: 10.1016/j.jacc.2006.06.071
29. Spencer CT.; Byrne BJ.; Gewitz MH.; Wechsler SB.; Kao AC.; Gerstenfeld EP.; et al. Ventricular Arrhythmia in the X-linked Cardiomyopathy Barth Syndrome. *Pediatr. Cardiol.,* Springer-Verlag; **2005**, 26, 632–7. doi: 10.1007/s00246-005-0873-z
30. Liu Y.; Sato T.; O'Rourke B.; and Marban E. Mitochondrial ATP-dependent potassium channels: novel effectors of cardioprotection? *Circulation,* American Heart Association, Inc.; **1998**, 97, 2463–9. doi: 10.1161/01.cir.97.24.2463
31. Spencer CT.; Byrne BJ.; Bryant RM.; Margossian R.; Maisenbacher M.; Breitenger P.; et al.

Impaired cardiac reserve and severely diminished skeletal muscle O_2 utilization mediate exercise intolerance in Barth syndrome. *Am. J. Physiol. Heart Circ. Physiol.,* American Physiological Society; **2011**, 301, H2122-9. doi: 10.1152/ajpheart.00479.2010
32. Steward CG.; Groves SJ.; Taylor CL.; Maisenbacher MK.; Versluys B.; Newbury-Ecob R.; et al. Barth Syndrome: An Under-Recognized Cause of Chronic Neutropenia. *Blood,* **2015**, 126,
33. Hauck F.; and Klein C. Pathogenic mechanisms and clinical implications of congenital neutropenia syndromes. doi: 10.1097/aci.0000000000000014
34. Kuijpers TW.; Maianski NA.; Tool ATJ.; Becker K.; Plecko B.; Valianpour F.; et al. Neutrophils in Barth syndrome (BTHS) avidly bind annexin-V in the absence of apoptosis. *Blood,* **2004**, 103,
35. van Raam BJ.; and Kuijpers TW. Mitochondrial defects lie at the basis of neutropenia in Barth syndrome. *Curr. Opin. Hematol.,* **2009**, 16, 14–9. doi: 10.1097/moh.0b013e32831c83f3
36. Collins S.; Bolyard AA.; Marrero TM.; Phan L.; and Dale DC. Barth Syndrome and Severe Chronic Neutropenia. *Blood,* **2015**, 116,
37. Makaryan V.; Kulik W.; Vaz FM.; Allen C.; Dror Y.; Dale DC.; et al. The cellular and molecular mechanisms for neutropenia in Barth syndrome. *Eur. J. Haematol.,* NIH Public Access; **2012**, 88, 195–209. doi: 10.1111/j.1600-0609.2011.01725.x
38. Su B.; and Ryan RO. Metabolic biology of 3-methylglutaconic acid-uria: a new perspective. *J. Inherit. Metab. Dis.,* Springer Netherlands; **2014**, 37, 359–68. doi: 10.1007/s10545-013-9669-0
39. Ikon N.; and Ryan RO. Barth Syndrome: Connecting Cardiolipin to Cardiomyopathy. *Lipids,* Springer Berlin Heidelberg; **2017**, 52, 99–108. doi: 10.1007/s11745-016-4229-7
40. Yen T-Y.; Hwu W-L.; Chien Y-H.; Wu M-H.; Lin M-T.; Tsao L-Y.; et al. Acute metabolic decompensation and sudden death in Barth syndrome: report of a family and a literature review. *Eur. J. Pediatr.,* Springer-Verlag; **2008**, 167, 941–4. doi: 10.1007/s00431-007-0592-y
41. Ørstavik KH.; Ørstavik RE.; Naumova AK.; D'Adamo P.; Gedeon A.; Bolhuis PA.; et al. X Chromosome Inactivation in Carriers of Barth Syndrome. *Am. J. Hum. Genet.,* **1998**, 63, 1457–63. doi: 10.1086/302095
42. Bissler JJ.; Tsoras M.; Göring HHH.; Hug P.; Chuck G.; Tombragel E.; et al. Infantile dilated X-linked cardiomyopathy, G4.5 mutations, altered lipids, and ultrastructural malformations of mitochondria in heart, liver, and skeletal muscle. *Lab. Invest.,* **2002**, 82, 335–44.
43. Acehan D.; Xu Y.; Stokes DL.; and Schlame M. Comparison of lymphoblast mitochondria from normal subjects and patients with Barth syndrome using electron microscopic tomography. *Lab. Invest.,* NIH Public Access; **2007**, 87, 40–8. doi: 10.1038/labinvest.3700480
44. Xu Y.; Sutachan JJ.; Plesken H.; Kelley RI.; and Schlame M. Characterization of lymphoblast mitochondria from patients with Barth syndrome. *Lab. Investig.,* Nature Publishing Group; **2005**, 85, 823–30. doi: 10.1038/labinvest.3700274
45. McKenzie M.; Lazarou M.; Thorburn DR.; and Ryan MT. Mitochondrial respiratory chain supercomplexes are destabilized in Barth Syndrome patients. *J. Mol. Biol.,* **2006**, 361, 462–9. doi: 10.1016/j.jmb.2006.06.057
46. Barth PG.; Wanders RJ.; Vreken P.; Janssen EA.; Lam J.; and Baas F. X-linked cardioskeletal myopathy and neutropenia (Barth syndrome): respiratory-chain abnormalities in cultured fibroblasts. *J. Inherit. Metab. Dis.,* **1996**, 22, 555–67.
47. Schlame M.; Kelley RI.; Feigenbaum A.; Towbin JA.; Heerdt PM.; Schieble T.; et al. Phospholipid abnormalities in children with Barth syndrome. *J. Am. Coll. Cardiol.,* **2003**, 42, 1994–9.
48. Schlame M.; Towbin JA.; Heerdt PM.; Jehle R.; DiMauro S.; and Blanck TJJ. Deficiency of tetralinoleoyl-cardiolipin in Barth syndrome. *Ann. Neurol.,* **2002**, 51, 634–7. doi:

10.1002/ana.10176
49. Xu Y.; Zhang S.; Malhotra A.; Edelman-Novemsky I.; Ma J.; Kruppa A.; et al. Characterization of tafazzin splice variants from humans and fruit flies. *J. Biol. Chem.,* **2009**, 284, 29230–9. doi: 10.1074/jbc.m109.016642
50. Vaz FM.; Houtkooper RH.; Valianpour F.; Barth PG.; and Wanders RJA. Only one splice variant of the human TAZ gene encodes a functional protein with a role in cardiolipin metabolism. *J. Biol. Chem.,* American Society for Biochemistry and Molecular Biology; **2003**, 278, 43089–94. doi: 10.1074/jbc.m305956200
51. Hijikata A.; Yura K.; Ohara O.; and Go M. Structural and functional analyses of Barth syndrome-causing mutations and alternative splicing in the tafazzin acyltransferase domain. *Meta gene,* Elsevier B.V.; **2015**, 4, 92–106. doi: 10.1016/j.mgene.2015.04.001
52. Claypool SM.; Boontheung P.; McCaffery JM.; Loo JA.; and Koehler CM. The cardiolipin transacylase, tafazzin, associates with two distinct respiratory components providing insight into Barth syndrome. *Mol. Biol. Cell,* **2008**, 19, 5143–55. doi: 10.1091/mbc.e08-09-0896
53. Liu J.; Faeder JR.; and Camacho CJ. Toward a quantitative theory of intrinsically disordered proteins and their function. *Proc. Natl. Acad. Sci. U. S. A.,* **2009**, 106, 19819–23. doi: 10.1073/pnas.0907710106
54. Claypool SM.; Whited K.; Srijumnong S.; Han X.; and Koehler CM. Barth syndrome mutations that cause tafazzin complex lability. *J. Cell Biol.,* **2011**, 192, 447–62. doi: 10.1083/jcb.201008177
55. Lu Y-W.; Galbraith L.; Herndon JD.; Lu Y-L.; Pras-Raves M.; Vervaart M.; et al. Defining functional classes of Barth syndrome mutation in humans. *Hum. Mol. Genet.,* Oxford University Press; **2016**, 25, 1754–70. doi: 10.1093/hmg/ddw046
56. Claypool SM.; McCaffery JM.; and Koehler CM. Mitochondrial mislocalization and altered assembly of a cluster of Barth syndrome mutant tafazzins. *J. Cell Biol.,* **2006**, 174, 379–90. doi: 10.1083/jcb.200605043
57. Whited K.; Baile MG.; Currier P.; and Claypool SM. Seven functional classes of Barth syndrome mutation. doi: 10.1093/hmg/dds447
58. Xu Y.; Malhotra A.; Claypool SM.; Ren M.; and Schlame M. Tafazzins from Drosophila and mammalian cells assemble in large protein complexes with a short half-life. *Mitochondrion,* **2015**, 21, 27–32. doi: 10.1016/j.mito.2015.01.002
59. Khuchua Z.; Yue Z.; Batts L.; and Strauss AW. A zebrafish model of human Barth syndrome reveals the essential role of tafazzin in cardiac development and function. *Circ. Res.,* **2006**, 99, 201–8. doi: 10.1161/01.res.0000233378.95325.ce
60. Xu Y.; Kelley RI.; Blanck TJJ.; and Schlame M. Remodeling of cardiolipin by phospholipid transacylation. *J. Biol. Chem.,* **2003**, 278, 51380–5. doi: 10.1074/jbc.m307382200
61. Xu Y.; Malhotra A.; Ren M.; and Schlame M. The enzymatic function of tafazzin. *J. Biol. Chem.,* **2006**, 281, 39217–24. doi: 10.1074/jbc.m606100200
62. Schlame M.; Acehan D.; Berno B.; Xu Y.; Valvo S.; Ren M.; et al. The physical state of lipid substrates provides transacylation specificity for tafazzin. *Nat. Chem. Biol.,* Nature Publishing Group, a division of Macmillan Publishers Limited. All Rights Reserved.; **2012**, 8, 862–9. doi: 10.1038/nchembio.1064
63. Schlame M. Thematic Review Series: Glycerolipids. Cardiolipin synthesis for the assembly of bacterial and mitochondrial membranes. *J. Lipid Res.,* **2008**, 49, 1607–20. doi: 10.1194/jlr.r700018-jlr200
64. Mejia EM.; Nguyen H.; and Hatch GM. Mammalian cardiolipin biosynthesis. *Chem. Phys. Lipids,* **2014**, 179, 11–6. doi: 10.1016/j.chemphyslip.2013.10.001
65. Claypool SM.; and Koehler CM. The complexity of cardiolipin in health and disease. ***Trends***

Biochem. Sci., 2012. p. 32–41. doi: 10.1016/j.tibs.2011.09.003
66. Helms B.; van Meer G.; Schlame M.; and Ren M. Barth syndrome, a human disorder of cardiolipin metabolism. *FEBS Lett.,* **2006**, 580, 5450–5.
67. Chen R.; Tsuji T.; Ichida F.; Bowles KR.; Yu X.; Watanabe S.; et al. Mutation analysis of the G4.5 gene in patients with isolated left ventricular noncompaction. *Mol. Genet. Metab.,* **2002**, 77, 319–25. doi: 10.1016/s1096-7192(02)00195-6
68. Acehan D.; Vaz F.; Houtkooper RH.; James J.; Moore V.; Tokunaga C.; et al. Cardiac and skeletal muscle defects in a mouse model of human Barth syndrome. *J. Biol. Chem.,* **2011**, 286, 899–908. doi: 10.1074/jbc.m110.171439
69. Xu Y.; Condell M.; Plesken H.; Edelman-Novemsky I.; Ma J.; Ren M.; et al. A Drosophila model of Barth syndrome. *Proc. Natl. Acad. Sci. U. S. A.,* **2006**, 103, 11584–8. doi: 10.1073/pnas.0603242103
70. Han X.; Yang J.; Yang K.; Zhao Z.; Abendschein DR.; and Gross RW. Alterations in myocardial cardiolipin content and composition occur at the very earliest stages of diabetes: a shotgun lipidomics study. *Biochemistry,* **2007**, 46, 6417–28. doi: 10.1021/bi7004015
71. Lesnefsky EJ.; Minkler P.; and Hoppel CL. Enhanced modification of cardiolipin during ischemia in the aged heart. *J. Mol. Cell. Cardiol.,* **2009**, 46, 1008–15. doi: 10.1016/j.yjmcc.2009.03.007
72. Claypool SM. Cardiolipin, a critical determinant of mitochondrial carrier protein assembly and function. *Biochim. Biophys. Acta,* **2009**, 1788, 2059–68. doi: 10.1016/j.bbamem.2009.04.020
73. Raja V.; and Greenberg ML. The functions of cardiolipin in cellular metabolism-potential modifiers of the Barth syndrome phenotype. *Chem. Phys. Lipids,* **2014**, 179, 49–56. doi: 10.1016/j.chemphyslip.2013.12.009
74. Li X-X.; Tsoi B.; Li Y-F.; Kurihara H.; and He R-R. Cardiolipin and Its Different Properties in Mitophagy and Apoptosis. *J. Histochem. Cytochem.,* **2015**, 0022155415574818-. doi: 10.1369/0022155415574818
75. Ren M.; Phoon CKL.; and Schlame M. Metabolism and function of mitochondrial cardiolipin. *Prog. Lipid Res.,* **2014**, 55, 1–16. doi: 10.1016/j.plipres.2014.04.001
76. Pfeiffer K.; Gohil V.; Stuart RA.; Hunte C.; Brandt U.; Greenberg ML.; et al. Cardiolipin stabilizes respiratory chain supercomplexes. *J. Biol. Chem.,* **2003**, 278, 52873–80. doi: 10.1074/jbc.m308366200
77. Haines TH.; and Dencher NA. Cardiolipin: a proton trap for oxidative phosphorylation. *FEBS Lett.,* **2002**, 528, 35–9. doi: 10.1016/s0014-5793(02)03292-1
78. Schägger H.; and Pfeiffer K. Supercomplexes in the respiratory chains of yeast and mammalian mitochondria. *EMBO J.,* EMBO Press; **2000**, 19, 1777–83. doi: 10.1093/emboj/19.8.1777
79. Maranzana E.; Barbero G.; Falasca AI.; Lenaz G.; and Genova ML. Mitochondrial respiratory supercomplex association limits production of reactive oxygen species from complex I. *Antioxid. Redox Signal.,* **2013**, 19, 1469–80. doi: 10.1089/ars.2012.4845
80. He Q.; Harris N.; Ren J.; and Han X. Mitochondria-targeted antioxidant prevents cardiac dysfunction induced by tafazzin gene knockdown in cardiac myocytes. *Oxid. Med. Cell. Longev.,* **2014**, 2014, 654198. doi: 10.1155/2014/654198
81. Wang G.; McCain ML.; Yang L.; He A.; Pasqualini FS.; Agarwal A.; et al. Modeling the mitochondrial cardiomyopathy of Barth syndrome with induced pluripotent stem cell and heart-on-chip technologies. *Nat. Med.,* **2014**, 20, 616–23. doi: 10.1038/nm.3545
82. Bayir H.; Fadeel B.; Palladino MJ.; Witasp E.; Kurnikov I V.; Tyurina YY.; et al. Apoptotic interactions of cytochrome c: redox flirting with anionic phospholipids within and outside of mitochondria. *Biochim. Biophys. Acta,* **2006**, 1757, 648–59. doi: 10.1016/j.bbabio.2006.03.002

83. Li P.; Nijhawan D.; Budihardjo I.; Srinivasula SM.; Ahmad M.; Alnemri ES.; et al. Cytochrome c and dATP-dependent formation of Apaf-1/caspase-9 complex initiates an apoptotic protease cascade. *Cell,* **1997**, 91, 479–89.
84. Kapralov AA.; Yanamala N.; Tyurina YY.; Castro L.; Samhan-Arias A.; Vladimirov YA.; et al. Topography of tyrosine residues and their involvement in peroxidation of polyunsaturated cardiolipin in cytochrome c/cardiolipin peroxidase complexes. *Biochim. Biophys. Acta,* NIH Public Access; **2011**, 1808, 2147–55. doi: 10.1016/j.bbamem.2011.04.009
85. Kagan VE.; Borisenko GG.; Tyurina YY.; Tyurin VA.; Jiang J.; Potapovich AI.; et al. Oxidative lipidomics of apoptosis: redox catalytic interactions of cytochrome c with cardiolipin and phosphatidylserine. *Free Radic. Biol. Med.,* **2004**, 37, 1963–85. doi: 10.1016/j.freeradbiomed.2004.08.016
86. Sani M-A.; Dufourc EJ.; and Gröbner G. How does the Bax-alpha1 targeting sequence interact with mitochondrial membranes? The role of cardiolipin. *Biochim. Biophys. Acta,* **2009**, 1788, 623–31. doi: 10.1016/j.bbamem.2008.12.014
87. Gonzalvez F.; and Gottlieb E. Cardiolipin: setting the beat of apoptosis. *Apoptosis,* **2007**, 12, 877–85. doi: 10.1007/s10495-007-0718-8
88. Claypool SM.; Oktay Y.; Boontheung P.; Loo JA.; and Koehler CM. Cardiolipin defines the interactome of the major ADP/ATP carrier protein of the mitochondrial inner membrane. *J. Cell Biol.,* **2008**, 182, 937–50. doi: 10.1083/jcb.200801152
89. Hoffmann B.; Stöckl A.; Schlame M.; Beyer K.; and Klingenberg M. The reconstituted ADP/ATP carrier activity has an absolute requirement for cardiolipin as shown in cysteine mutants. *J. Biol. Chem.,* **1994**, 269, 1940–4.
90. NOEL H.; and PANDE S V. An essential requirement of cardiolipin for mitochondrial carnitine acylcarnitine translocase activity. Lipid requirement of carnitine acylcarnitine translocase. *Eur. J. Biochem.,* **1986**, 155, 99–102. doi: 10.1111/j.1432-1033.1986.tb09463.x
91. Kadenbach B.; Mende P.; Kolbe HVJ.; Stipani I.; and Palmieri F. The mitochondrial phosphate carrier has an essential requirement for cardiolipin. *FEBS Lett.,* **1982**, 139, 109–12. doi: 10.1016/0014-5793(82)80498-5
92. Phoon CKL.; Acehan D.; Schlame M.; Stokes DL.; Edelman-Novemsky I.; Yu D.; et al. Tafazzin knockdown in mice leads to a developmental cardiomyopathy with early diastolic dysfunction preceding myocardial noncompaction. *J. Am. Heart Assoc.,* Lippincott Williams & Wilkins; **2012**, 1, jah3-e000455. doi: 10.1161/jaha.111.000455
93. Soustek MS.; Falk DJ.; Mah CS.; Toth MJ.; Schlame M.; Lewin AS.; et al. Characterization of a transgenic short hairpin RNA-induced murine model of Tafazzin deficiency. *Hum. Gene Ther.,* **2011**, 22, 865–71. doi: 10.1089/hum.2010.199
94. Powers C.; Huang Y.; Strauss A.; and Khuchua Z. Diminished Exercise Capacity and Mitochondrial bc1 Complex Deficiency in Tafazzin-Knockdown Mice. *Front. Physiol.,* **2013**, 4, 74. doi: 10.3389/fphys.2013.00074
95. Kiebish MA.; Yang K.; Liu X.; Mancuso DJ.; Guan S.; Sims HF.; et al. Dysfunctional Cardiac Mitochondrial Bioenergetic , Lipidomic , and Signaling in a Murine Model of Barth Syndrome *.
96. Cadalbert LC.; Ghaffar FN.; Stevenson D.; Bryson S.; Vaz FM.; Gottlieb E.; et al. Mouse Tafazzin Is Required for Male Germ Cell Meiosis and Spermatogenesis. *PLoS One,* Public Library of Science; **2015**, 10, e0131066. doi: 10.1371/journal.pone.0131066
97. Uhlig T.; Kyprianou T.; Martinelli FG.; Oppici CA.; Heiligers D.; Hills D.; et al. The emergence of peptides in the pharmaceutical business: From exploration to exploitation. *EuPA Open Proteomics,* European Proteomics Association (EuPA); **2014**, 4, 1–12. doi: 10.1016/j.euprot.2014.05.003

98. Copolovici DM.; Langel K.; Eriste E.; and Langel Ü. Cell-penetrating peptides: design, synthesis, and applications. *ACS Nano,* American Chemical Society; **2014**, 8, 1972–94. doi: 10.1021/nn4057269
99. Green M.; Ishino M.; and Loewenstein PM. Mutational analysis of HIV-1 Tat minimal domain peptides: Identification of trans-dominant mutants that suppress HIV-LTR-driven gene expression. *Cell,* **1989**, 58, 215–23. doi: 10.1016/0092-8674(89)90417-0
100. Derossi D.; Calvet S.; Trembleau A.; Brunissen A.; Chassaing G.; and Prochiantz A. Cell Internalization of the Third Helix of the Antennapedia Homeodomain Is Receptor-independent. *J. Biol. Chem.,* **1996**, 271, 18188–93. doi: 10.1074/jbc.271.30.18188
101. Milletti F. Cell-penetrating peptides: classes, origin, and current landscape. *Drug Discov. Today,* **2012**, 17, 850–60. doi: 10.1016/j.drudis.2012.03.002
102. Falanga A.; Galdiero M.; and Galdiero S. Membranotropic Cell Penetrating Peptides: The Outstanding Journey. *Int. J. Mol. Sci.,* Multidisciplinary Digital Publishing Institute; **2015**, 16, 25323–37. doi: 10.3390/ijms161025323
103. Sónia Troeira Henriques ‡.; Júlia Costa § and.; and Miguel A. R. B. Castanho* ‡. Translocation of β-Galactosidase Mediated by the Cell-Penetrating Peptide Pep-1 into Lipid Vesicles and Human HeLa Cells Is Driven by Membrane Electrostatic Potential†. American Chemical Society; **2005**,
104. Deshayes S.; Heitz A.; Morris MC.; Charnet P.; Divita G.; and Heitz F. Insight into the mechanism of internalization of the cell-penetrating carrier peptide Pep-1 through conformational analysis. *Biochemistry,* American Chemical Society; **2004**, 43, 1449–57. doi: 10.1021/bi035682s
105. Richard JP.; Melikov K.; Vives E.; Ramos C.; Verbeure B.; Gait MJ.; et al. Cell-penetrating peptides. A reevaluation of the mechanism of cellular uptake. *J. Biol. Chem.,* **2003**, 278, 585–90. doi: 10.1074/jbc.m209548200
106. Duchardt F.; Fotin-Mleczek M.; Schwarz H.; Fischer R.; and Brock R. A Comprehensive Model for the Cellular Uptake of Cationic Cell-penetrating Peptides. *Traffic,* **2007**, 8, 848–66. doi: 10.1111/j.1600-0854.2007.00572.x
107. Console S.; Marty C.; García-Echeverría C.; Schwendener R.; and Ballmer-Hofer K. Antennapedia and HIV transactivator of transcription (TAT) "protein transduction domains" promote endocytosis of high molecular weight cargo upon binding to cell surface glycosaminoglycans. *J. Biol. Chem.,* **2003**, 278, 35109–14. doi: 10.1074/jbc.m301726200
108. Richard JP.; Melikov K.; Brooks H.; Prevot P.; Lebleu B.; and Chernomordik L V. Cellular uptake of unconjugated TAT peptide involves clathrin-dependent endocytosis and heparan sulfate receptors. *J. Biol. Chem.,* **2005**, 280, 15300–6. doi: 10.1074/jbc.m401604200
109. Nakase I.; Tadokoro A.; Kawabata N.; Takeuchi T.; Katoh H.; Hiramoto K.; et al. Interaction of arginine-rich peptides with membrane-associated proteoglycans is crucial for induction of actin organization and macropinocytosis. *Biochemistry,* American Chemical Society; **2007**, 46, 492–501. doi: 10.1021/bi0612824
110. Munsell E V.; Ross NL.; and Sullivan MO. Journey to the Center of the Cell: Current Nanocarrier Design Strategies Targeting Biopharmaceuticals to the Cytoplasm and Nucleus. *Curr. Pharm. Des.,* **2015**,
111. Madani F.; Lindberg S.; Langel U.; Futaki S.; and Gräslund A. Mechanisms of cellular uptake of cell-penetrating peptides. *J. Biophys.,* **2011**, 2011, 414729. doi: 10.1155/2011/414729
112. Tünnemann G.; Martin RM.; Haupt S.; Patsch C.; Edenhofer F.; and Cardoso MC. Cargo-dependent mode of uptake and bioavailability of TAT-containing proteins and peptides in living cells. *FASEB J.,* **2006**, 20, 1775–84. doi: 10.1096/fj.05-5523com

113. Erazo-Oliveras A.; Muthukrishnan N.; Baker R.; Wang T-Y.; and Pellois J-P. Improving the endosomal escape of cell-penetrating peptides and their cargos: strategies and challenges. *Pharmaceuticals (Basel).,* **2012**, 5, 1177–209. doi: 10.3390/ph5111177
114. Akita H.; Masuda T.; Nishio T.; Niikura K.; Ijiro K.; and Harashima H. Improving in vivo hepatic transfection activity by controlling intracellular trafficking: the function of GALA and maltotriose. *Mol. Pharm.,* American Chemical Society; **2011**, 8, 1436–42. doi: 10.1021/mp200189s
115. Saar K.; Lindgren M.; Hansen M.; Eiríksdóttir E.; Jiang Y.; Rosenthal-Aizman K.; et al. Cell-penetrating peptides: a comparative membrane toxicity study. *Anal. Biochem.,* **2005**, 345, 55–65. doi: 10.1016/j.ab.2005.07.033
116. El-Andaloussi S.; Järver P.; Johansson HJ.; and Langel U. Cargo-dependent cytotoxicity and delivery efficacy of cell-penetrating peptides: a comparative study. *Biochem. J.,* Portland Press Limited; **2007**, 407, 285–92. doi: 10.1042/bj20070507
117. Verdurmen WPR.; and Brock R. Biological responses towards cationic peptides and drug carriers. *Trends Pharmacol. Sci.,* **2011**, 32, 116–24. doi: 10.1016/j.tips.2010.11.005
118. Michiue H.; Eguchi A.; Scadeng M.; and Dowdy SF. Induction of in vivo synthetic lethal RNAi responses to treat glioblastoma. *Cancer Biol. Ther.,* Taylor & Francis; **2014**, 8, 2304–11. doi: 10.4161/cbt.8.23.10271
119. Rothbard JB.; Garlington S.; Lin Q.; Kirschberg T.; Kreider E.; McGrane PL.; et al. Conjugation of arginine oligomers to cyclosporin A facilitates topical delivery and inhibition of inflammation. *Nat. Med.,* Nature Publishing Group; **2000**, 6, 1253–7. doi: 10.1038/81359
120. Aguilera TA.; Olson ES.; Timmers MM.; Jiang T.; and Tsien RY. Systemic in vivo distribution of activatable cell penetrating peptides is superior to that of cell penetrating peptides. *Integr. Biol. (Camb).,* The Royal Society of Chemistry; **2009**, 1, 371–81. doi: 10.1039/b904878b
121. Khafagy E-S.; Kamei N.; Nielsen EJB.; Nishio R.; and Takeda-Morishita M. One-month subchronic toxicity study of cell-penetrating peptides for insulin nasal delivery in rats. *Eur. J. Pharm. Biopharm.,* Elsevier B.V.; **2013**, 85, 736–43. doi: 10.1016/j.ejpb.2013.09.014
122. Inagaki K.; Chen L.; Ikeno F.; Lee FH.; Imahashi K.; Bouley DM.; et al. Inhibition of delta-protein kinase C protects against reperfusion injury of the ischemic heart in vivo. *Circulation,* **2003**, 108, 2304–7. doi: 10.1161/01.cir.0000101682.24138.36
123. Bates E.; Bode C.; Costa M.; Gibson CM.; Granger C.; Green C.; et al. Intracoronary KAI-9803 as an adjunct to primary percutaneous coronary intervention for acute ST-segment elevation myocardial infarction. *Circulation,* **2008**, 117, 886–96. doi: 10.1161/circulationaha.107.759167
124. Zhang J.; Yang PL.; and Gray NS. Targeting cancer with small molecule kinase inhibitors. *Nat. Rev. Cancer,* Nature Publishing Group; **2009**, 9, 28–39. doi: 10.1038/nrc2559
125. Pisani A.; Visciano B.; Roux GD.; Sabbatini M.; Porto C.; Parenti G.; et al. Enzyme replacement therapy in patients with Fabry disease: State of the art and review of the literature. ***Mol. Genet. Metab.,*** 2012. p. 267–75. doi: 10.1016/j.ymgme.2012.08.003
126. Baldo B a. Enzymes Approved for Human Therapy: Indications, Mechanisms and Adverse Effects. *BioDrugs,* **2015**, 31–55. doi: 10.1007/s40259-015-0116-7
127. Lawlor MW.; Armstrong D.; Viola MG.; Widrick JJ.; Meng H.; Grange RW.; et al. Enzyme replacement therapy rescues weakness and improves muscle pathology in mice with X-linked myotubular myopathy. *Hum. Mol. Genet.,* **2013**, 22, 1525–38. doi: 10.1093/hmg/ddt003
128. Honda F.; Hane Y.; Toma T.; Yachie A.; Kim E-S.; Lee S-K.; et al. Transducible form of p47phox and p67phox compensate for defective NADPH oxidase activity in neutrophils of patients with chronic granulomatous disease. *Biochem. Biophys. Res. Commun.,* **2012**, 417, 162–8.

doi: 10.1016/j.bbrc.2011.11.077
129. Vyas PM.; Tomamichel WJ.; Pride PM.; Babbey CM.; Wang Q.; Mercier J.; et al. A TAT-Frataxin fusion protein increases lifespan and cardiac function in a conditional Friedreich's ataxia mouse model. *Hum. Mol. Genet.,* **2012**, 21, 1230–47. doi: 10.1093/hmg/ddr554
130. Malhotra A.; Edelman-Novemsky I.; Xu Y.; Plesken H.; Ma J.; Schlame M.; et al. Role of calcium-independent phospholipase A2 in the pathogenesis of Barth syndrome. *Proc. Natl. Acad. Sci. U. S. A.,* **2009**, 106, 2337–41. doi: 10.1073/pnas.0811224106
131. Zou L-L.; Ma J-L.; Wang T.; Yang T-B.; and Liu C-B. Cell-penetrating Peptide-mediated therapeutic molecule delivery into the central nervous system. *Curr. Neuropharmacol.,* Bentham Science Publishers; **2013**, 11, 197–208. doi: 10.2174/1570159x11311020006
132. Zahid M.; Phillips BE.; Albers SM.; Giannoukakis N.; Watkins SC.; and Robbins PD. Identification of a cardiac specific protein transduction domain by in vivo biopanning using a M13 phage peptide display library in mice. *PLoS One,* **2010**, 5, e12252. doi: 10.1371/journal.pone.0012252
133. Tsai SQ.; Wyvekens N.; Khayter C.; Foden JA.; Thapar V.; Reyon D.; et al. Dimeric CRISPR RNA-guided FokI nucleases for highly specific genome editing. *Nat. Biotechnol.,* NIH Public Access; **2014**, 32, 569–76. doi: 10.1038/nbt.2908
134. Gregorevic P.; Plant DR.; Leeding KS.; Bach LA.; and Lynch GS. Improved contractile function of the mdx dystrophic mouse diaphragm muscle after insulin-like growth factor-I administration. *Am. J. Pathol.,* **2002**, 161, 2263–72. doi: 10.1016/s0002-9440(10)64502-6
135. Folch J.; Lees M.; and Sloane GH. A SIMPLE METHOD FOR THE ISOLATION AND PURIFICATION OF TOTAL LIPIDES FROM ANIMAL TISSUES*. *J. Biol. Chem.,* **1957**, 226, 497–509.
136. Bowron A.; Frost R.; Powers VEC.; Thomas PH.; Heales SJR.; and Steward CG. Diagnosis of Barth syndrome using a novel LC-MS/MS method for leukocyte cardiolipin analysis. *J. Inherit. Metab. Dis.,* **2013**, 36, 741–6. doi: 10.1007/s10545-012-9552-4
137. Weldy CS.; Liu Y.; Chang Y-C.; Medvedev IO.; Fox JR.; Larson T V.; et al. In utero and early life exposure to diesel exhaust air pollution increases adult susceptibility to heart failure in mice. *Part. Fibre Toxicol.,* **2013**, 10, 59. doi: 10.1186/1743-8977-10-59
138. Sakamoto O.; Kitoh T.; and Ohura T. Novel missense mutation (R94S) in the TAZ (G4 . 5) gene in a Japanese patient with Barth syndrome. **2002**, 2, 3–5.
139. Herndon JD.; Claypool SM.; and Koehler CM. The Taz1p transacylase is imported and sorted into the outer mitochondrial membrane via a membrane anchor domain. *Eukaryot. Cell,* **2013**, 12, 1600–8. doi: 10.1128/ec.00237-13
140. Chacinska A.; Koehler CM.; Milenkovic D.; Lithgow T.; and Pfanner N. Importing Mitochondrial Proteins: Machineries and Mechanisms. *Cell,* **2009**, 138, 628–44. doi: 10.1016/j.cell.2009.08.005
141. Dudek J.; Rehling P.; and van der Laan M. Mitochondrial protein import: Common principles and physiological networks. *Biochim. Biophys. Acta - Mol. Cell Res.,* **2013**, 1833, 274–85. doi: 10.1016/j.bbamcr.2012.05.028
142. Stojanovski D.; Müller JM.; Milenkovic D.; Guiard B.; Pfanner N.; and Chacinska A. The MIA system for protein import into the mitochondrial intermembrane space. *Biochim. Biophys. Acta - Mol. Cell Res.,* **2008**, 1783, 610–7. doi: 10.1016/j.bbamcr.2007.10.004
143. Abe Y.; Shodai T.; Muto T.; Mihara K.; Torii H.; Nishikawa S.; et al. Structural basis of presequence recognition by the mitochondrial protein import receptor Tom20. *Cell,* **2000**, 100, 551–60.
144. Neupert W.; and Herrmann JM. Translocation of Proteins into Mitochondria. *Annu. Rev. Biochem.,* **2007**, 76, 723–49. doi: 10.1146/annurev.biochem.76.052705.163409

145. Sugiura A.; McLelland G-L.; Fon EA.; and McBride HM. A new pathway for mitochondrial quality control: mitochondrial-derived vesicles. *EMBO J.,* **2014**, 33, 2142–56. doi: 10.15252/embj.201488104
146. WRIESSNEGGER T.; GUBITZ G.; LEITNER E.; INGOLIC E.; CREGG J.; DELACRUZ B.; et al. Lipid composition of peroxisomes from the yeast Pichia pastoris grown on different carbon sources. *Biochim. Biophys. Acta - Mol. Cell Biol. Lipids,* **2007**, 1771, 455–61. doi: 10.1016/j.bbalip.2007.01.004
147. Settembre C.; Fraldi A.; Medina DL.; and Ballabio A. Signals from the lysosome: a control centre for cellular clearance and energy metabolism. *Nat. Rev. Mol. Cell Biol.,* NIH Public Access; **2013**, 14, 283–96. doi: 10.1038/nrm3565
148. Chacinska A.; Lind M.; Frazier AE.; Dudek J.; Meisinger C.; Geissler A.; et al. Mitochondrial Presequence Translocase: Switching between TOM Tethering and Motor Recruitment Involves Tim21 and Tim17. *Cell,* **2005**, 120, 817–29. doi: 10.1016/j.cell.2005.01.011
149. Harner M.; Neupert W.; and Deponte M. Lateral release of proteins from the TOM complex into the outer membrane of mitochondria. *EMBO J.,* **2011**, 30, 3232–41. doi: 10.1038/emboj.2011.235
150. Dhillon VS.; and Fenech M. Mutations that affect mitochondrial functions and their association with neurodegenerative diseases. *Mutat. Res. - Rev. Mutat. Res.,* Elsevier B.V.; **2014**, 759, 1–13. doi: 10.1016/j.mrrev.2013.09.001
151. Dudek J.; Cheng I-F.; Chowdhury A.; Wozny K.; Balleininger M.; Reinhold R.; et al. Cardiac-specific succinate dehydrogenase deficiency in Barth syndrome. *EMBO Mol. Med.,* Wiley-Blackwell; **2016**, 8, 139–54. doi: 10.15252/emmm.201505644
152. Minkler PE.; and Hoppel CL. Separation and characterization of cardiolipin molecular species by reverse-phase ion pair high-performance liquid chromatography-mass spectrometry. *J. Lipid Res.,* **2010**, 51, 856–65. doi: 10.1194/jlr.d002857
153. Sparagna GC.; Chicco AJ.; Murphy RC.; Bristow MR.; Johnson CA.; Rees ML.; et al. Loss of cardiac tetralinoleoyl cardiolipin in human and experimental heart failure. *J. Lipid Res.,* American Society for Biochemistry and Molecular Biology; **2007**, 48, 1559–70. doi: 10.1194/jlr.m600551-jlr200
154. Bowron A.; Honeychurch J.; Williams M.; Tsai-Goodman B.; Clayton N.; Jones L.; et al. Barth syndrome without tetralinoleoyl cardiolipin deficiency: a possible ameliorated phenotype. *J. Inherit. Metab. Dis.,* Springer Netherlands; **2015**, 38, 279–86. doi: 10.1007/s10545-014-9747-y
155. Iverson SJ.; Lang SLC.; and Cooper MH. Comparison of the bligh and dyer and folch methods for total lipid determination in a broad range of marine tissue. *Lipids,* **2001**, 36, 1283–7. doi: 10.1007/s11745-001-0843-0
156. Kulik W.; van Lenthe H.; Stet FS.; Houtkooper RH.; Kemp H.; Stone JE.; et al. Bloodspot assay using HPLC-tandem mass spectrometry for detection of Barth syndrome. ***Clin. Chem.,*** 2008doi: 10.1373/clinchem.2007.095711
157. Augusto V.; Padovani CR.; Eduardo G.; and Campos R. Skeletal Muscle Fiber Types in C57Bl6J Mice. *Braz J Morphol Sci,* **2004**, 21, 89–94.
158. Horowitz JF.; and Klein S. Lipid metabolism during endurance exercise. *Am. J. Clin. Nutr.,* American Society for Nutrition; **2000**, 72, 558S–63S.
159. Acehan D.; Khuchua Z.; Houtkooper RH.; Malhotra A.; Kaufman J.; Vaz FM.; et al. Distinct effects of tafazzin deletion in differentiated and undifferentiated mitochondria. *Mitochondrion,* **2009**, 9, 86–95. doi: 10.1016/j.mito.2008.12.001
160. Branco AF.; Pereira SP.; Gonzalez S.; Gusev O.; Rizvanov AA.; and Oliveira PJ. Gene Expression Profiling of H9c2 Myoblast Differentiation towards a Cardiac-Like Phenotype.

PLoS One, Public Library of Science; **2015**, 10, e0129303. doi: 10.1371/journal.pone.0129303
161. Ronchi JA.; Figueira TR.; Ravagnani FG.; Oliveira HCF.; Vercesi AE.; and Castilho RF. A spontaneous mutation in the nicotinamide nucleotide transhydrogenase gene of C57BL/6J mice results in mitochondrial redox abnormalities. *Free Radic. Biol. Med.,* **2013**, 63, 446–56. doi: 10.1016/j.freeradbiomed.2013.05.049
162. Huang Y.; Powers C.; Moore V.; Schafer C.; Ren M.; Phoon CKL.; et al. The PPAR pan-agonist bezafibrate ameliorates cardiomyopathy in a mouse model of Barth syndrome. *Orphanet J. Rare Dis.,* BioMed Central; **2017**, 12, 49. doi: 10.1186/s13023-017-0605-5
163. Soustek MS.; Baligand C.; Falk DJ.; Walter GA.; Lewin AS.; and Byrne BJ. Endurance training ameliorates complex 3 deficiency in a mouse model of Barth syndrome. *J. Inherit. Metab. Dis.,* **2015**, 38, 915–22. doi: 10.1007/s10545-015-9834-8
164. Cade WT.; Reeds DN.; Peterson LR.; Bohnert KL.; Tinius RA.; Benni PB.; et al. Endurance Exercise Training in Young Adults with Barth Syndrome: A Pilot Study. *JIMD Rep.,* Springer; **2017**, 32, 15–24. doi: 10.1007/8904_2016_553
165. Ikon N.; Su B.; Hsu F-F.; Forte TM.; and Ryan RO. Exogenous cardiolipin localizes to mitochondria and prevents TAZ knockdown-induced apoptosis in myeloid progenitor cells. *Biochem. Biophys. Res. Commun.,* NIH Public Access; **2015**, 464, 580–5. doi: 10.1016/j.bbrc.2015.07.012
166. Ries M. Enzyme replacement therapy and beyond—in memoriam Roscoe O. Brady, M.D. (1923–2016). *J. Inherit. Metab. Dis.,* Springer Netherlands; **2017**, 40, 343–56. doi: 10.1007/s10545-017-0032-8
167. Lopaschuk GD.; and Jaswal JS. Energy Metabolic Phenotype of the Cardiomyocyte During Development, Differentiation, and Postnatal Maturation. *J. Cardiovasc. Pharmacol.,* **2010**, 56, 130–40. doi: 10.1097/fjc.0b013e3181e74a14
168. Lopaschuk GD.; Spafford MA.; and Marsh DR. Glycolysis is predominant source of myocardial ATP production immediately after birth. *Am. J. Physiol.,* **1991**, 261, H1698-705.
169. Schlame M.; and Ren M. The role of cardiolipin in the structural organization of mitochondrial membranes. *Biochim Biophys Acta,* **2009**, 1788, 2080–3. doi: 10.1016/j.bbamem.2009.04.019
170. He Q.; and Spinale FG. Tafazzin knockdown causes hypertrophy of neonatal ventricular myocytes. *Am. J. Physiol. Heart Circ. Physiol.,* American Physiological Society; **2010**, 299, H210-6. doi: 10.1152/ajpheart.00098.2010
171. He Q.; Wang M.; Harris N.; and Han X. Tafazzin knockdown interrupts cell cycle progression in cultured neonatal ventricular fibroblasts. *Am. J. Physiol. Heart Circ. Physiol.,* **2013**, 305, H1332-43. doi: 10.1152/ajpheart.00084.2013
172. van Raam, Bram J; Kuijpers TW.; van Raam BJ.; and Kuijpers TW. Mitochondrial defects lie at the basis of neutropenia in Barth syndrome. Lippincott Williams & Wilkins, Inc.; **2009**, 16, 14–9. doi: 10.1097/moh.0b013e32831c83f3